72-13,440

COHEN, Jonathan Brewer, 1944-
MICROWAVE-MICROWAVE DOUBLE RESONANCE
INVESTIGATIONS OF COLLISIONAL TRANSFER OF
ROTATIONAL ENERGY.

Harvard University, Ph.D., 1972
Chemistry, physical

University Microfilms, A XEROX Company, Ann Arbor, Michigan

THIS DISSERTATION HAS BEEN MICROFILMED EXACTLY AS RECEIVED

Reproduced with permission of the copyright owner. Further reproduction prohibited without permission.

MICROWAVE-MICROWAVE DOUBLE RESONANCE INVESTIGATIONS OF COLLISIONAL TRANSFER OF ROTATIONAL ENERGY

A thesis presented

by

Jonathan Brewer Cohen

to

The Department of Chemistry

in partial fulfillment of the requirements

for the degree of

Doctor of Philosophy

in the subject of

Chemistry

Harvard University

Cambridge, Massachusetts

July, 1971

Copyright reserved by the author.

Reproduced with permission of the copyright owner. Further reproduction prohibited without permission.

PLEASE NOTE:

Some pages have indistinct print. Filmed as received.

UNIVERSITY MICROFILMS.

Reproduced with permission of the copyright owner. Further reproduction prohibited without permission.

Microwave-Microwave Double Resonance Investigations of

Collisional Transfer of Rotational Energy

Summary

Research Director
E. Bright Wilson

Jonathan B. Cohen
July, 1971

Four level, modulated microwave double resonance has been used to study rotational energy transfer in dilute polar gases. A survey has been made of double resonance signals observable in four asymmetric rotors: trimethylene oxide, β-propiolactone, cyclobutanone, and cis-difluoroethylene. Double resonance intensities have been measured in vibrational ground and excited states. Also, angular momentum reorientation caused by intermolecular collisions has been studied by microwave double resonance. Four level experiments have been performed on individual $|JM\rangle$ components of ethylene oxide and 3,3,3-trifluoropropyne and on $|JF\rangle$ components of ICN. These experiments provide evidence that the energy transfer and momentum reorientation occurring during collisions are determined by the long range dipole-dipole interaction. Qualitatively, a first order perturbation theory description of the collision process accounts for the selection rules of the observed collision induced transitions.

Double resonance studies have been made of collision induced transitions occurring in pure HCN and in HCN in the presence of He, Ar, or Xe. Double resonance intensities and phase shifts have been determined for a number of HCN ℓ-doublets. Also, collision broadening rotational linewidth parameters have been determined for pure HCN and for each rare gas collision partner. A computer program is used to calculate intensities and phase shifts in terms of a set of collisional rate constants. It has been found that it is not possible to determine a unique set of rate constants on the basis of the experimental data. However, general theoretical arguments are presented that allow a preferred set to be determined for each collision partner. Experimental studies are presented that provide evidence that quantum coherence effects are being observed that must be accounted for in any improved analysis of double resonance data.

Reproduced with permission of the copyright owner. Further reproduction prohibited without permission.

ACKNOWLEDGEMENTS

I would like to express my gratitude to Prof. E. Bright Wilson for his encouragement and guidance during the course of this research.

I also wish to thank Prof. Roy Gordon for his help and Prof. Rollie Myers for his encouragement during recent months.

The fellow members of the Wilson research group have been a constant source of assistance and encouragement. I am grateful to Drs. Raymond Azrak and Robert Ford for the help they gave me as they introduced me to the intricacies of microwave spectroscopy. Talks with Dr. Herbert Pickett helped clarify many confusions, and the aid and friendship of Frank Wodarczyk and Mike Fuller are truly appreciated.

I am grateful to the National Science Foundation and to Harvard University for their financial support.

Reproduced with permission of the copyright owner. Further reproduction prohibited without permission.

TABLE OF CONTENTS

CHAPTER I. AN INTRODUCTION TO MICROWAVE DOUBLE RESONANCE

I. Four-level Double Resonance, General Considerations....I-2

II. Microwave Linewidth Theory and Double Resonance Experiments.....I-5

III. A Kinetic Model to Describe Double Resonance.....I-11

IV. Application of the Kinetic Model.....I-23

V. Future Chapters.....I-27

CHAPTER II. ROTATIONAL ENERGY TRANSFER IN PURE POLAR GASES

I. Introduction

A. Absorption Coefficient of Double Resonance Signals..II-3

B. Perturbation Theory Description of Collisions.....II-6

C. Summary of Results.....II-11

D. Molecular Energy Levels.....II-12

II. Experimental

A. Apparatus.....II-15

B. Procedure.....II-17

C. Results

1. Trimethylene Oxide.....II-19

2. β-Propiolactone and Cyclobutanone.....II-22

3. Cis-difluoroethylene.....II-22

III. Discussion.....II-22

Reproduced with permission of the copyright owner. Further reproduction prohibited without permission.

CHAPTER III. COLLISION-INDUCED ANGULAR MOMENTUM REORIENTATION IN POLAR GASES

I. Introduction.....III-1

II. M-Dependence of Rotational Energy Transfer.....III-2

A. Ethylene Oxide.....III-2

B. 3,3,3-Trifluoropropyne.....III-7

III. Angular Momentum Reorientation in ICN-ICN Collisions...III-13

A. Introduction.....III-13

B. Choice of Four-level System.....III-16

C. Apparatus and Procedure.....III-18

D. Results.....III-20

E. Discussion.....III-30

IV. ENERGY TRANSFER IN HCN-RARE GAS MIXTURES

I. Introduction.....IV-1

II. Energy Levels in HCN.....IV-3

III. Experimental

A. MMDR Experiments.....IV-8

1. The Spectrometer.....IV-8

2. Procedure.....IV-13

3. Results.....IV-19

a. Relative Intensities.....IV-19

b. Phase.....IV-24

B. Pressure Broadening Linewidth Parameters.....IV-33

Reproduced with permission of the copyright owner. Further reproduction prohibited without permission.

IV. Analysis of Experimental Results

A. First Set of Rate Constants.....IV-41

1. HCN-HCN.....IV-47

2. HCN-Argon, HCN-Xenon.....IV-51

3. HCN-Helium.....IV-52

B. Refinements of Results.....IV-54

1. HCN-HCN Parameters.....IV-55

2. Argon Analysis.....IV-58

3. Helium Analysis.....IV-64

4. Back to Pure HCN.....IV-68

V. Discussion.....IV-75

A. Perturbation Theory Description of HCN-Rare Gas Collisions.....IV-76

B. Parity Selection Rules.....IV-82

C. Relative Magnitude of Rate Constants.....IV-84

VI. Further Experiments and Discussion about Phase Shifts..IV-90

VII. Conclusions and Summary.....IV-100

APPENDIX I. Observed Transitions of cis-Difluoroethylene.....AI-1

APPENDIX II. Further Details about Chapter IV Calculations.....AII-1

Reproduced with permission of the copyright owner. Further reproduction prohibited without permission.

CHAPTER I

AN INTRODUCTION TO MICROWAVE DOUBLE RESONANCE

Most work in gas phase microwave rotational spectroscopy has been oriented towards the determination of molecular structural parameters. However, the microwave spectra of molecules also include much information about intermolecular interactions. Although the widths of microwave absorption lines are determined by several different factors, over a great pressure range the dominant line-broadening mechanism is the intermolecular collision. Chemists and physicists have devoted considerable effort to experimental and theoretical analyses of rotational linewidth parameters in an effort to gain greater understanding about the intermolecular potential through which molecules interact.

In recent years microwave double resonance techniques have been developed that allow the determination of cross-sections (rates) for collision-induced transitions between specified initial and final states. These partial cross sections are more closely related to individual collision encounters than the total cross section. There is still an average over all possible collision partners, but the partial cross section eliminates the necessity of summing over all possible final states.

From inspection of the experimental linewidth parameter, one can only say whether the total cross section is large or small--a measure of the strength of the interaction. From just the qualitative inspection of double resonance data, one has a considerably finer picture of

Reproduced with permission of the copyright owner. Further reproduction prohibited without permission.

the intermolecular interaction. By determining the preferred "selection rules" for collision-induced transitions, one can make statements about the symmetry of the important parts of the intermolecular potential.

Four Level Double Resonance. General Considerations

Two microwave double resonance techniques have been developed to study rotational energy transfer in dilute polar gases, a technique utilizing Stark modulation[1,2] (SMDR) and a microwave modulation technique[3,4] (MMDR). The two techniques have many features in common. A sample of gas in a waveguide is irradiated simultaneously with two radiation fields, a high power field called the "pump," and a low power field called the "signal." When at the frequency of a dipole-allowed rotational transition, the pump is of sufficient intensity to cause equalization or near equalization of populations of the two pumped levels. This perturbation of the population from equilibrium will be transmitted to other rotational levels by rotationally inelastic collisions. The signal field is introduced at another resonant frequency. The absorption at a resonant frequency is proportional to the difference

---

1. T. Oka, J. Chem. Phys. 45, 754 (1966).
2. T. Oka, J. Chem. Phys. 47, 13 (1967).
3. R. C. Woods, A. M. Ronn, and E. B. Wilson, Rev. Sci. Inst. 37, 927 (1966).
4. A. M. Ronn and E. B. Wilson, J. Chem. Phys. 46, 3262 (1967).

Reproduced with permission of the copyright owner. Further reproduction prohibited without permission.

in population between the two levels. In the Stark experiment, the signal absorption is monitored by traditional Stark techniques, and the change in intensity of the signal is monitored as the pump field passes through a rotational resonance. In the modulation experiment, the pump field is modulated on and off a resonance. The signal field is monitored at the modulation frequency, and a signal is detected only if the population difference between the signal levels has a time dependent component at the modulation frequency. If the signal and pump transitions have no energy level in common, an MMDR signal is detected only if there is collisionally induced population transfer between the pumped and observed levels. Analogously, in SMDR, a change in intensity of the Stark signal can only be caused by collisionally induced transitions.

The four level problem is presented schematically in Figure 1. If the transition ab is saturated, level b becomes a source of molecules while level a is a sink for molecules as collisions tend to return the system to equilibrium. Let us consider some possible collision interactions in terms of the SMDR technique. Clearly, if molecules are only very rarely transferred from ab to cd there will be no change in cd intensity as we turn on pump ab. If molecules are transferred from b to d only, there will be a decrease in the Stark signal cd on pumping ab. Molecules transferred from b to c will cause an increase in the signal. If molecules are transferred with equal probability to c and d, the double resonance signal will be very weak. Also, the strongest signals will occur if the preferred collision transfer is $b \longleftrightarrow d$ and $c \longleftrightarrow a$.

The effects of multiple collisions can also be accounted for

Reproduced with permission of the copyright owner. Further reproduction prohibited without permission.

Figure 1

Four Level MMDR

Energy Levels

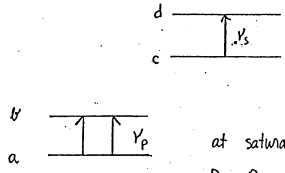

Reproduced with permission of the copyright owner. Further reproduction prohibited without permission.

qualitatively. If collision induced transitions favor b $\longleftrightarrow$ c and c $\longleftrightarrow$ d, we see that the effects of multiple collisions would tend to diminish the effect of a single collision as we monitor the cd transition. Lastly, there is one factor that must be important. How many levels do we expect to be involved in the dominant relaxation processes? If levels a and b are each connected with essentially comparable probability to 30 other levels, then the expected double resonance effect would be very weak at any signal transition, while if levels a and b can relax only through one or two levels, we might expect to see rather strong signals.

Microwave Linewidth Theory and Double Resonance Experiments

Four level microwave signals were first reported by Dr. Oka[1] in 1966. That they were observed is not surprising from a theoretical vantage point since all useful theories of collision-broadening predict that there should be dominant relaxation pathways. The basic formulation of microwave lineshape theory of Van Vleck-Weisskopf[5] and the Karplus-Schwinger[6] extension for saturation effects derived lineshape expressions based on the assumption that there was a single characteristic relaxation time, τ, by which collisions restored populations to equilibrium. In this manner each rotational state is described by the

---

5. J. H. Van Vleck and V. Weisskopf, Rev. Mod. Phys 17, 227 (1945).

6. R. Karplus and J. Schwinger, Phys. Rev. 73, 1020 (1948).

Reproduced with permission of the copyright owner. Further reproduction prohibited without permission.

same characteristic time, and the halfwidth at half height, $\Delta\nu$, of the Lorentzian shape is related to this time

$$\tau = \frac{1}{2\pi\Delta\nu}. \tag{1}$$

For transitions between states i and f,

$$\Delta\nu = \frac{1}{2}(\Delta\nu_i + \Delta\nu_f) \equiv \frac{1}{4\pi}\left(\frac{1}{\tau_i} + \frac{1}{\tau_f}\right). \tag{1a}$$

Most calculations of microwave linewidths are based on a general impact theory derived by Anderson.[7] The widths and shifts are determined by collisions that interrupt the radiation process of a free molecule. Extensions and modifications have been made by Tsao and Curnutte,[8] Boggs,[9] Krishnaji,[10] Rabitz[11] and others. These extensions have focused on different means of utilizing perturbation theory to evaluate the general expression derived by Anderson. There is a recent review by Birnbaum.[12]

The basic result is that resolved lines should be Lorentzians with a linewidth that is determined by the real part of an effective inter-

---

7. P. W. Anderson, Phys. Rev. 76, 647 (1949).
8. C. J. Tsao and B. Curnutte, J. Quant. Spectrosc. and Radiat. Transfer 2, 41 (1962).
9. J. Murphy and J. Boggs, J. Chem. Phys. 51, 3891 (1969) contains references to earlier articles.
10. Krishnaji and S. Srivastava, J. Chem. Phys. 43, 1345 (1965) contains references to earlier work.
11. H. Rabitz and R. G. Gordon, J. Chem. Phys. 53, 1815 and 1831 (1970).
12. G. Birnbaum, Adv. Chem. Phys. 12, 487 (1967).

Reproduced with permission of the copyright owner. Further reproduction prohibited without permission.

action cross section, $\sigma = \sigma' + i\sigma''$.

$$2\pi\Delta\nu = N_1 v_{11} \sigma'_{11} + N_2 v_{12} \sigma'_{12} \qquad (2)$$

for N_i molecules per volume and mean relative velocities v_{ij}. The subscript 1 refers to absorbers and 2 to perturbers. For single component gases, $N_2 = 0$.

The collision cross section can be computed from perturbation theory. In order to render the molecular interactions tractable, assumptions are usually made:

(1) Only bimolecular collisions are important and the duration of collision is much less than the time between collisions.

(2) While the internal molecular coordinates are treated quantum mechanically, the translational motion is treated classically. Most often the perturber is assumed to follow a straight line trajectory of impact parameter b. This latter assumption restricts calculations to those situations where the energy transferred from translation to internal modes must be a small fraction of the kinetic energy, and the angular momentum transferred must be only a small part of the orbital angular momentum.

More details of the perturbation theory description of the collision process will be presented later (Chapters II and IV). The interaction potential is implicitly a function of time since the distance between molecules is a function of time. As the translational motion is described by a classical trajectory, the interaction potential is converted to a function of time and the internal mode problem becomes a time-dependent perturbation theory problem.

Reproduced with permission of the copyright owner. Further reproduction prohibited without permission.

The cross section can be expressed as

$$\sigma = \pi b^{*2} + \int_{b^*}^{\infty} 2\pi b \, S(b) \, db \qquad (3)$$

where b is an impact parameter, b* some critical distance below which the perturbation theory is invalid (usually $S(b^*) = 1$), and S(b) is the collision interruption function, the probability that a collision at impact parameter b will disturb the behavior of an emitting molecule and hence contribute to line broadening. The determination of the distance b* is, unfortunately, crucial. Different procedures have been developed[7, 9, 11] to estimate the effects of the short range collisions. The linewidth is determined by Re[S(b)], while shifts are determined by Im[S(b)].

As one develops the collision interruption function by treating the collision to first order in a perturbation expansion one finds that the real cross section is more complicated than a simple average of contributions from states i and f. There is one part of σ' that is due to an average interruption function for i and f ($S_2(b)_o$ in Anderson's[7] notation),

$$S_2(b)_o \propto \frac{1}{2} \{ \sum_{J_i'} |\langle J_i M_i | P | J_i' M_i' \rangle|^2 + \sum_{J_f'} |\langle J_f M_f | P | J_f' M_f' \rangle|^2 \} \qquad (3a)$$

but there is also a contribution, $S_2(b)_m$, that is a cross term between the component levels i and f and depends on reorientation effects within the degenerate sublevels of J_i and J_f.

$$S_2(b)_m \propto \langle J_i M_i | P | J_i M_i' \rangle \times \langle J_f M_f | P | J_f M_f' \rangle \qquad (3b)$$

where

Reproduced with permission of the copyright owner. Further reproduction prohibited without permission.

$$P = \int_{-\infty}^{\infty} dt\ e^{iH_o t/h}\ V(t)\ e^{-iH_o t/h}. \qquad (3c)$$

H_o is the free molecule Hamiltonian and V(t) the interaction potential.

These results necessitate that the microwave linewidths contain information other than the rates of collision-induced transitions, the latter contributing only to $S_2(b)_o$. In general, then, the linewidth parameters are complementary to the collision-induced transition rates as a means of gaining further information about intermolecular forces. However, for many situations $(S_2)_o$ is the main contributor to the cross section. In that case the linewidths and double resonance transition rates should be comparable, and in all cases the fact that one can experimentally determine quantities closely related to individual terms in $S_2(b)_o$ serves as a powerful check on any theoretical formulation.

The theory predicts clearly that there will be preferred collision-induced transitions with partial cross sections determined by the intermolecular potential. For long range interactions the attractive interactions can be expressed in terms of the multipole moment expansion of the non-overlapping charge distributions. The fact that the theory had been reasonably successful in accounting for microwave linewidths, including the dependence on J state and temperature, suggested that the preferred relaxation processes should exist and should be more important than the cruder hard collision model.

After the many years during which this model of linewidth theory had been utilized, Oka's first observation[1] of a four level microwave double resonance must have been received with both relief and satisfaction. Using the SMDR technique described previously, he observed

Reproduced with permission of the copyright owner. Further reproduction prohibited without permission.

several signals in ethylene oxide, an asymmetric rotor with μ_b = 1.88 D. The signals were observed for levels that were doubly connected by possible collision induced transitions. In the notation of Figure 1, a $\longleftrightarrow$ c and b $\longleftrightarrow$ d were both dipole allowed.

Subsequently Oka[2,13-18] has utilized the SMDR technique to study energy transfer in many different systems. He has studied energy transfer in pure polar gases (H_2CO, HCN, H_2CCO, NH_3, CH_3OH, CH_3NH_2) and in mixtures (NH_3 with He, Ar, Xe, H_2, HD, D_2, O_2, N_2, CH_4, or SF_6; CH_3OH with He or H_2; and CH_3NH_2 with He). The experiments have been primarily qualitative in nature. Where complex systems have been studied, no attempt was made to reduce the experimental results to specific rate constants. For the pure polar gases, the results agree with what one expects from a dominant dipolar interaction. In some cases, transitions are observed for $\Delta J = \pm 2$, 3 or 4. These signals might be caused by multiple dipole collisions or by direct processes due to different types of interactions (either higher order dipole interactions or higher multipole moments). In an elegant experiment, Oka[16] used triple resonance to experimentally distinguish between the results of direct high ΔJ

---

13. T. Oka, J. Chem. Phys. 47, 4852 (1967).
14. T. Oka, J. Chem. Phys. 48, 4919 (1968).
15. T. Oka, J. Chem. Phys. 49, 3135 (1968).
16. T. Oka, J. Chem. Phys. 49, 4234 (1968).
17. R. M. Lees and T. Oka, J. Chem. Phys. 51, 3027 (1969).
18. P. Daly and T. Oka, J. Chem. Phys. 53, 3272 (1970).

Reproduced with permission of the copyright owner. Further reproduction prohibited without permission.

transitions and a cascade process.

The many experiments on NH_3-rare gas mixtures[13,15] have emphasized the power of the double resonance technique even without the determination of specific rates. By tracing out the preferred collision-induced transitions one is able to see the J and K dependence. The results emphasize the complexity of the interactions and, in particular, the cause of the variation from one collision partner to another is not readily apparent.

After Oka's initial report, Ronn[4] used the MMDR technique to confirm Oka's result and to make a preliminary survey of "selection rules" for some asymmetric rotors. His conclusions were that the MMDR technique was definitely sensitive enough to see signals where there were multiple connections between pumped and observed levels. The chances of observation were less likely if there was only a single connection. Furthermore, he felt that the technique would not be sensitive enough if there were dipole moment components along more than one principal axis. In that case there would be too many relaxation mechanisms. Also, molecules with low lying vibrational states would probably have individual rotational absorptions that were insufficiently intense to observe the small double resonance perturbations.

A Kinetic Model to Describe Double Resonance

Ronn's initial use of the MMDR technique consisted of a qualitative

Reproduced with permission of the copyright owner. Further reproduction prohibited without permission.

survey. Subsequently, Gordon[19] presented an analysis of the information contained in the four level MMDR experiments in terms of a linear kinetic model. It was shown that by using the model to analyze the experimental data, it should be possible to obtain values for the dominant collision-induced transition rates, and this has been done by Larson, et al.[20]

The starting point for the analysis is that the time dependent rotational populations can be described by a classical linear rate expression

$$\frac{d\underset{\sim}{n}(t)}{dt} = -\underset{\approx}{\Pi} \cdot \underset{\sim}{n}(t) \tag{4}$$

where n is the vector of populations, and $\underset{\approx}{\Pi}$ is the matrix of rate coefficients. The diagonal elements, Π_{ii}, equal the total rate at which molecules are transferred out of level i. The off diagonal elements, Π_{ij}, give minus the rate at which molecules are transferred from state j to i. The matrix as constructed assures that there is mass conservation if

$$\sum_i \Pi_{ij} = 0 \quad \text{for all } j. \tag{5}$$

In an MMDR experiment two levels are being pumped during one half cycle while for the other half cycle there is no pumping. Hence, if we consider $\underset{\approx}{\Pi}$ to contain all the equilibrium collision transfer rates and

---

19. R. G. Gordon, J. Chem. Phys. 46, 4399 (1967).

20. R. G. Gordon, P. E. Larson, C. H. Thomas and E. B. Wilson, J. Chem. Phys. 50, 1388 (1969).

Reproduced with permission of the copyright owner. Further reproduction prohibited without permission.

$\delta\underset{\approx}{\Pi}$ to contain the effects of the pump, then during one half cycle the rate equation is given by (4), and during the other half it is given by

$$\frac{d\underset{\sim}{n}(t)}{dt} = -(\underset{\approx}{\Pi} + \delta\underset{\approx}{\Pi})\cdot\underset{\sim}{n}(t). \tag{6}$$

Using matrix notation, equations (4) and (6) have solutions

$$\underset{\sim}{n}(t) = \exp(-\underset{\approx}{\Pi}t)\cdot\underset{\sim}{n}(0) \qquad t \geq 0 \tag{7a}$$

$$\underset{\sim}{n}(t) = \exp[(-\underset{\approx}{\Pi} - \delta\underset{\approx}{\Pi})t]\cdot\underset{\sim}{n}(0) \qquad t \geq 0 \tag{7b}$$

Before outlining the specific solution of the problem for the case of the square wave pump perturbation, it is desirable to consider some general properties of the linear relaxation theory. These equations are the starting point for discussing many relaxation processes, in particular chemical relaxation[21] and vibrational relaxation,[22] and, therefore, the general properties of these types of problems have been considered.

The simplest way to evaluate the formal exponential solution to the coupled linear equations is in terms of the "normal modes" of the problem, the eigenvalues and eigenvectors of the rate matrix. If there is a similarity transformation that diagonalizes $\underset{\approx}{\Pi}$,

$$\underset{\approx}{T}^{-1}\cdot\underset{\approx}{\Pi}\cdot\underset{\approx}{T} = \underset{\approx}{\Lambda}$$

where $\underset{\approx}{\Lambda} = \lambda_i\delta_{ij}$, then Eq.(7a) becomes

$$\underset{\sim}{n}(t) = \{\underset{\approx}{T}\, e^{-\lambda_i t}\, \delta_{ij}\, \underset{\approx}{T}^{-1}\}\cdot\underset{\sim}{n}(0). \tag{8}$$

The matrix $\underset{\approx}{\Pi}$ in our problem has been defined to contain the

---

21. G. Schwartz, Rev. Mod. Phys. 40, 206 (1968).

22. E. Montroll and K. Shuler , Adv. Chem. Phys. 1, 361 (1958).

Reproduced with permission of the copyright owner. Further reproduction prohibited without permission.

equilibrium collisional transfer rates. However, for relaxation processes about the thermodynamic equilibrium, the "principle of detailed balance" must hold,[23,24] namely that

$$\Pi_{ij} n_j^{eq} = \Pi_{ji} n_i^{eq} \qquad \text{for all i and j.} \tag{9}$$

This property of the equilibrium state is much "stronger" than the steady state condition,

$$\sum_j A_{ij} n_j^{ss} = 0,$$

and its basis is not found in a classical thermodynamic treatment of equilibrium.

Because the $\underset{\approx}{\Pi}$ matrix must satisfy detailed balancing, the matrix is symmetrizable. If

$$S_{ij} = \Pi_{ij} \sqrt{n_j^{eq}} / \sqrt{n_i^{eq}}, \tag{10}$$

then Eq. (9) guarantees that $S_{ij} = S_{ji}$. Furthermore, it can be shown that any symmetric matrix has only real eigenvalues. Mass conservation guarantees that there is one zero eigenvalue. Herzfeld and Litovitz[25] discuss conditions for which a symmetric matrix will have eigenvalues of one sign. All the principal minors must be positive. The general

---

23. R. H. Fowler, Statistical Mechanics (Cambridge University Press, London, 1929).

24. L. Onsager, Phys. Rev. 37, 405 (1931); 38, 2265 (1932).

25. Herzfeld and Litovitz, Absorption and Dispersion of Ultrasonic Waves, p. 120 (Academic Press, New York, 1959).

Reproduced with permission of the copyright owner. Further reproduction prohibited without permission.

proof is not presented, but clearly any physically meaningful matrix would require that to be the case. Hence, for the half cycle after the pump is turned off, each level n_j will relax toward equilibrium. The decay need not be a monotonically decreasing process and there might be some overshoot. The system will not, however, oscillate about the equilibrium populations.

For the half cycle when the pump is on, the problem is more complicated. The populations start out at or near equilibrium and relax toward a non-equilibrium steady state solution. The principle of detailed balance that must hold for $\underset{\approx}{\Pi}$ will not hold for $\underset{\approx}{\Pi} + \delta\underset{\approx}{\Pi}$ unless $\delta\underset{\approx}{\Pi}$ satisfies detailed balance. In general it will not, and, in fact, the simplest form that might be appropriate for the MMDR problem will have $\delta\Pi_{pq} = \delta\Pi_{qp}$. Because the matrices are built to conserve mass,

$$\sum_j (\underset{\approx}{\Pi} + \delta\underset{\approx}{\Pi})_{ij} = 0,$$

and there will be a steady state solution associated with the zero eigenvalue

$$(\underset{\approx}{\Pi} + \delta\underset{\approx}{\Pi}) \cdot \underset{\sim}{n}^{ss} = 0. \qquad (11)$$

$\underset{\sim}{n}^{ss}$ will not symmetrize the matrix $(\underset{\approx}{\Pi} + \delta\underset{\approx}{\Pi})$. This means that for the half cycle with the pump on, the eigenvalues need not be real, and the transformation matrix need not be unitary. Oscillating solutions are possible, and all these possibilities must be examined as one tries to perform actual calculations using the model. Previous work[20] has assumed that $(\underset{\approx}{\Pi} + \delta\underset{\approx}{\Pi})$ is symmetrizable. This assumption is examined in detail later (Chapter IV) as calculations are presented for a particular rotational

Reproduced with permission of the copyright owner. Further reproduction prohibited without permission.

energy transfer problem.

At this point, however, let us return to the formal analysis of the MMDR experiment. In terms of the MMDR experiment we want Eq. (4) to be valid for the time when the pump is off, from $t = -t_o$ to $t = 0$ and Eq. (6) to hold from $t = 0$ to $t = +t_o$. We must find the appropriate solution for Eq. (4) subject to an initial condition at $t = -t_o$:

$$\underset{\sim}{n}(t) = e^{-\underset{\approx}{\Pi}(t+t_o)}\,\underset{\sim}{n}(-t_o) \qquad -t_o \le t \le 0. \tag{12a}$$

In this case, $\underset{\sim}{n}(0) = e^{-\underset{\approx}{\Pi}t_o}\cdot\underset{\sim}{n}(-t_o)$, and hence,

$$\underset{\sim}{n}(t) = e^{-\underset{\approx}{\Pi}t}\cdot\underset{\sim}{n}(0) \qquad -t_o \le t \le 0. \tag{12}$$

$\underset{\sim}{n}(0)$ must have the same value in Eq. (12) as in Eq. (7b) because the populations must be continuous at $t = 0$. The boundary condition for a periodic solution is that $\underset{\sim}{n}(+t_o) = \underset{\sim}{n}(-t_o) \equiv \underset{\sim}{n}(\pm t_o)$. $\underset{\sim}{n}(0)$ and $\underset{\sim}{n}(\pm t_o)$ are the solutions to homogeneous matrix equations. Utilizing Eq. (12) and Eq. (7b),

$$\underset{\sim}{n}(-t_o) = \exp(\underset{\approx}{\Pi}t_o)\cdot\underset{\sim}{n}(0) = \underset{\sim}{n}(+t_o) = \exp[-(\underset{\approx}{\Pi} + \delta\underset{\approx}{\Pi})t_o]\cdot\underset{\sim}{n}(0),$$

and $\underset{\sim}{n}(0)$ is determined by

$$[\exp(\underset{\approx}{\Pi}t_o) - \exp(-(\underset{\approx}{\Pi} + \delta\underset{\approx}{\Pi})t_o)]\cdot\underset{\sim}{n}(0) = 0. \tag{13}$$

If one substitutes Eq. (12a) into Eq. (7b),

$$\underset{\sim}{n}(+t_o) = \exp[-(\underset{\approx}{\Pi} + \delta\underset{\approx}{\Pi})t_o]\cdot\underset{\sim}{n}(0) = \exp[-(\underset{\approx}{\Pi} + \delta\underset{\approx}{\Pi})t_o]\cdot\exp(-\underset{\approx}{\Pi}t_o)\cdot\underset{\sim}{n}(-t_o)$$

and, therefore,

$$[\underset{\approx}{1} - \exp(-\underset{\approx}{\Pi} + \delta\underset{\approx}{\Pi})t_o\cdot\exp(-\underset{\approx}{\Pi}t_o)]\cdot\underset{\sim}{n}(\pm t_o) = 0 \tag{14}$$

determines $\underset{\sim}{n}(\pm t_o)$.

Reproduced with permission of the copyright owner. Further reproduction prohibited without permission.

As the pump is turned on and off a rotational resonance for a time t_o with the fundamental modulation frequency of $\omega = \frac{\pi}{t_o}$, the full time dependent solutions of $\underset{\sim}{n}(t)$ will have frequency components at the fundamental and its harmonic frequencies, $\omega_n = (n + 1)\frac{\pi}{t_o}$.

If in the experimental arrangement one detects at the fundamental modulation frequency, the absorption signal will be related to the Fourier analysis of the time dependent populations:

$$\underset{\sim}{A}(\omega) = \int_{-t_o}^{+t_o} e^{-i\omega t} \underset{\sim}{n}(t)\, dt. \tag{15}$$

The observed absorption is due to the difference in populations between the two levels. If we define a vector $\underset{\sim}{d}_{fi}$ whose non-zero elements are the ith element which is +1 and f^{th} element which is -1, then

$$A_{fi} = \underset{\sim}{d}_{fi} \cdot \underset{\sim}{A} \tag{16}$$

is the population factor for the net absorption of the if transition. Discussion of the other factors determining the absorption coefficient of a double resonance signal will be presented in Chapter II.

For the fundamental component,

$$A_{fi} = -2i\, \underset{\sim}{d}_{fi} \cdot ([\underset{\approx}{\omega} - i(\underset{\approx}{\Pi} + \delta\underset{\approx}{\Pi})]^{-1} - (\underset{\approx}{\omega} - i\underset{\approx}{\Pi})^{-1}) \cdot \underset{\sim}{\bar{n}}, \tag{17}$$

where $\underset{\approx}{\omega}$ is the fundamental frequency ω times the unit matrix and $\underset{\sim}{\bar{n}}$ is the average population defined by

$$\underset{\sim}{\bar{n}} = \frac{1}{2}[\underset{\sim}{n}(0) + \underset{\sim}{n}(\pm t_o)]. \tag{18}$$

Eq. (17) is obtained from an evaluation of Eq. (15) using Eq.s (7b) and (12) to determine $\underset{\sim}{n}(t)$.

Reproduced with permission of the copyright owner. Further reproduction prohibited without permission.

Experimentally it is difficult to measure absolute absorptions in the microwave region and it is much easier to compare the double resonance amplitude A_{fi} to the Stark-modulation signal amplitude. If we assume that the Stark signal is fully modulated in a perfect square wave form, then the zero field absorption would be proportional to

$$\begin{cases} \underset{\sim}{d}_{fi} \cdot \underset{\sim}{n}^{eq} & -t_o \leq t \leq 0 \qquad \text{field off} \\ 0 & 0 \leq t \leq t_o \qquad \text{field on} \end{cases} \tag{19}$$

The modulation amplitude at the fundamental frequency is then given by

$$S_{fi} = \int_{-t_o}^{0} dt \, [\underset{\sim}{d}_{fi} \cdot \underset{\sim}{n}^{eq}] \exp(-i\omega t) + 0$$

$$= 2i(\underset{\sim}{d}_{fi} \cdot \underset{\sim}{n}^{eq})/\omega. \tag{20}$$

The ratio between the power modulated line and the Stark signal is given by

$$R_{fi} = -A_{fi}/S_{fi} = \omega \, \underset{\sim}{d}_{fi} \cdot \{[\underset{\approx}{\omega} - i(\underset{\approx}{\Pi} + \delta\underset{\approx}{\Pi})]^{-1} - (\underset{\approx}{\omega} - i\underset{\approx}{\Pi})^{-1}\} \cdot \underset{\sim}{\bar{n}} / (\underset{\sim}{d}_{fi} \cdot \underset{\sim}{n}^{eq}). \tag{21}$$

The relative intensity, R_{fi}, is a complex number whose modulus is the ratio of the intensity of the double resonance signal to the intensity of the same line observed by Stark modulation. The argument of R_{fi} is the phase shift between the fundamental of the double resonance signal and the fundamental of the applied modulation. This will be made clearer in Figure 2 where typical curves of the pump perturbation and the n(t) are presented. As the time scale is defined in Figure 2,

Reproduced with permission of the copyright owner. Further reproduction prohibited without permission.

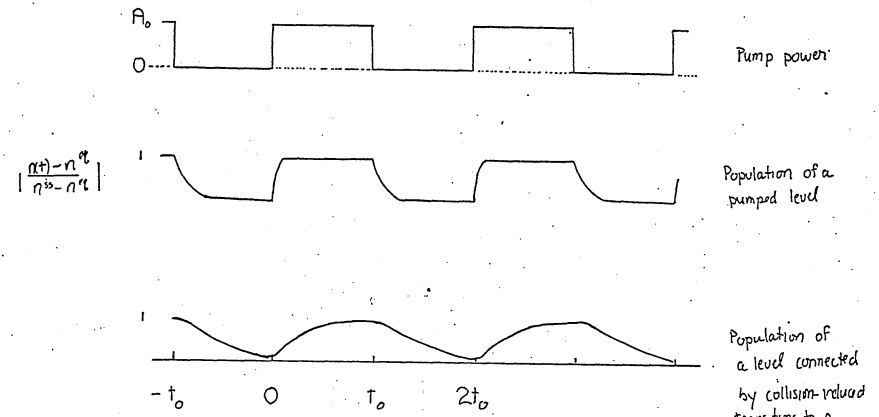

Time Dependence of Pump Field and Rotational Populations

Figure 2

Reproduced with permission of the copyright owner. Further reproduction prohibited without permission.

the pump square will have only sine components

$$f(t) = \frac{A_o}{2} + \frac{2A_o}{\pi} \sum_{j=0}^{\infty} \frac{1}{2j+1} \sin \omega(2j+1)t \quad . \qquad \omega = \frac{\pi}{t_o} \quad .$$

Even if a population $\underset{\sim}{d}_{fi} \cdot \underset{\sim}{n}(t)$ could be described by a single exponential relaxation time, its Fourier component at the fundamental would be of the form

$$A_1 \sin \omega t + B_1 \cos \omega t = \sqrt{A_1^2 + B_1^2} \sin(\omega t + \phi)$$

where $\tan^{-1}\phi = B_1/A_1$.

The magnitudes of A_1 and B_1 will be determined by the magnitude of the exponential risetime. As the risetime becomes shorter, the waveform becomes more like the applied pump square wave and ϕ goes to zero, while for slow risetimes there will be considerable phase shifts.

In fact, the populations must be described as a sum of exponentials, and the matrix expression of Eq. (21) denotes the equivalent information for the more complicated problem. In this model the pressure dependent phase shift is due entirely to the double resonance relaxation process. The Stark signal absorption has been assumed to have a perfect square wave time behavior, and in this case the phase shift of the double resonance signal is being implicitly referenced to the time scale of the pump or to the identical Stark time scale.

The analysis emphasizes that there are two experimentally different pieces of information: the relative intensity of the signal and its phase shift (or time lag) relative to the applied modulation time scale. The relative intensity and phase shift should be pressure dependent.

Reproduced with permission of the copyright owner. Further reproduction prohibited without permission.

At higher pressures there are more molecular collisions per unit time and the pump "information" should be transmitted faster by the collisions to the signal levels. At higher pressures we expect the phase to go to zero or π (relative to the Stark phase), depending on whether the effect of the pump is to cause an increase or decrease in signal absorption. At low pressures the relative intensities should reflect the effects of a small number of collisions while at high pressures we see the effects of many collisions. For some sufficiently high pressure the double resonance signals will reflect the steady state populations. In this case the time during which the pump is on, t_o, is much longer than any of the relaxation times of the system and the populations will be given at $t = 0$ by $\underset{\sim}{n}^{eq}$ while at $t = t_o$ by $\underset{\sim}{n}^{ss}$ of Eq. (11).

This formulation is directly applicable to the MMDR experiment. It should be noted that the SMDR experiment may also be interpreted by this formulation. The time scale in that technique is established by the Stark field. If the pump is set at the zero field resonance, for the time from $t = -t_o$ to $t = 0$ where the Stark field is on, the pump is off, and for the other half cycle the pump is on. In this case instead of determining the magnitude of the double resonance signal directly, one determines the change in magnitude of the Stark signal, ΔI_{St}. This quantity represents the projection of the double resonance signal on the Stark phase direction. If one also monitors the magnitude of the signal 90° out of phase with the Stark component, $\Delta I_{90°}$, one will have the same information as in the MMDR experiment. Figure 3

Reproduced with permission of the copyright owner. Further reproduction prohibited without permission.

Relation Between Four Level Signals

Detected by

SMDR and MMDR

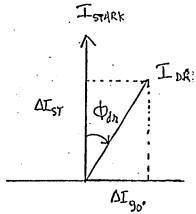

Figure 3

Reproduced with permission of the copyright owner. Further reproduction prohibited without permission.

presents this pictorially. The phase information of the MMDR experiment will be determined by the angle

$$\phi_{DR} = \arctan \frac{\Delta I_{90^\circ}}{\Delta I_{Stark}} .$$

In this case, at the high pressure limit $\Delta I_{90^\circ} \to 0$. Hence,

$$\left. \frac{\Delta I_{Stark}}{I_{Stark}} \right|_p = |R_{fi}(p)|$$

in the high pressure region. Oka in his work generally reports only the signals in the region where the steady state equations hold. Furthermore, he uses pump klystrons of sufficiently high power to assure that the pumped levels are saturated.

The potential equivalence of the two techniques depends on the fact that the Stark field is of sufficient intensity to fully modulate the pump levels. When the Stark field is on, there should be no pumping of the Stark levels. In the MMDR technique, the on-off process is caused by moving the pump frequency off resonance. Frequency shifts of 20-40 MHz can easily be accomplished. It is certainly not as easy to assure comparable modulation of the pump Stark levels, but the information is there in principle. However, in all that follows, only the MMDR technique is used.

Application of the Model

All that must be known to apply this quantitative model to a problem are the elements of $\underset{\approx}{\Pi}$ and $\delta\underset{\approx}{\Pi}$. Π_{ii} has been defined as the rate at

Reproduced with permission of the copyright owner. Further reproduction prohibited without permission.

which molecules leave a state due to collision processes. Hence, in many cases the diagonal elements Π_{ii} will be determinable from the linewidth parameters, particularly if the linewidths are determined by $S_2(b)_o$ of our earlier discussion. The off diagonal elements Π_{ij} might be calculated from an appropriate theoretical analysis of the collision process or they can be considered to be unknowns, and one can try to find values of those parameters that reproduce the double resonance experimental results.

Karplus and Schwinger[6] developed a first order perturbation theory treatment for the saturation of a rotational transition $q \leftrightarrow p$ by a strong microwave field. In that case

$$\delta\Pi_{pq} = \frac{1}{2} \frac{|\langle q|\mu\cdot E|p\rangle|^2/\tau}{\hbar^2[(\omega-\omega_o)^2 + 1/\tau^2]} \tag{22}$$

where ω_o is the molecular resonant frequency, ω the microwave frequency, and τ the collisional parameter defined by Eq. (1).

For $\omega = \omega_o$ Eq. (22) reduces to

$$\delta\Pi_{pq} = \frac{1}{2} \frac{|\langle q|\mu\cdot E|p\rangle|^2}{\hbar^2 2\pi\Delta\nu} = \frac{|\langle q|\mu\cdot E|p\rangle|^2}{\hbar^2 \Delta\omega_{1/2}} \tag{22a}$$

where $\Delta\omega_{1/2}$ is the full width at half height in angular frequency of the absorption in the absence of saturation effects. This is the expression for the steady state radiation-induced transition rate. It does not include any possible time-dependent coherence effects. In keeping with the original classical rate equations and our treatment of the Stark absorption as an ideal square wave absorption, it is appropriate

Reproduced with permission of the copyright owner. Further reproduction prohibited without permission.

to consider the Karplus-Schwinger expression to be a plausible first functional form to use for $\delta\underset{\approx}{\Pi}$. In this case $\delta\Pi_{pq} = \delta\Pi_{qp} = -\delta\Pi_{pp} = -\delta\Pi_{qq}$ and all other elements of $\delta\underset{\approx}{\Pi}$ are zero.

From the functional form of Eq. (22a) we see that $\delta\Pi_{pq}$ is proportional to 1/P. As pressure increases, a given field strength will less effectively saturate a transition. If the microwave field distribution in the cell were known and the matrix elements of the pumped transition were known, then $\delta\Pi_{pq}$ is calculable. In everything that has been said to this point, the state n_i has not been explicitly defined. Each rotational energy level has a 2J + 1 spatial degeneracy. The experimental observations described previously make no attempt to distinguish between these M components. Since all matrix elements over rotational wave functions are functions of the M quantum number, $\delta\Pi_{pq}$ will actually represent an average pumping of level pq unless higher order corrections are made. Furthermore, the elements of $\underset{\approx}{\Pi}$ will represent an average over the different M contributions unless an experiment is specifically designed to lift the spatial degeneracy.

This quantitative theory was first tested by Larson et al.[20] MMDR experiments were performed in pure HCN where double resonance signals were monitored $\Delta J = 1$, 2, and 3 units from a pumped level. A computer program was developed to calculate R_{fi} for known values of $\underset{\approx}{\Pi}$ and $\delta\underset{\approx}{\Pi}$. Because of the system studied, it was possible to make certain restrictive assumptions about $\underset{\approx}{\Pi}$. In fact the double resonance data could be reproduced by constructing $\underset{\approx}{\Pi}$ in terms of 5 rate constants. A parameter was determined for $\delta\underset{\approx}{\Pi}$ and another parameter was necessary to scale the

Reproduced with permission of the copyright owner. Further reproduction prohibited without permission.

phase data. The results were gratifying. To the level of accuracy of the work, the quantitative theory seemed to be very adequate, and they were able to determine the partial cross sections for the collision-induced transitions.

The MMDR technique used in conjunction with an appropriate kinetic model allows one to determine a set of rate constants that reproduce the data. As in the interpretation of all relaxation experiments, some care must be taken before one feels confident that the rates actually have physical meaning. How many rate matrices might reproduce the data?

In many relaxation techniques, real time experiments are performed. $\underset{\sim}{n}(t)$ is monitored directly after the application of a step function perturbation and from $\underset{\sim}{n}(t)$ one attempts to extract the relaxation times of the system. Furthermore, if $\underset{\sim}{n}(t)$ is very well known, one can hope to find the eigenvectors also. Then one can relate these quantities to appropriate rate matrices. Schwartz[21] discusses the difficulties in extracting useful information for processes where the relaxation times are not distinct. By using a modulated perturbation one can improve signal/noise by averaging the real time experiment or by using harmonic detection with the attendant advantage of reduced bandwidths.

In the MMDR technique, a periodic perturbation is used and harmonic detection is used. In fact, all work done to date has utilized the information contained at the fundamental frequency of the perturbation. Unfortunately, because of the nature of rotational energy transfer processes, many states must be considered, and, hence, large matrices and many relaxation times. When in the MMDR technique one

Reproduced with permission of the copyright owner. Further reproduction prohibited without permission.

varies the pressure, the information obtained should be equivalent to performing the real time experiment at one pressure or by extracting information from all harmonics at one pressure. Also, the relative intensity and phase information are not actually independent (Kramers-Kronig relations). Once the $\underset{\approx}{\Pi}$ matrix is specified, both quantities are specified for all pressure and time. Alternatively, if the relative intensity or phase information were very well known for all R_{fi}, the $\underset{\approx}{\Pi}$ matrix would be specified. In practice one only has information about a limited number of double resonance signals, and that information is known with only finite precision. Because the relative intensity and phase data represent different combinations of eigenvalues and eigenvectors, they will effectively be independent pieces of information as one tries to find rate matrices that fit the data.

Onward, Future Chapters

The work in this thesis consists of various extensions of four level MMDR. In Chapter II we describe a series of experiments that test the sensitivity of the technique. We will see that it is possible to detect preferred collision processes in asymmetric rotors where there are low-lying vibrational states. In Chapter III are described a series of experiments that examine the M dependence of rotational energy transfer. Two methods are used: the use of a static dc field that lifts the spatial degeneracy, and the study of energy transfer in the presence of a nuclear spin. In the former case direct observation

Reproduced with permission of the copyright owner. Further reproduction prohibited without permission.

of |JM> levels is possible and in the latter case a study of the ΔF collision-induced selection rules gives comparable information. Those two sections are essentially qualitative in nature; no attempt is made to determine the rate constants of a $\underset{\approx}{\Pi}$ matrix that would reproduce the data.

In Chapter IV we present various studies related to the use of MMDR for quantitative purposes. The basic work is the determination of rate constants for collision-induced transitions in HCN-rare gas mixtures. It is found that it is not possible to determine a unique set of rate constants for each collision partner because of uncertainty in the experimental data, but on the basis of general theoretical arguments a preferred set is determined. Furthermore, it is shown that as one tries to improve the experimental accuracy, one finds evidence that there are quantum coherence effects being observed in both the Stark and double resonance signals, and in regions where these phenomena are important, the classical $\underset{\approx}{\Pi}$ matrix formulation will no longer be valid.

Reproduced with permission of the copyright owner. Further reproduction prohibited without permission.

CHAPTER II

ROTATIONAL ENERGY TRANSFER IN PURE POLAR GASES

I INTRODUCTION

Rotational relaxation processes in dilute polar gases are dominated by long range dipolar interactions that lead to collision-induced rotational transitions. Because the population of a single rotational energy state can relax only through a limited number of other states, one can monitor the preferential population transfer pathways by the use of four level microwave double resonance techniques. Previous work has shown that for some pure polar gases, collision-induced transitions will lead to detectable double resonance signals in accordance with the dominant relaxation pathways expected for dipole-dipole interactions. Using the MMDR technique, Ronn[1,2] was able to observe rotational relaxation signals for four level systems in three of seven asymmetric rotors studied. For only one case was a magnitude of the signal reported, namely a $\Delta J = +1$ relaxation signal with a relative intensity $I_{dr}/I_{st} \approx 11\%$ in 1,1-difluoroethylene. Oka[3,4] has examined rotational relaxation pathways for two classes of asymmetric rotors: slightly asymmetric

---

1. A. M. Ronn, Ph. D. Thesis, Harvard U., Cambridge, Mass. 1967.
2. A. M. Ronn and E. B. Wilson, J. Chem. Phys. 46, 3263 (1967).
3. T. Oka, J. Chem. Phys. 47, 13 (1967).
4. R. M. Lees and T. Oka, J. Chem. Phys. 51, 3027 (1969).

Reproduced with permission of the copyright owner. Further reproduction prohibited without permission.

rotors whose energy levels consist of a series of doublets with the two levels of a doublet separated by microwave frequencies while the different doublets are separated by far infrared frequencies and molecules whose energy levels are complicated by internal rotation (CH_3OH and CH_3NH_2). In the latter case, no signals were detected for CH_3NH_2 ($\Delta I_{st}/I_{st} < 1\%$) and weak signals were detected in CH_3OH ($\Delta I_{st}/I_{st} \lesssim 3\%$) for $\Delta J = +1$ collision-induced transitions. In the former case signals were considerably stronger, the largest being $\Delta I_{st}/I_{st} \approx 30\%$ for $\Delta J = -1$ in HCN, with weaker signals detected for $\Delta J = -2$, -3, and -4.

In this chapter we present a series of MMDR experiments on several asymmetric rotors that extend our understanding of relaxation processes for polar gases that are small asymmetric rotors. The results and accompanying discussion provide evidence that it should be possible to predict (to within an order of magnitude) the relative intensities of rotational relaxation signals for many small molecules. Experiments are reported on three molecules that are four-membered rings, trimethylene oxide, ß-propiolactone, and cyclobutanone. Also, energy transfer experiments in cis-difluoroethylene are reported. For the ring compounds relaxation processes have been studied in the vibrational ground state and in the lowest level of the ring puckering mode. In the fluoroethylene four-level systems in the vibrational ground state and in the lowest vibrationally excited state, the symmetric $^{F}\!\diagdown\!C\text{-}C\!\diagup^{F}$ bend is reported.

These molecules were chosen for study for several reasons. They are all reasonably rigid rotors with large dipole moments. ß-propiolactone possesses large dipole moment components along two principal

Reproduced with permission of the copyright owner. Further reproduction prohibited without permission.

axes, but the other molecules possess only one component. It is possible to study relaxation processes where each pumped level is expected to relax through as many as six other levels. Because of the nature of the asymmetric rotor energy levels, the energy gaps for the important collision-induced transitions will all be much less than kT. In that case, the J state of the collision partner will be less important than for a molecule such as HCN where the ΔJ spacings are far-infrared. Lastly, the four-level systems studied include cases where a rotational transition in the vibrationally excited state was pumped while ground state rotational transitions were monitored. Those systems were chosen in an attempt (unsuccessful) to detect evidence of vibrational relaxation.

The search for four-level signals can be made without any reference to Stark spectroscopy if one is using the MMDR technique. However, for reference purposes it is useful to calibrate the sensitivity of the MMDR experiment in terms of the corresponding Stark signal where that is possible. In that manner, when no double resonance signal is detected it is possible to report the negative result as an upper limit on the magnitude of the double resonance effect ($|I_{dr}/I_{st}| < A\%$). This is useful because one can then determine an operational sensitivity for a given spectrometer on different days or for different spectrometers.

A. Absorption Coefficient of Double Resonance Signal

Also, the intensity of the double resonance signal relative to the Stark signal is physically an important quantity. The factors

Reproduced with permission of the copyright owner. Further reproduction prohibited without permission.

determining the strength of the double resonance signal absorption are the same as for the Stark signal except for the population difference. In Chapter I we have outlined how the population differences in the double resonance experiment are generated, but no mention has been made of the other factors involved in the absorption coefficient. The absorption coefficient for a transition $i \rightarrow j$ is given by[5]

$$\gamma_{max} = \frac{8\pi^2}{3ch} |\mu_{ij}|^2 \frac{\nu^2}{\nu_s} \frac{\Delta\nu}{(\nu-\nu_s)^2 + (\Delta\nu)^2} \Delta n_{ij} \qquad \text{(II-1)}$$

where $|\mu_{ij}|^2$ = square of the dipole moment matrix element for the transition, summed over the three perpendicular transitions in space,

ν = frequency

ν_s = resonant frequency of the absorption

$\Delta\nu$ = halfwidth at half height

Δn_{ij} = difference in population between upper and lower levels, $n_i - n_j$.

For Stark absorption $\Delta n_{ij} = n_i(1 - e^{-h\nu_s/kT}) \approx n_i[\frac{h\nu_s}{kT}]$, and at $\nu = \nu_s$,

$$\gamma_{max} \alpha |\mu_{ij}|^2 \nu_s^2 n_i \,. \qquad \text{(II-2a)}$$

For the MMDR signal, the difference in population Δn_{ij} must be calculated as indicated in Chapter I. To make an estimate of Δn_{ij}, however,

---

5. C. H. Townes and A. Schawlow, Microwave Spectroscopy (McGraw Hill, New York, 1955) p. 341

Reproduced with permission of the copyright owner. Further reproduction prohibited without permission.

one may assume that all the population perturbation of the pumped levels has been transmitted to the signal levels. In this case, $\Delta n_{ij} \approx n_{pump} \frac{h\nu_p}{kT}$. For a double resonance signal

$$\gamma_{max} \propto |\mu_{ij}|^2 \nu_s^2 \frac{\nu_p}{\nu_s} n_{pump} . \qquad \text{(II-2b)}$$

However, for energy level spacings in the asymmetric rotors of interest, the populations of pump and signal levels are essentially the same for transitions within a single vibrational state.

This rather crude estimate serves to point out several facts that are pertinent. If a Stark signal is weak because $|\mu_{ij}|^2$ is small, a double resonance signal must also be weak. The double resonance signals will be relatively stronger for those experiments where ν_p is as large as possible. The ν_p/ν_s ratio suggests that relative intensities of double resonance signals will be somewhat larger for experiments where $\nu_p/\nu_s \approx 2$ (pump in K band, observe K_u band) than for an otherwise analogous experiment where $\nu_p/\nu_s \approx \frac{1}{2}$ (pump in K band, observe in R band).

The emphasis on relative intensities of four level signals has been made because all the work in this and subsequent chapters consists of MMDR experiments performed in cells capable of Stark detection as well. However, for higher sensitivity the double resonance cell may be made longer than a Stark cell can be conveniently made. Before presenting the experimental work, it is proper to present a primitive picture of the collision interaction that is useful in determining the types of relaxation processes that are important.

Reproduced with permission of the copyright owner. Further reproduction prohibited without permission.

B. Perturbation Theory Description of the Collision Process

To a first approximation the "selection rules" for collision-induced transitions and the ordering of dominant relaxation pathways can be predicted on the basis of first order time-dependent perturbation theory. In that case, the probability of collision-induced transition $i \to f$ is given by[6]

$$P_{i\to f} = \frac{1}{\hbar^2} \left| \int_{-\infty}^{\infty} V_{if}(\vec{r}(t)) \exp(i\omega_{if}t)\, dt \right|^2 \qquad \text{(II-3)}$$

where $V_{if}(\vec{r}(t))$ is the interaction potential matrix element. The integral over time results from the integration over the full collision trajectory. $|i\rangle$ and $|f\rangle$ are the two molecule states $|n_1^i\rangle|n_2^i\rangle$ and $|n_1^f\rangle|n_2^f\rangle$. $|n_i\rangle$ indicates a rotational wave function $|J_{K_{-1}K_1}M\rangle$. The frequency $\omega_{if} = (E_f - E_i)/\hbar$ depends on the energy mismatch between the final and initial state, the energy that must be converted to an internal mode from translational energy during the collision. If $E_{n_1}{}_i - E_{n_1}{}_f = -(E_{n_2}{}_i - E_{n_2}{}_f)$, $\omega_{if} = 0$.

The quantity of interest in the double resonance experiment is the probability that a molecule initially in one of the rotational levels being pumped will be transferred to another particular energy level because of interactions with all possible collision partners. For the dipole-dipole interaction, the long range attractive potential will be of the form

---

6. This is discussed in any suitable quantum mechanics text such as A. Messiah, Quantum Mechanics (John Wiley & Sons, 1962) p. 724 ff.

Reproduced with permission of the copyright owner. Further reproduction prohibited without permission.

$$V = \frac{\vec{\mu}_1 \cdot \vec{\mu}_2 - 3(\vec{\mu}_1 \cdot \hat{r}(t))(\vec{\mu}_2 \cdot \hat{r}(t))}{\vec{r}(t)^3} \qquad \text{(II-4)}$$

where $\vec{r}$ is the vector between the centers of mass of the two dipoles $\vec{\mu}_1$ and $\vec{\mu}_2$ ($\hat{r}$, the corresponding normal vector). The perturbation formulation has been developed by many authors, most recently by Rabitz and Gordon.[7] The transition probability of Eq. (II-3) is part of the collision interruption function expression $S_2(b_o)$, Eq. (I-3). Evaluation of the collision couple transition probability for a straight line collision trajectory with a distance of closest approach b leads to the result

$$P_{i \to f} \propto \frac{\mu_1^2 \mu_2^2}{v^2 b^4} \left[\frac{{}^{x}S_{J_1 J_1'}(\kappa)}{2J_1+1} \right] \left[\frac{{}^{x'}S_{J_2 J_2'}(\kappa)}{2J_2+1} \right] R(X) \qquad \text{(II-5)}$$

where μ_1, μ_2 are the dipole moments for molecules 1 and 2

v = the average collision velocity

b = impact parameter for a collision

${}^{x}S_{JJ'}(\kappa)$ = line strength[7a] of a rotational transition for a molecule with a moment along body axis x

$X = |\omega_{if} \frac{b}{v}|$, parameter measuring the resonant character of the collision

---

7. H. Rabitz and R. G. Gordon, J. Chem. Phys. 53, 1815 and 1831 (1970).

7a. The rotational linestrength is defined in reference 5, p. 557. Values of rotational linestrengths for various asymmetry parameters (κ) have been tabulated in Walker and Pratto, Microwave Spectral Tables Vol. II (N.B.S. Mimeograph 70, Washington D.C., 1964).

Reproduced with permission of the copyright owner. Further reproduction prohibited without permission.

R(X) = resonance function that has been calculated for dipolar interactions.

It is not obvious from the form of the potential (Eq. (II-4)) that is to be substituted into the basic perturbation expression (Eq. (II-3)) that the transition probability will be proportional to the rotational line strengths, expressions that are familiar to microwave spectroscopists. The formal derivation has not been made for the asymmetric rotor, but consideration of the derivation for the symmetric rotor shows that this is the analogous result.[8] The linestrengths enter into the first order transition probability because the intermolecular potential is dipolar and the transition probability must be independent of M_i because the plane in which the collision occurs must be randomly oriented with respect to the space fixed axis determined by the polarized microwave radiation. Also the probability must include transitions to all possible final M' states since all those levels are degenerate. In the evaluation of P_{if} of Eq. (II-3) there are, then, sums and averages

$$\left(\frac{1}{2J_1+1} \frac{1}{2J_2+1} \sum_{M_1,M_2} \sum_{M_1',M_2'} \right)$$

which when performed lead to simplifications of matrix elements that

---

8. This problem has been considered in calculations of linewidths of asymmetric rotors; see, for example:
Krishnaji and S. Chandra, J. Chem. Phys. 38, 2690 (1963) or
W. S. Benedict and L. Kaplan, J. Chem. Phys. 30, 388 (1959).

Reproduced with permission of the copyright owner. Further reproduction prohibited without permission.

lead to the final result in terms of line strengths.

The resonance function in Eq. (II-5) increases from 1 to 1.2 as X varies from 0 to 1, and then it decreases monotonically reaching a value of 0.7 at X = 2, and less than 0.1 for X = 4.

The transition probability of Eq. (II-5) must be averaged over all collision partners and over all impact parameters before a cross section for a particular collision-induced transition is obtained. However, the number of relaxation pathways through which a given level $|n_1^i>$ can relax will be determined by the number of levels to which $|n_1^i>$ is connected by significant line strengths. A molecule with dipole moment components along more than one principal axis may have a greater number of relaxation pathways than a molecule with a single dipole component. In the first order transition probability a given pair of asymmetric rotor levels ($|n_1^i>$ and $|n_1^f>$) will be connected by only a single dipole moment component. Of course, it is known that the first order theory is not adequate. Preferred population transfer can be detected in pure polar gases for $\Delta J = 4$[3] and it has been shown that these signals can not be attributed to multiple $\Delta J = 1$ transitions.[9] Rabitz and Gordon[7] have extended the impact theory to second order.

The basic analysis of the dominant collision interaction suggests the possibility that another relaxation might be detectable, the

---

9. R. G. Gordon, P. E. Larson, C. H. Thomas, and E. B. Wilson, J. Chem. Phys. 50, 1388 (1969).

Reproduced with permission of the copyright owner. Further reproduction prohibited without permission.

resonant transfer of vibrational energy. If one considers an expansion of the dipole moment in terms of the normal modes,

$$\mu = \mu_o + \sum_{\substack{i \\ \text{modes}}} \frac{\partial \mu}{\partial Q_i} Q_i \ .$$

Just as the permanent moment of an asymmetric rotor can have components along any or all of the axes, the transition moment will also have components along particular axes depending on the molecular symmetry of the normal mode of interest. Traditionally[10] vibrational relaxation has been considered in terms of vibration-translation energy transfer. Because in that case large (infrared) amounts of energy must be exchanged between the internal and the translational modes, the important collisional interaction is the relatively infrequent but strong short range collision that can be represented by an exponential repulsive potential.

However, if there is resonant vibrational energy transfer, (Fig. 1)

Figure 1

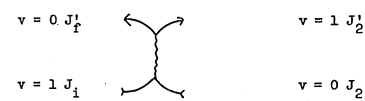

10. See, for example, Herzfeld and Litovitz, Absorption and Dispersion of Ultrasonic Waves (Academic Press, New York, 1959).

Reproduced with permission of the copyright owner. Further reproduction prohibited without permission.

the problem is essentially the same as the pure rotational energy transfer problem. The net energy mismatch will be on the order of the rotational energy spacings and will generally be much less than kT. For this case the "selection rules" will be determined by the rotational line strengths and the vibrational matrix element $\langle v|Q|v'\rangle$. The analog of the permanent dipole is now the transition moment. For any molecule for which a pure rotational transition can be observed or pumped, there must be a permanent as well as a transition moment. In this circumstance, the vibrational relaxation process will be at best one of several relaxation pathways.

C. Summary of Results

The experiments to be presented here lead to the following conclusions.

(1) The dominant rotational relaxation pathway can be well predicted by the line strengths of possible collision-induced transitions. The first order treatment predicts $\Delta J = 0, \pm 1$ collision-induced transitions, but the signals detected with $\Delta J > 1$ can be correlated with multiple collisions of a dipole-allowed nature without specifying whether the signals are due to cascades of $\Delta J = 1$ transitions or direct $\Delta J > 1$ transitions caused by interactions other than first order dipole.

(2) Rotational relaxation can be observed for molecules with dipole moment components along more than one principal axis, and four-level signals can be observed within low-lying excited vibrational states. In the latter case the relative intensities (I_{dr}/I_{st}) are the same magnitude as the ground state signals within experimental uncertainty.

Reproduced with permission of the copyright owner. Further reproduction prohibited without permission.

(3) No evidence has been found for relaxation via a resonant vibrational energy transfer process. This means that in the presence of large permanent moments, the cross section for pure rotational relaxation is much larger than the vibrational relaxation process.

D. Molecular Energy Levels

The rotational spectra of the ring compounds in their ground and low-lying vibrational states have been characterized previously. Trimethylene oxide[11] (TMO) is a near oblate rotor (κ = +0.88) with a ground state dipole moment μ_a = 1.93 D. The first excited state of the ring puckering mode is about 60 cm^{-1} above the vibrational ground state which itself lies about 8 cm^{-1} above a small barrier. Cyclobutanone[12] is a moderately asymmetric prolate rotor (κ = -0.65) whose ground state dipole is μ_a = 2.9 D. As with TMO, the ground state lies slightly above a low ($\approx$ 8 cm^{-1}) bump in the quartic oscillator potential function and the first puckering state lies about 36 cm^{-1} above the ground state. β-propiolactone[13] (κ = -0.68) has ground state dipole components along two axes (μ_a = 3.7 D, μ_b = 2.0 D), and the puckering mode states appear to be fit by a harmonic potential function with the

---

11. S. I. Chan, J. Zinn, J. Fernandez, and W. D. Gwinn, J. Chem. Phys. 33, 1643 (1960).

12. L. H. Scharpen and V. W. Laurie, J. Chem. Phys. 49, 241 (1968).

13. D. W. Boone, C. O. Britt, and J. E. Boggs, J. Chem. Phys. 43, 1190 (1965).

Reproduced with permission of the copyright owner. Further reproduction prohibited without permission.

first state about 160 cm^{-1} above the ground state. For all three compounds the transition dipole for the ring puckering mode is c-type.

For two compounds, β-propiolactone and TMO, it was necessary to determine the frequencies of most of the signal transitions that were to be used in the four-level experiments. By using the published rotational constants in a program[14] to compute rotational energy levels and transition frequencies, it was possible to assign transitions that had not been reported previously. For $J \leq 10$ the centrifugal distortion corrections were generally small. In one instance the assignment of a transition to be pumped was ambiguous. For TMO the $v = 1$ $6_{33}-6_{52}$ transition had been reported[11] at 25928 MHz. Examination of the Stark spectrum showed two lines of similar intensity, and a better assignment is

		calc	obs
$6_{33}-6_{52}$	v = 1	25925.5	25926.1
$5_{23}-5_{42}$	GS	25927.7	25928.2

Cis-difluoroethylene is a near prolate rotor ($\kappa = -0.84$) with a ground state dipole $\mu_b = 2.4$ D. Low J lines have been assigned[15] for the ground state and $\nu_5 = 1$ symmetric CF bend that lies about 255 cm^{-1} above the ground state. Ground state high J transitions were

---

14. The asymmetric rotor energies and transition frequencies were calculated with the computer program TOP supplied by Dr. C. H. Thomas.

15. V. W. Laurie, J. Chem. Phys. 34, 291 (1961).

Reproduced with permission of the copyright owner. Further reproduction prohibited without permission.

assigned[16] in an application of a second order centrifugal distortion theory. As a preliminary analysis for the four-level double resonance experiments, an analogous assignment was made of the $\nu_5 = 1$ rotational transitions. By use of a computer program[17] that adjusts P^4 and P^6 centrifugal distortion constants to reproduce the observed spectrum, it has been possible to assign 40 transitions up to $J = 40$. The assignments are presented in a brief appendix. The transition dipole for the $\nu_5 = 1$ mode is in the direction of the molecular b axis.

A few numbers will be useful to get a rough picture of the energy level spacings. For the four molecules the maximum of the Boltzmann distribution occurs in the region $45 \leq J_{max} \leq 55$. (This is found by assuming that the molecules are approximately spherical tops, and the average energy of a J level will be given by $\frac{1}{3}(A+B+C)\cdot J\cdot(J+1)$ while each J level is $(2J+1)^2$ degenerate. In this case, $J_{max} \approx \sqrt{3kT/(A+B+C)}$.) For TMO, all $J = 12$ levels are less than $\frac{1}{3}$ kT above the 0_{00} level. In all the double resonance experiments performed, the four level systems were lower than $J = 15$ and usually less than $J = 10$. In this situation the main cause of the energy mismatch will be $\Delta E_{J_2 J_2'}$. For the molecules of interest, if $J \approx 50$, then for $\Delta J = +1$, the energy gap is about 10 cm^{-1} while it is at most 2 cm^{-1} for $J \approx 10$. However,

---

16. C. H. Thomas, Ph. D. Thesis, University of Notre Dame, Notre Dame, Indiana (1965).

17. The program, DISTO, was provided by Dr. C. H. Thomas.

Reproduced with permission of the copyright owner. Further reproduction prohibited without permission.

for high J collision partners, there will also be $\Delta J = 0$ transitions at considerably lower energies than the $\Delta J = 1$ transitions. Still, it must be remembered that $kT \approx 210\ cm^{-1}$ at room temperature, and for these molecules the resonance function factor may be near unity for many important collision partners.

II EXPERIMENTAL

A. Apparatus

The four level systems studied for the three ring compounds were chosen so that all the pump transitions were in K band while all the signal transitions were at higher frequencies (28-40 GHz). An Oki 24V11 was used as the pump klystron, the basic principles of the double resonance modulation spectrometer have been presented previously,[18] and the apparatus used for these experiments is similar. The modulation frequency used in this work was 80 kHz, and the sample cell was a fifteen foot copper X Band Stark cell. The arrangement of microwave hardware for the K-R double resonance spectrometer is presented in detail in Chapter IV (Block diagram is Figure 2 of Chapter IV).

When the pump is below the signal frequency, the signal detector, source, and hardware can be isolated from the modulated pump power by waveguide cutoff filters. When the pump frequency is higher than the

---

18. R. C. Woods, A. M. Ronn, and E. B. Wilson, Rev. Sci. Inst. 37, 927 (1966).

Reproduced with permission of the copyright owner. Further reproduction prohibited without permission.

signal frequency, the separation of the pump and signal radiation fields is more difficult. In this case band pass filters must be used. The four levels systems studied in cis-difluoroethylene were all characterized by a pump transition between 20-26 GHz and a signal transition in K_u-band (12-18 GHz). Once again 80 kHz modulation was used and the sample cell was a 15 foot copper X-band Stark cell. The arrangement of microwave hardware was known to be far from ideal, but it was the best obtainable with the available equipment. In particular, only one band-pass filter was available that blocked K-band radiation. This was placed before the signal detector, but there was still evidence of pump radiation reaching the signal detector.

Furthermore, it was not possible to prevent pump radiation from entering the signal arm. Pump radiation could be monitored on the signal arm frequency mixer. That is a disastrous situation because with the K and K_u radiation fields, the difference between the two frequencies is also K_u band radiation that will then reach the detector. It was necessary to use attenuators to isolate the signal arm, and then to apply a dc bias to the signal detector to maintain the crystal at a reasonable operating point. Further practices that were sometimes necessary to minimize spurious signals were to remove all crystals except the detector crystal and also to use a point reflector in front of the detector crystal to try to set up standing waves at the pump frequency that would effectively prevent the pump radiation from reaching the detector crystal. Obviously matters could have been improved if more band pass filters were available, and this has since been done.

Reproduced with permission of the copyright owner. Further reproduction prohibited without permission.

B. Procedure

The three ring compounds were obtained from commercial sources while the cis-difluoroethylene was provided by Prof. L. Pierce of Notre Dame. Once placed in sample tubes, they were degassed by the freeze-pump-thaw method and they were used without further purification. All double resonance experiments were performed at sample pressures of about 10-20 μ of Hg, pressures at which the steady state condition (Eq. I-11) generally holds at the end of the pump cycle.

For a given four level experiment, one of the pump frequencies would be adjusted to within 1 MHz of the desired resonance and the signal klystron would be frequency swept through a 10 MHz region including the signal resonance. The other frequency of the pump klystron would be more than 20 MHz off resonance. Either before the sample is introduced or with the sample frozen out in a cold finger, the spectrometer is adapted to minimize spurious signals. Then with the sample present the phase of the phase sensitive detector is adjusted to maximize the double resonance signal if it is present. The output of the phase sensitive detector was monitored on an oscilloscope.

If there is no detectable signal at first, one must vary the amplifier phase shifter over an adequate interval to ascertain that the signal is not detectable at any phase. Generally, it is adequate to search at the phase setting for which the Stark signal would be maximized and then 90° out of phase with that.

Even when the four level signals are only of the same size as spurious signals, it is easy to distinguish between the two. Since the

Reproduced with permission of the copyright owner. Further reproduction prohibited without permission.

exact frequencies of the rotational resonances are known, one can check whether the signal being observed is maximized with one of the pump frequencies on resonance and whether it occurs exactly at the signal resonance. Furthermore, a four level double resonance signal that is Lorentzian in shape will be shifted in phase by 180° as one places alternately the upper and lower frequency pump field on resonance. Lastly, if there is still some confusion, one can always remove the sample from the cell.

Either after of before performing the double resonance experiment one can measure the size of the corresponding Stark absorption under the same experimental conditions--the same signal radiation level and the same sample pressure. Unfortunately, it is not always possible to determine the magnitudes of the Stark signals. For some of the signal transitions studied the Stark effect was so small that even at the maximum voltages attainable (1600 V) the signals were only partially modulated. In other instances the lines were obscured by lobes from nearby lines that were more intense. An effort has been made to estimate the size of the Stark signals in order to allow a presentation of results in terms of the relative intensity of the double resonance signal, $\frac{I_{dr}}{I_{st}}$ ($|R_{fi}|$ of Eq. (I-21)). Some of the values of $\frac{I_{dr}}{I_{st}}$ may have uncertainty as large as 50%, but the information that is of interest primarily is whether the relative intensity is 10%, 1% or .1% or when a four level signal was not detected, what the upper limit can be said to be.

Reproduced with permission of the copyright owner. Further reproduction prohibited without permission.

C. Results

1. Trimethylene oxide

The observed values of I_{dr}/I_{st} for the systems studied are presented in Table 1. In that table v = 0 or 1 refers to the vibrational ground state or the first excited state of the ring puckering mode. Eighteen pairs of ground state transitions were examined. Of these, four were pairs related by $\Delta J = 0, \pm 1$ but without a-type connections. In those cases no signals were detected (placing an upper limit of $I_{dr}/I_{st} < 0.1\%$). Six pairs were related by $\Delta J = 0, \pm 1$ with a μ_a connection between each pump level and a signal level. Signals were detected in each instance except for the one that was expected to be weakest in terms of the line strength factors. Signals were detected for two $\Delta J = +2$ systems but not for two $\Delta J = -2$ systems. A "$\Delta J = +3$" signal was detected that would be expected from a dipole cascade process. No signal was detected at the analogous $\Delta J = +4$ transition, but the sensitivity of the apparatus was such that the $\Delta J = +4$ signal would not have been detectable had the relative intensities continued to drop:

$\Delta J =$	+1	+2	+3	+4
$\frac{I_{dr}}{I_{st}}$	$\approx 5\%$	$\approx +0.8\%$	-0.2%	$<0.05\%$

A $\Delta J = +1$ rotational relaxation was observed in the first excited state that was of the same relative intensity as the corresponding ground state experiment. No signals were detected in four cases where a rotational transition was pumped in the excited state and a ground state transition was monitored that was connected to the pumped levels by a

Reproduced with permission of the copyright owner. Further reproduction prohibited without permission.

TABLE 1

Observed values of $\frac{I_{dr}}{I_{st}}$ in pure trimethylene oxide

Pump J''+J	v	Signal J'''-J''	v	ν_p(MHz)	ν_s(MHz)	$\frac{I_{dr}}{I_{st}}$ *	"Selection rules" [a]
7_{52}-7_{53}	0	8_{53}-8_{54}	0	24592	35825	-5±2%	ΔJ=+1 double dipole 4.3, 0, 0, 3.7
		8_{63}-8_{44}	0		36011	N(<.05%)	ΔJ=+1 μ_a forbidden
		6_{43}-6_{24}	0		36055.7	N(<.1%)	ΔJ=+1 μ_a forbidden
		6_{33}-6_{34}	0		36022.6	-0.6±3%	ΔJ=-1 weak double dipole 0.4, 0, 0, 0.7
		9_{73}-9_{54}	0		35994	+0.8±2%	ΔJ=+2 dipole cascade
		10_{73}-10_{74}	0		35330	≈ -0.2%	ΔJ=+3 dipole cascade
		10_{83}-10_{64}	0		36008.6	N(<.05%)	ΔJ=+3 forbidden
		11_{93}-11_{74}	0		36062.1	N(<.05%)	ΔJ=+4 cascade
		5_{23}-5_{24}	0		36063.5	N(<.1%)	ΔJ=-2 μ_a forbidden
		5_{33}-5_{14}	0		36074.8	N(<1%)	ΔJ=-2 weak μ_a cascade
7_{52}-7_{53}	v=1	8_{53}-8_{54}	v=1	24240	35501.5	-5±3%	ΔJ=+1 double dipole
		9_{73}-9_{54}	1		35720	N(<1%)	ΔJ=+2
		7_{44}-7_{43}	0		35948.3	N(<.1%)	vibrational relax. μ_c allowed

a For $|\Delta J|$=0,1 rotational linestrengths are presented $S_{JJ'''}$, $S_{JJ'''}$, $S_{J'J''}$, $S_{J'J'''}$.

* N indicates no detectable signal; quantity in parenthesis is upper limit to I_{dr}/I_{st}. I_{dr}/I_{st} is negative as signal absorption decreases in presence of pump field.

Reproduced with permission of the copyright owner. Further reproduction prohibited without permission.

TABLE 1, continued

Pump $J'+J$	v	Signal $J'''-J''$	v	ν_p	ν_s	$\frac{I_{dr}}{I_{st}}$	"Selection rules"
$6_{52}-6_{33}$	v=0	$7_{53}-7_{34}$	0	26081	36032.7	P signal observed	$\Delta J=+1$ double dipole
		$5_{33}-5_{14}$			36074	N(<.1%)	$\Delta J=-1$ weak dipole 0.2, 0, 0, 0.5
$5_{42}-5_{23}$	0	$7_{43}-7_{44}$	0	25928	35948	-.8±.3%	$\Delta J=+2$ cascade
$7_{62}-7_{43}$	0	$8_{63}-8_{44}$	0	26331	36010.5	-4±1%	$\Delta J=+1$ double dipole 4.3, 0, 0, 3.7
		$7_{53}-7_{34}$	0		36033	N(<.1%)	$\Delta J=0$ μ_a forbidden
		$6_{33}-6_{34}$	0		36023	N(<.1%)	$\Delta J=-1$ μ_a forbidden
		$6_{43}-6_{24}$	0		36055.7	~-1%	$\Delta J=-1$ μ_a allowed 0.7, 0, 0, 0.4
		$5_{23}-5_{24}$	0		36033	N(<.1%)	$\Delta J=-2$ cascade
$6_{52}-6_{33}$	v=1	$7_{43}-7_{44}$	0		35947	N(<.1%)	vibrational relax μ_c allowed
$8_{62}-8_{63}$	v=1	$8_{53}-8_{54}$	0	23460	35825	N(<.05%)	"
		$9_{73}-9_{54}$	0		35998	N(<.1%)	"

Reproduced with permission of the copyright owner. Further reproduction prohibited without permission.

c-type transition moment. Signals would have been detected that were 0.1% of the Stark signal.

2. β-propiolactone and cyclobutanone

The results of experiments on these molecules are presented in Tables 2 and 3. Despite the fact that β-propiolactone possesses a and b dipole components, rotational relaxation was observed in the ground state. Signals were detected for a-type connections, and the four-level system connected by b-type transitions where no signal was observed would be expected to have been the weakest signal. The three systems examined for possible vibrational relaxation in cyclobutanone were connected by strong μ_c line strengths, but there were also strong μ_a connections for each of the pumped levels.

3. Cis 1,2-difluoroethylene

Rotational relaxation in the ground and lowest lying vibrationally excited state were observed in selected systems in cis-fluoroethylene. The results are presented in Table 4. Once again, no evidence of vibrational relaxation was observed, but the weakness of the Stark signals and the added difficulty of performing K-K_u double resonance led to the result that the smallest detectable relative intensities were an order of magnitude larger for this molecule than for the ring compounds.

III DISCUSSION

Though there have been cases [3,9] where the four-level $\Delta J = 1$ double resonance signal was about 30% of the Stark signal, those strong

Reproduced with permission of the copyright owner. Further reproduction prohibited without permission.

TABLE 2

Observed values of $\frac{I_{dr}}{I_{st}}$ in β-Propiolactone

Pump J'-J	v	Signal J'''-J''	v	ν_p(MHz)	ν_s(MHz)	$\frac{I_{dr}}{I_{st}}$	"Selection rules" [a]
$7_{25}-7_{16}$	0	$6_{15}-6_{06}$	0	23724	28821.6	+3%	ΔJ=-1 single μ_a μ_c, 6.6, 0.06; μ_c
$7_{25}-7_{16}$	1	$6_{15}-6_{06}$	0	23611.0	"	N(<.5%)	vibrational relax. μ_c connections
		$8_{35}-8_{26}$	0		29873.4	N(<.1%)	"
$2_{21}-2_{12}$	0	$3_{12}-2_{11}$	0	25610.6	29283.4	N(<.1%)	weak J=+1,0 .8, 0, 0, .2
$3_{13}-2_{12}$	0	$3_{12}-2_{11}$	0	25172.3	"	~-6%	μ_a connections .8, 0, 0, .6

a For ΔJ=0,1 selection rules, rotational linestrengths are presented $S_{JJ'''}$, $S_{JJ''''}$, $S_{J'J'''}$, $S_{J'J''''}$.

Reproduced with permission of the copyright owner. Further reproduction prohibited without permission.

TABLE 3

Cyclobutanone -4 Levels Systems Examined

Pump	v	Signal	v	ν_p	ν_s	$\frac{I_{dr}}{I_{st}}$	"Selection rules" [a]
$3_{13}-2_{12}$	v=1	$4_{23}-3_{22}$	v=0	23226.7	33322.8	N(<.5%)	vibrational relax. strong μ_c connections
$3_{03}-2_{02}$	v=1	$4_{13}-3_{12}$	v=0	24510.3	35554.6	N(<.5%)	"
		$4_{31}-3_{30}$	0	"	33862.0	N(<.5%)	no strong μ_c connections

a For $\Delta J=0,1$ selection rules, rotational linestrengths are presented $S_{JJ'''}$, $S_{JJ''''}$, $S_{J'J'''}$, $S_{J'J''''}$.

Reproduced with permission of the copyright owner. Further reproduction prohibited without permission.

TABLE 4

Observed values of $\frac{I_{dr}}{I_{st}}$ in 1,2 cis-difluoroethylene

Pump J'←J	v	Signal	v	ν_p(MHz)	ν_s(MHz)	$\frac{I_{dr}}{I_{st}}$	"Selection rules" [a]
$13_{311}-12_{48}$	0	$15_{511}-14_{6,8}$	0	24852.2	11893	P(~5%)	ΔJ=+2 strong cascade
		$14_{4,10}-13_{5,9}$	0	"	12997	P(~10%)	ΔJ=+1 μ_b double connection 5.7, 0, 0, 3.7
$13_{3,11}-12_{48}$	v=1	$14_{4,10}-13_{5,9}$	v=1	23913	11716.6	P(12±4%)	" excited state rotational relaxation
$5_{23}-4_{32}$	v=0	$4_{14}-3_{21}$	0	24091	12416	P(~10%)	strong μ_b connection 2.5, 0, 0, 1.2 but weak transitions-linestrengths for each ~.3
"	v=1	"	v=1	24774	12849	N(<10%)	
$11_{47}-10_{56}$	v=1	$12_{3,10}-11_{47}$	v=0	24813	15780	N	possible μ_b vibrational relaxation
$13_{311}-12_{48}$	1	$14_{410}-13_{59}$	v=0	23913	12997	N(<1%)	
		$12_{48}-11_{57}$	0		11876	N(<1%)	

a Including linestrengths for ΔJ = 0,1 transitions.

Reproduced with permission of the copyright owner. Further reproduction prohibited without permission.

signals occur only in unusual circumstances. Where the molecules are near symmetric rotors and where the K-doubling transitions that are being monitored have small line strengths relative to the $\Delta J = \pm 1$ transitions, it is not surprising that the double resonance signals are reasonably intense. These energy level patterns are discussed elsewhere (Chapter IV). For the more general asymmetric rotors studied in this chapter where the pump and signal transitions are "strong" and there are as many as five or six other strong connections for each level of the four level system, it is seen that under favorable circumstances relative intensities of about 10% can be expected. As an example of this situation, we present in Fig. 2 different energy levels and line strengths for some of the TMO systems that were studied. Comparison of this information with the experimental results (Table 1) confirms that the linestrengths do order the signals adequately.

A question that merits further consideration is the resonant vibrational relaxation problem. Is it possible that it is detectable by the microwave-microwave double resonance technique? The permanent dipole moments are generally much larger than transition moments. For comparison, let us consider the relative sizes for OCS and SO_2, two molecules whose infrared intensities have been well studied and, hence, for which transition moments may be calculated. The integrated absorption coefficient of a vibration-rotation band can be related to the transition moment.[19]

---

19. E. B. Wilson, J. C. Decius and P. L. Cross, Molecular Vibrations (McGraw Hill, New York, 1955) p. 162 ff.

Reproduced with permission of the copyright owner. Further reproduction prohibited without permission.

Reproduced with permission of the copyright owner. Further reproduction prohibited without permission.

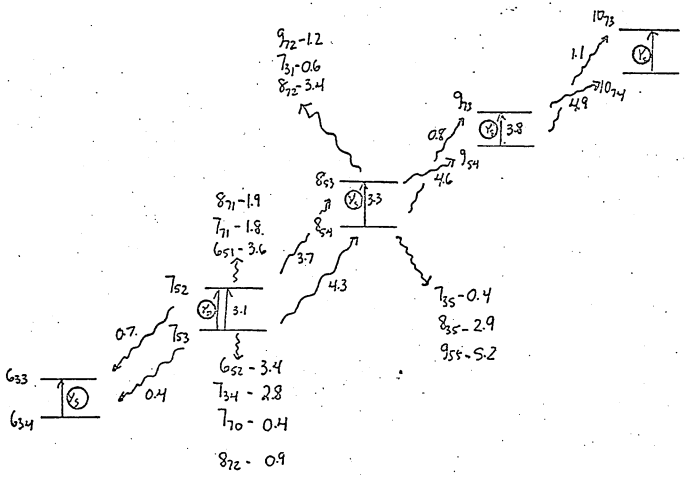

Linestrengths for Selected Rotational Transitions

of Trimethylene Oxide

Figure 2

The quantity of interest in the four-level MMDR experiments must be the importance of the permanent moment relative to the transition moment. As a measure of this property one can consider the ratio

$$r = \frac{(\frac{\partial \mu}{\partial Q})^2 (Q_{01})^2}{\mu^2}$$

where μ is the permanent moment, Q_{01} is the vibrational matrix element for the $v = 0 \rightarrow v = 1$ transition and $\partial\mu/\partial Q$ is the transition moment. In the harmonic oscillator approximation,

$$Q_{01} = (\frac{\hbar}{4\pi\nu})^{1/2}$$

where ν is the oscillator transition frequency. Also, the transition moment can be found from the integrated absorption intensity

$$A_i = \frac{\pi}{3c} (\frac{\partial \mu}{\partial Q_i})^2$$

where A_i is the absorption per molecule in units of $cm^2 sec^{-1}$ and c is the speed of light. Using intensities from the literature,[20] one can find that for the symmetric bend at 519 cm^{-1} of SO_2 and the degenerate bending mode at 521 cm^{-1} of OCS:

---

20. L. A. Gribov and V. N. Smirnov, Usp. Fiz. Nauk. 75, 527 (1961). (English translation Soviet Phys. Usp. 4, 919 (1962)).

Reproduced with permission of the copyright owner. Further reproduction prohibited without permission.

	$SO_2(\nu_2)$	OCS (ν_2)
$(\frac{\partial\mu}{\partial Q})^2$ esu^2/gm	4040	200
μ (D)	1.59	0.75
$\frac{(\frac{\partial\mu}{\partial Q})^2 Q_{01}^2}{\mu^2}$	0.009	0.002

Furthermore the possible vibrational relaxation signals must be smaller than a rotational relaxation signal by the Boltzmann factor between the ground and excited state. Even if the four level system could only relax through the resonant vibrational energy transfer, the perturbation of the pumped levels, $\delta n \approx \frac{h\nu_p}{kT} n_1(v) \approx \frac{h\nu_p}{kT} \cdot n_1(GS) \cdot e^{-h\nu_{vib}/kT}$ This latter factor would be negligible for the ring puckering modes of the compounds examined, but there is every reason to expect that the permanent moment is much more important than the transition moment for the four-level systems studied.

These factors suggest that the only hope is for molecules that possess very small permanent moments, but in that case the signal absorptions will be correspondingly weak. Furthermore, recent work on relaxation processes in the CO_2 laser has been interpreted[21] (without proof) in terms of rotational relaxation within the excited state. This interpretation would suggest that some permanent high order moment of CO_2

---

21. T. O. Carroll and S. Marcus, Phys. Letters 27A, 590 (1968).
P. K. Cheo and R. L. Abrams, App. Phys. Letters 14, 47 (1969).

Reproduced with permission of the copyright owner. Further reproduction prohibited without permission.

is more important than the transition moment. Recently the importance of resonant vibrational energy transfer has been emphasized[22] in the interpretation of CO_2 laser relaxation processes. If, however, there actually is rotational relaxation at a rate faster than resonant vibrational energy transfer processes even in non-polar CO_2, then it is unlikely that vibrational relaxation processes will be detectable by microwave double resonance.

In conclusion, let us summarize the results for energy transfer in polar gases. The work reported here suggests that the dominant interaction is the long range dipolar interaction. For a variety of asymmetric rotors we have seen that for the $\Delta J = 1$ signals, steady state relative intensities of about 10% ± 5% can be expected for four-level systems that are doubly connected but where each pumped level is also strongly connected to about five other levels. It has been shown[9] in HCN that the $|\Delta J| > 1$ signals can not be accounted for by multiple $\Delta J = 1$ collisions, and there is no reason to believe that this will not be true also for asymmetric rotors with large dipoles ($\mu > 1$ D). To show that direct $\Delta J > 1$ transitions are occuring one can try to use a mathematical analysis to evaluate rate constants. However, the analysis will be difficult for general asymmetric rotors because of the number of energy levels involved. The magnitudes of the $|\Delta J| > 1$ signals

---

22. R. D. Sharma, Phys. Rev. 177, 102 (1969) contains references to earlier article.

Reproduced with permission of the copyright owner. Further reproduction prohibited without permission.

reported here are not inconsistent with some contributions of direct $|\Delta J| > 1$ transitions since they are somewhat larger than one expects from the cascade process. Also, we see that the relative intensities for various transitions are ordered by the rotational line strengths connecting the pump and signal levels.

Reproduced with permission of the copyright owner. Further reproduction prohibited without permission.

CHAPTER III

COLLISION-INDUCED ANGULAR MOMENTUM REORIENTATION IN POLAR GASES

I. Introduction

In addition to monitoring rotational energy transfer in polar gases, four-level microwave double resonance techniques can also be used to study angular momentum reorientation caused by the long range interactions between polar molecules. We present here a series of experiments that use two different molecular phenomena to monitor the angular momentum transfer. In the presence of a static dc field the (2J + 1) spatial degeneracy of the molecular rotational wavefunctions is lifted.[1] For selected molecules, the degeneracies can be lifted to a sufficient extent such that it is possible to perform four-level MMDR experiments on individual M components. In this case in addition to the ΔJ selection rules, the ΔM selection rules and relaxation pathways can be determined. Such experiments have been performed for four-level systems in an asymmetric rotor, ethylene oxide, and in a symmetric top, 3,3,3-trifluoropropyne (CF_3CCH). It is possible to obtain similar information about angular momentum transfer by studying the collision-induced transitions between the hyperfine components of a molecule

---

1. See Chapter 10 of C. H. Townes and H. Schawlow, Microwave Spectroscopy (McGraw Hill, New York 1955).

Reproduced with permission of the copyright owner. Further reproduction prohibited without permission.

whose rotational energy levels have been split by the presence of a nuclear quadrupole moment. It has been found that $I^{127}CN$ is a molecule that is suited for four level MMDR experiments on the resolved hyperfine transitions, and the experimental results are presented here.

The experimental results presented demonstrate that the preferred selection rules for $\Delta J = \pm 1$ are transitions $\Delta M = \pm 1$ and $\Delta M = 0$; analogously the results for ICN are consistent with $\Delta J = \pm 1$, $\Delta F = \pm 1$ collision-induced transitions being preferred, though other pathways are weakly allowed. These selection rules for orientation changes of J are the ones expected from a first order perturbation theory treatment of the collision process.[2]

II. M-Dependence of Rotational Energy Transfer

A. Ethylene Oxide

Ethylene oxide (C_2H_4O, μ_b = 1.88 D) was the molecule for which four-level double resonance signals were first observed.[3] The assigned rotational spectrum[4] suggested that it would be possible to find low-J

---

2. For a recent presentation of the perturbation theory-impact approximation description of rotational energy transfer, see H. Rabitz and R. G. Gordon, J. Chem. Phys. 53, 1815 (1970).
3. T. Oka, J. Chem. Phys. 45, 754 (1966).
4. G. Cunningham, A. Boyd, R. Myers, W. D. Gwinn, and W. LeVan, J. Chem. Phys. 19, 676 (1951).

Reproduced with permission of the copyright owner. Further reproduction prohibited without permission.

transitions on which one can perform four-level double resonance experiments on individual M components. Examination of the Stark spectrum confirmed that the individual M components were reasonably intense and that they could be sufficiently well resolved at the voltages attainable to permit the effective pumping of only single M components.

The dc electric field is applied to the septum of a conventional X-band copper Stark cell. In the experiments with ethylene oxide, the dc power supply was a series of dry cells that provided a voltage of up to 700 volts. Because the direction of the applied electric field is parallel to the direction of polarization of the microwave radiation E field in the waveguide, the allowed rotational transitions must follow the $\Delta M = 0$ selection rule.[1]

The zero field transition 3_{12}-3_{21} of ethylene oxide occurs at 23611.0 MHz, and with 1100 volts dc bias applied to the septum, the M = 1, 2, and 3 components occur at 23616, 23628, and 23644 MHz respectively. With only 600 V dc bias, the M = 3 and 2 lobes are separated by 15 MHz. At pressures in the 10-20 μ Hg region these splittings are about ten linewidths, and when the pump radiation field is coincident with the M = 3 transition, there is essentially no pumping of the M = 2 or 1 lobes.

The four-level system chosen for study involved the M components of the 3_{12}-3_{21} transition occurring in K band (23611.0 MHz) and the 2_{12}-2_{21} transition occurring in R-band (34157 MHz). The microwave spectrometer used was the modulated microwave double resonance

Reproduced with permission of the copyright owner. Further reproduction prohibited without permission.

spectrometer arranged for K-R double resonance.[5] The high power (about 1 watt) saturating klystron is frequency modulated at 80 KHz. To pump the M = 3 lobe, the lower frequency of the pump klystron was adjusted to the M = 3 absorption and the upper frequency was then 30 MHz above that absorption and even further off resonance from the M = 2 and 1 lobes. To pump the M = 2 lobe, more care is necessary. The upper pump frequency was set on the resonance and the lower frequency was kept 20 MHz below the M = 1 lobe. The pump power is blocked from the R-band detector crystal by a waveguide cutoff filter. The signal transitions are observed at low power. It is possible to sweep electronically through both the M = 2 and M = 1 lobes, and the crystal output is observed through a phase sensitive detector tuned to 80 KHz. The final signal is displayed on an oscilloscope.

The experiments on the M components led to the following results:

TABLE 1

Pump ($3_{12} - 3_{21}$)	Signal ($2_{12} - 2_{21}$)	I_{dr}/I_{st} (P signal detected) (N no signal detected)
M = 3	M = 2	P ≈ 1%
	M = 1	N < 0.1%
M = 2	M = 2	P ≈ 1%
	M = 1	P ≈ 4%

5. The basic MMDR spectrometer has been described in:

R. C. Woods, A. M. Ronn, and E. B. Wilson, Rev. Sci. Inst. 37, 927 (1966) and the particular arrangement of microwave hardware for these experiments is presented in Chapter IV.

Reproduced with permission of the copyright owner. Further reproduction prohibited without permission.

These results do confirm that the dipolar interaction dominates the angular momentum reorientation occurring during a collision. No calculations have been made of M-dependent rotational energy transfer cross sections because the angular momenta algebra becomes very involved where it is not possible to sum over degenerate M components. However, in terms of a first order perturbation treatment of the collision process as outlined in Chapter II, the only possible collision-induced transitions must obey the selection rule $\Delta J = 1$, $\Delta M = 0, \pm 1$. The dipolar interaction potential will have non-vanishing matrix elements only in those cases. The rotational transitions in the presence of the microwave field must obey the $\Delta M = 0$ rule because the microwave field and the electric field are parallel, but the collision-induced transitions will follow the more general dipolar selection rule because the plane of any particular collision will be randomly oriented with respect to the space-fixed axis system determined by the applied electric field.

The matrix elements that enter into the first order perturbation expressions have been tabulated because they also determine the intensities of the Stark components.[1] The squares of the matrix elements are presented in Table 2. The dominant relaxation pathway expected from the matrix elements present in the first order theory would be for $\Delta J = -1$, $\Delta M = -1$ and a less favored pathway would be $\Delta J = -1$, $\Delta M = 0$. A $\Delta J = -1$, $\Delta M = -2$ collision-induced transition is not allowed for a single collision in the first order theory. The results presented for ethylene oxide are consistent with such expectations. These selection

Reproduced with permission of the copyright owner. Further reproduction prohibited without permission.

TABLE 2

Relative Intensities of Stark Components

	$J' = J + 1$	$J' = J$	$J' = J - 1$
$\Delta M=0 \leftrightarrow \lvert\langle J'M\rvert \mu_z \rvert JM\rangle\rvert^2$	$(J+1)^2 - M^2$	M^2	$J^2 - M^2$
$\Delta M=+1 \leftrightarrow \lvert\langle J'M+1\rvert \mu_x+i\mu_y \rvert JM\rangle\rvert^2$	$(J+M+1)(J+M+2)$	$(J-M)(J+M+1)$	$(J-M)(J-M-1)$
$\Delta M=-1 \leftrightarrow \lvert\langle J'M-1\rvert \mu_x-i\mu_y \rvert JM\rangle\rvert^2$	$(J-M+1)(J-M)$	$(J-M+1)(J+M)$	$(J+M-1)(J+M)$

Reproduced with permission of the copyright owner. Further reproduction prohibited without permission.

rules can be presented pictorially as in Fig. 1. In this classical picture the reorientation of the angular momentum is emphasized. The ΔM selection rules for the dominant relaxation pathway is that change for which the angular momentum reorientation is minimized.

Figure 1

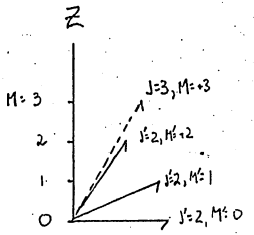

Vector Diagram of Angular Momentum Reorientation

$J, M = 3, 3 \rightarrow J', M' = 2, M'$

$|J| = \sqrt{(3)(3+1)}$

B. 3, 3, 3 Trifluoropropyne

Four-level double resonance experiments have also been performed on individual M components of rotational transitions of the symmetric top 3,3,3-trifluoropropyne (CF_3CCH, μ = 2.36 D). To use the equipment

Reproduced with permission of the copyright owner. Further reproduction prohibited without permission.

available in the laboratory for four-level experiments on a linear or symmetric rotor, the rotational constant must be subject to the constraint

$$22000 \text{ MHz} < 2B(J + 1) < 26300 \text{ MHz},$$

$$2B(J + 3) < 42000 \text{ MHz}.$$

For CF_3CCH[6], $J = 3 \rightarrow 4$ falls in K-band (23023 MHz) and $J = 5 \rightarrow 6$ occurs around 34536 MHz. By performing the double resonance experiments on M components of these intermediate J transitions, it is possible to better determine the ΔM selection rules.

The symmetric top seemed interesting because it is possible to use the first order Stark effect to separate the individual M, K components more effectively with the available electric fields than can be done for molecules characterized by second order Stark effects. The $J = 3 \rightarrow 4$ transition of CF_3CCH splits into 12 first order and four second order components, while the $J = 5 \rightarrow 6$ transition splits into 28 first order and six second order components. All the M components can be assigned and the frequencies determined as a function of electric field strength, but the complexity of the first order spectrum makes it ill-suited for four-level double resonance experiments. The individual MK signals are seriously broadened (presumably by electric field inhomogeneities

---

6. J. N. Shoolery, R. G. Shulman, W. F. Sheehan, V. Schomaker, and D. Yost, J. Chem. Phys. 19, 1364 (1957).
W. Anderson, R. Trambarulo, J. Sheridan, and W. Gordy, Phys. Rev. 82, 58 (1957).

Reproduced with permission of the copyright owner. Further reproduction prohibited without permission.

caused by deviations of the position of the Stark septum) before they are split far enough apart to permit the pumping of individual signals. The simpler second order transitions were used for four-level experiments. All work was performed at dry ice temperature (200°K).

Once again the double resonance spectrometer is arranged for K-R double resonance, as for ethylene oxide. The dc bias is applied to the Stark septum, and for these experiments a klystron power supply was used as the source of the dc bias. In this manner 1500 V with ripple less than 10 mv can be provided easily. As for the ethylene oxide experiments, the applied field is parallel to the polarized microwave E field in the guide. The assignment of the particular Stark components is critical. It must be remembered that the observed $\Delta M = 0$ transitions are still partially degenerate since the second order energy shifts of a rotational level are completely symmetric in M and K.[1] Thus, the second order shifts contain pairs of sub-levels, $|J, M=\pm a, K = 0\rangle$ and $|J, M=0, K=\pm a\rangle$. Because the selection rules for detectable absorptions are always $\Delta K = 0$ and $\Delta M = 0$ for the electric field parallel to the microwave field, the observed M component transitions will include these pairs of levels. In Table 3A we present the frequencies of the second order transition at 1500 volts dc bias. Examination of the frequencies of the $J = 3 \rightarrow 4$ transitions shows that it is possible to pump the transition at 23007 with the higher frequency of the modulated pump klystron while keeping the lower frequency at least 20 MHz below the transition at 22997 MHz. Similarly, it is possible to pump the transition at 23039 MHz with the lower of the two pump

Reproduced with permission of the copyright owner. Further reproduction prohibited without permission.

TABLE 3

4 Level Experiments on CF_3CCH M-Components

A. Frequencies of $\Delta M = 0$, $\Delta K = 0$ Rotational Transitions at 1500 V dc bias (X Band Cell)

M,K	ν (MHz) J=3 → 4	ν (MHz) J=5 → 6
0,0	22996.8	34528.5
1,0 and 0,1	23007.5	34529.5
2,0 0,2	23039.3	34533.5
3,0 0,3	23091.1	34537.8
4,0 0,4	-	34546.5
5,0 0,5	-	(not assigned)

B. 4 Level Double Resonance Experiments

Pump	Signal		I_{dr}/I_{st}
23007.5 { M=1,K=0 M=0,K=1	34529.5	P[a]	~2%
	34533	P	~1%
	34537	N	$< \frac{1}{4}$ %
23039.3 M,K= { 2,0 0,2	34529	N	$< \frac{1}{2}$ %
	34533	P	} several %
	34537	P	
	34547	N	$< \frac{1}{2}$ %

a P or N indicates positive--signal detected, N--no signal detected.

Reproduced with permission of the copyright owner. Further reproduction prohibited without permission.

frequencies and keep the upper pump frequency at least 20 MHz from the 23091 transition.

Four level experiments were performed using those transitions as the pump levels, and the results are presented in Table 3B. These experiments were performed at about 14 μ Hg pressure at dry ice temperature. The double resonance signals were very weak, the best obtainable signal to noise ratio only being 4/1, and the size of the Stark signals can only be estimated because the different signals are still very close together. Because of these difficulties, the most important conclusion that can be drawn from the work is that the first order dipole selection rules are followed. (The actual relative intensities may be uncertain to a factor of two.) The observed four level signals are consistent with the selection rules $\Delta J = +1$, $\Delta M = +1$ or 0. Signals were not observed for $\Delta J = +1$, $\Delta M = -1$ or $+2$. Furthermore, for a dipole-dipole interaction $\Delta K = 0$ selection rules are expected,[2] and the results presented here are consistent with $\Delta K = 0$ preferred collision-induced transitions.

In terms of the relative squared matrix elements listed in Table 2, it is expected that the $\Delta J = +1$, $\Delta M = +1$ collision-induced transition would be more preferred than the $\Delta J = +1$, $\Delta M = 0$ transition. However, one must extend the analysis a little further to take into account the state degeneracy of the symmetric rotor energy levels and the K dependence of the line strengths.

One of the experiments involved saturating

$$J = 3 \rightarrow 4 \ (M = 1,\ K = 0 \text{ and } M = 0,\ K = 1).$$

Reproduced with permission of the copyright owner. Further reproduction prohibited without permission.

From the upper level, dipole-allowed transitions would be

$$J = 4,\ M = 1,\ K = 0 \left\{ \begin{array}{ll} \Delta M = +1 & \rightarrow J = 5,\ M = 2,\ K = 0 \\ 0 & \rightarrow J = 5,\ M = 1,\ K = 0 \\ -1 & \rightarrow J = 5,\ M = 0,\ K = 0 \end{array} \right.$$

$$J = 4,\ M = 0,\ K = 1 \left\{ \begin{array}{ll} +1 & \rightarrow J = 5,\ M = 1,\ K = 1 \\ 0 & \rightarrow J = 5,\ M = 0,\ K = 1 \\ -1 & \rightarrow J = 5,\ M = -1,\ K = 1 \end{array} \right.$$

The two $\Delta M = 0$ transitions would populate two degenerate levels of the $J = 5$ state. If one estimates the relative magnitude of the collision cross sections by the relative intensities of the appropriate Stark M, K transitions, then one concludes

$$\frac{I_{dr}}{I_{st}} \alpha \frac{I_{J = 4 \rightarrow 5}}{I_{J = 5 \rightarrow 6}} = \begin{array}{ll} 1.3 & J = 5;\ M, K = 2, 0 \\ 1.4 & M, K = 1, 0 \\ 0.4 & M, K = 0, 0 \end{array}$$

as one pumps $J = 3 \rightarrow 4$ (M, K = 1, 0 and 0, 1). As can be seen in Table 3B the observed relative intensity was apparently 2 to 1 in favor of the $\Delta M = 0$ transition rather than 1 to 1. This discrepancy is not serious given the level of significance of the calculation. The purpose of the experiment was to determine whether the M selection rules expected for the dipolar interaction are found to be dominant, and this has been found to be the case. No evidence was found for transitions following $\Delta J = +1$, $\Delta M = +2$ selection rules.

The basic complexity of the symmetric rotor spectrum necessitates that any further work that is to be done must focus on linear molecules

Reproduced with permission of the copyright owner. Further reproduction prohibited without permission.

if one is to be able to determine M dependent cross sections quantitatively. The linear molecule (K = 0 symmetric rotor) has each J level split into only J + 1 components and it should be possible to perform an analysis of the energy transfer results in terms of the linear kinetic theory. However, with the equipment available, the only linear molecules that are suitable also have nuclear spins greater than $\frac{1}{2}$, and, hence, each rotational energy level is perturbed by the spin-rotation interaction. Fortunately that spin-rotation interaction can be used to collect equivalent information about the angular momentum reorientation occurring during collisions.

III. Angular Momentum Reorientation in ICN-ICN Collisions

A. Introduction

A nucleus that is characterized by a spin greater than $\frac{1}{2}$ possesses a nuclear quadrupole moment that couples with the gradient of the molecular electric field to split each rotational J level into a set of sublevels.[7] In vector notation, the nuclear spin $\underset{\sim}{I}$ couples with the rotational angular momentum $\underset{\sim}{J}$ to produce a total angular momentum $\underset{\sim}{F}$

$$\underset{\sim}{F} = \underset{\sim}{I} + \underset{\sim}{J} .$$

Because the dominant collision interaction for polar molecules that can be monitored by four level double resonance will be the long range dipole-dipole interaction, the orientation of $\underset{\sim}{I}$ will be unperturbed during

---

7. See reference 1, Chapter 6.

Reproduced with permission of the copyright owner. Further reproduction prohibited without permission.

a collision. The collision-invariant $\underset{\sim}{I}$ orientation can be used as a reference by which one can monitor changes in angular momentum during collisions. The nuclear spin becomes an internal reference for the direction of angular momentum analogous to the external reference established by the use of a dc field in the preceding section.

The molecular energy levels are characterized by the values of I, J, and F. By the basic properties of angular momenta, F takes on the values $I + J$, $I + J - 1$, ..., $|I - J|$. A collision-induced transition might cause a transfer of population from I, J, F to I, J', F'. The value of F' relative to F is a measure of the reorientation of angular momentum occurring during the transition. This is indicated in Fig. 2 for $I = \frac{5}{2}$, $J = 4 \rightarrow J = 5$, and for different F values. The length of the vectors is taken as $\sqrt{a(a+1)}$. Clearly for $\Delta J = +1$, there will be the smallest reorientation of angular momentum for $\Delta F = +1$, with increasing reorientation for $\Delta F = 0$ and $\Delta F = -1$.

ΔF transitions other than 0, ± 1 are possible. In general, if one determines the cross sections for the various possible ΔF transitions associated with a given ΔJ collision-induced transition, one will be determining the dependence of the cross section on angular momentum transfer because the energy transferred will be the same for all transitions since the F levels are generally close together relative to the J spacings. Rabitz and Gordon[8] have considered a first order perturbation theory treatment of the F reorientation occurring during collisions

---

8. H. Rabitz and R. G. Gordon, J. Chem. Phys. 53, 1831 (1970).

Reproduced with permission of the copyright owner. Further reproduction prohibited without permission.

Figure 2

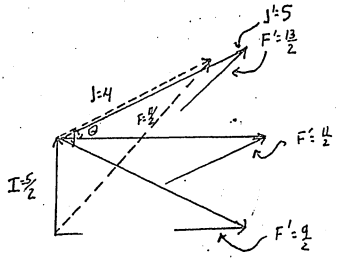

θ Reorientation angle for $\underset{\sim}{J} \rightarrow \underset{\sim}{J}'$

Vector Diagram, Angular Momentum($\underset{\sim}{J}$) Reorientation in Presence of Nuclear Spin($\underset{\sim}{I}$)

Reproduced with permission of the copyright owner. Further reproduction prohibited without permission.

for a dipole-dipole potential.

B. Choice of Four Level System

A molecule suited for four level double resonance experiments on individual hyperfine transitions must have the components sufficiently separated to permit the pumping of individual transitions. To use modulated double resonance one must be able to place one of the pump frequencies on a single resonance and have neither it nor the other frequency within 10 MHz of any other resonance. Furthermore, a linear molecule is desirable since there is nothing gained by the added complexity of an asymmetric rotor rotational spectrum. $I^{127}CN$ is a molecule well-suited for the purpose. With a rotational constant[9] B = 3225.6 MHz and a quadrupole coupling constant eqQ = -2420 MHz, the J = 3 → 4 transition occurs in K band (centered at 25804 MHz) and the J = 5 → 6 transition is centered about 38706 MHz. The J = 3 → 4 transitions and the J = 5 → 6 transitions are presented in Table 4. The effect of the N^{14} quadrupole moment is so small that it can be neglected.

Unfortunately iodine compounds tend to be unstable and ICN proved to be no exception. ICN was not stable in copper waveguides in general. It was found to be stable for a brief period in a new X-band copper cell in which there was no septum. Finally, it was found to be stable

---

9. C. H. Townes, A. N. Holden, and F. R. Merritt, Phys. Rev. 74, 113 (1948).

Reproduced with permission of the copyright owner. Further reproduction prohibited without permission.

TABLE 4

Hyperfine Components of ICN Rotational Transitions

$J = 3 \rightarrow 4$			$J = 5 \rightarrow 6$			
$F \rightarrow F'$	Freq. in MHz[a]	Relative Intensity[b]	$F \rightarrow F'$	ν_{pred}[b]	ν_{obs}[c]	Relative Intensity[b]
$\frac{5}{2} \rightarrow \frac{5}{2}$	25991.9	0.1	$\frac{7}{2} \rightarrow \frac{7}{2}$	38970.7		0.05
$\frac{3}{2} \rightarrow \frac{3}{2}$	25969.6	0.1	$\frac{9}{2} \rightarrow \frac{9}{2}$	38925.0		0.08
$\frac{7}{2} \rightarrow \frac{7}{2}$	25954.4	0.1	$\frac{11}{2} \rightarrow \frac{11}{2}$	38819.5		0.09
$\frac{9}{2} \rightarrow \frac{11}{2}$	25837.6	0.8	$\frac{13}{2} \rightarrow \frac{15}{2}$	38723.5	38723.0	0.8
$\frac{11}{2} \rightarrow \frac{13}{2}$	25823.1	1.0	$\frac{15}{2} \rightarrow \frac{17}{2}$	38716.0	38715.8	1.0
$\frac{9}{2} \rightarrow \frac{9}{2}$	25789.9	0.2	$\frac{11}{2} \rightarrow \frac{13}{2}$	38705.1	38704.1	0.7
$\frac{7}{2} \rightarrow \frac{9}{2}$	25783.5	0.6	$\frac{5}{2} \rightarrow \frac{7}{2}$	38688.4	38687.7	0.4
$\frac{1}{2} \rightarrow \frac{3}{2}$	25752.5	0.2	$\frac{9}{2} \rightarrow \frac{11}{2}$	38683.0	38682.0	0.6
$\frac{5}{2} \rightarrow \frac{7}{2}$	25728.8	0.4	$\frac{7}{2} \rightarrow \frac{9}{2}$	38673.7	38672.0	0.5
$\frac{3}{2} \rightarrow \frac{5}{2}$	25711.5	0.3	$\frac{13}{2} \rightarrow \frac{13}{2}$	38624.5		0.08
$\frac{11}{2} \rightarrow \frac{11}{2}$	25393.9	0.1	$\frac{15}{2} \rightarrow \frac{15}{2}$	38304.6		0.05

a Townes, Holden, and Merritt, Phys Rev. 74, 1113.

b Using first order perturbation theory description of spin-rotation interaction, as in Townes and Schawlow, Microwave Spectroscopy p. 150 ff.

c This work.

Reproduced with permission of the copyright owner. Further reproduction prohibited without permission.

in a nickel waveguide. An iodine compound that is considerably more stable is CF_3I. That molecule is not suited for four level double resonance experiments because each J level is split into distinct $|J,K,F\rangle$ components, and any particular transition is relatively weak.

C. Apparatus and Procedure

Four level double resonance experiments on individual hyperfine components of ICN rotational transitions have been performed under two sets of conditions. First the sample cell was an empty fifteen foot copper X-band waveguide. Secondly, a 10 foot nickel Stark cell has been used as the sample container. The spectrometer sensitivity was greater in the former case as is to be expected for the longer cell. The greater sensitivity was used to obtain a full survey of selection rules, but the sizes of the signals can not be experimentally referenced to the corresponding Stark signals. The nickel cell was used to obtain measurements of the double resonance signals (relative intensity and phase) as a function of pressure. In all cases, $J = 3 \rightarrow 4$ transitions were pumped and most experiments involved signal transitions in the $J = 5 \rightarrow 6$ manifold. Experiments are also reported where double resonance signals were detected at $J = 6 \rightarrow 7$ transitions. We note that $J = 4 \rightarrow 5$ transitions can not be used as signal transitions because three-level quantum effects[10] will obscure the weaker four-level energy

---

10. A. P. Cox, G. W. Flynn, and E. B. Wilson, J. Chem. Phys. 42, 3094 (1965).

Reproduced with permission of the copyright owner. Further reproduction prohibited without permission.

transfer signals.

The basic arrangement of the double resonance spectrometer is the same as for the M component experiments described in the preceding section. However, the high power klystron is frequency modulated at 100 KHz. Because the signal transitions are occurring at higher frequencies than the pumped transitions, the crystal detector is isolated from the pump radiation by waveguide cutoff filters. The crystal output is observed after amplification by a 100 KHz preamplifier and a phase sensitive detector tuned to 100 KHz. The final signal is monitored on an oscilloscope.

For the experiments performed in the nickel Stark cell, the relative intensity and phase measurements were obtained in the following manner. After the pump radiation frequency was set at the desired frequency, the variable phase shifter of the phase sensitive detector was set to maximize the double resonance signal by setting the phase first to null the signal and then shifting it 90°. For the weakest double resonance signals uncertainties of phase of up to 10° are possible, but generally they are less than 5°. Once the double resonance signal size is recorded, the modulation is switched from the pump klystron reflector circuit to the Stark cell and the magnitude of the Stark signal can be determined at its proper phase setting. In this manner the relative intensities and phase shifts can be determined as a function of pressure. The pressure measurements were made on an MKS Baratron capacitance gauge.

Reproduced with permission of the copyright owner. Further reproduction prohibited without permission.

D. Results

1. Experiments using the Fifteen Foot Copper Waveguide as Sample Cell

The first experiments involved pumping $J = 3 \rightarrow 4$, $F = \frac{9}{2} \rightarrow \frac{11}{2}$ at 25837 MHz with the upper pump frequency set around 25860 MHz. The sample pressure was estimated to be about 15 μ Hg from linewidth considerations and thermocouple gauge readings. When that transition is pumped, double resonance signals are observed for many transitions in the $J = 5 \rightarrow 6$ manifold as is indicated in Fig. 3. In that figure we indicate schematically the signal shape as it would be observed on the oscilloscope to emphasize that some of the signals are 180° out of phase with each other, since some signals represent increased gas absorption when the pump radiation is saturating the 3, $\frac{6}{2} \rightarrow 4$, $\frac{11}{2}$ transition while other signals are associated with decreased absorption. Also in the figure relative signal heights are presented, and a ratio of relative signal height to the theoretical magnitude of the different hyperfine components of the signal transition. In Fig. 3 we have associated the signal at 5, $\frac{13}{2} \rightarrow 6$, $\frac{15}{2}$ with an increase in absorption because that is what would be expected in terms of first order perturbation theory,[8] where the dominant collision-induced transition would be 4, $\frac{11}{2} \rightarrow 5$, $\frac{13}{2}$.

By determining the variation of signal height with pump frequency, it was seen that the signals denoted S1, S4, and S6 were due to the transition being pumped: the peak heights decreased regularly and symmetrically as the pump frequency was shifted either above or below the resonance. The signal at S2 appears to be a result of pumping the wing

Reproduced with permission of the copyright owner. Further reproduction prohibited without permission.

Figure 3

Signals Observed in J= 5→6 Manifold
on Pumping J= 3→4, F= $\frac{9}{2} \rightarrow \frac{11}{2}$

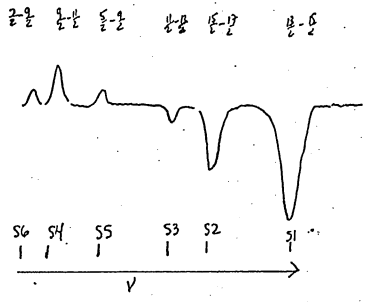

	S6	S4	S5	S3	S2	S1
Relative Peak Height	2	10	1	10	25	150
$\frac{\text{Relative Peak Height}}{\text{Relative Intensity of Hyperfine Comp}^*}$	2	7	1	6	10	80

* Theoretical value
see reference 1, chap. 6

Reproduced with permission of the copyright owner. Further reproduction prohibited without permission.

of the transition 25823 ($J = 3, \frac{11}{2} \rightarrow J = 4, \frac{13}{2}$) because the signal height increases as the pump frequency is shifted to lower frequencies. Also the signal denoted S3 can not simply be attributed to pumping the $J = 3, \frac{9}{2} \rightarrow J = 4, \frac{11}{2}$ transition. The phase setting of the phase sensitive detector for which the signal is maximized is not consistent with the settings for the other signals.

Other four level systems have also been examined. In each instance the strongest rotational relaxation signals are consistent with $\Delta J = +1$, $\Delta F = +1$ and 0 collision-induced transitions. The weaker signals may be due to a variety of causes. On the one hand, they may be due to collision-induced transitions related to the levels being pumped. Unfortunately, they may also be due to partial pumping of other transitions. Also, one must consider the possibility that the $|I,J,F>$ wave functions are not adequate descriptions of the rotational transitions. For the large I^{127} quadrupole coupling constant, second order perturbation theory is needed to predict the molecular energy levels accurately.[7] A calculation of the first order corrections to the ICN wave functions shows that $|I,J,F> = |\frac{5}{2}, 6, \frac{13}{2}>$ is mixed in with the $|\frac{5}{2}, 4, \frac{13}{2}>$ wave function by 5×10^{-3}. Such a correction is small, but finite, and it may be necessary to consider it if one tries to interpret the weakest double resonance signals. This effect has been detected by Oka[11] in three-level double resonance experiments on

---

11. T. Oka, J. Chem. Phys. 45, 752 (1966).

Reproduced with permission of the copyright owner. Further reproduction prohibited without permission.

ethyl iodide where it has been possible to pump a $\Delta J = +3$ transition that is made weakly allowed by the mixing of J and J + 2 wave functions.

2. Experiments using the Nickel Stark Cell

To better characterize the angular momentum changes occurring during collisions, data was collected of the intensities of the double resonance signals relative to the corresponding Stark signals and the phase shifts of the double resonance signals as a function of pressure. The four level systems for which the data was collected are indicated in Fig. 4. These systems were chosen because the pump transitions were relatively isolated, and the signal transitions were those for which the Stark intensities would be most accurately determined. The steady state relative intensities are presented in Table 5. In Fig.s 5 and 6 we present the relative intensities as a function of pressure for some of the four level systems studied and in Fig.s 7 and 8 we present phase shifts as a function of pressure. Because of the weakness of the signals it is not possible to collect data below 5 μ Hg for even the stronger signals, and for the weaker signals 10 μ Hg was the lowest attainable pressure.

Examination of the relative intensity data shows two interesting trends. Even though the pump radiation field is less than 1 watt, the pump transition is effectively saturated at pressures as high as 40 μ Hg. This is seen by the existence of the plateau region at high pressures, and is different from the results in

Reproduced with permission of the copyright owner. Further reproduction prohibited without permission.

Figure 4

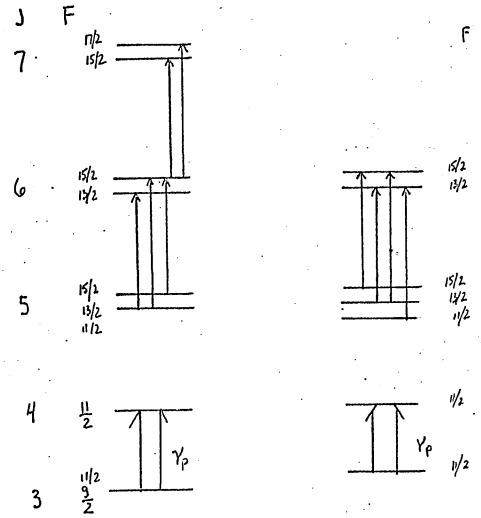

Four-Level Systems, ICN

Reproduced with permission of the copyright owner. Further reproduction prohibited without permission.

TABLE 5

Rotational Energy Transfer - ICN Hyperfine Transitions

Steady State Relative Intensities

Pump Transition (J=3→4)		Signal			$\frac{I_{dr}}{I_{st}}$ (%)
F → F'	ν (MHz)	J=5→6 F → F'		ν (MHz)	
$\frac{11}{2} - \frac{11}{2}$	25394		$\frac{13}{2} - \frac{13}{2}$	38625	+4.5±.5
$\frac{9}{2} - \frac{11}{2}$	25837		$\frac{13}{2} - \frac{13}{2}$		+2.5±.2
$\frac{11}{2} - \frac{11}{2}$			$\frac{13}{2} - \frac{15}{2}$	38723.5	+3.0±.2
$\frac{9}{2} - \frac{11}{2}$			$\frac{13}{2} - \frac{15}{2}$		+2.2±.3
$\frac{11}{2} - \frac{11}{2}$			$\frac{11}{2} - \frac{13}{2}$	38705	+0.5±.1
$\frac{11}{2} - \frac{11}{2}$			$\frac{15}{2} - \frac{15}{2}$	38304	-3.5±.3
$\frac{9}{2} - \frac{11}{2}$			$\frac{15}{2} - \frac{15}{2}$		-0.4±.2
		J=6→7			
$\frac{9}{2} - \frac{11}{2}$			$\frac{15}{2} - \frac{17}{2}$	45169.2	+0.6±.2
			$\frac{15}{2} - \frac{15}{2}$	45057	No signal (<.7%)

Reproduced with permission of the copyright owner. Further reproduction prohibited without permission.

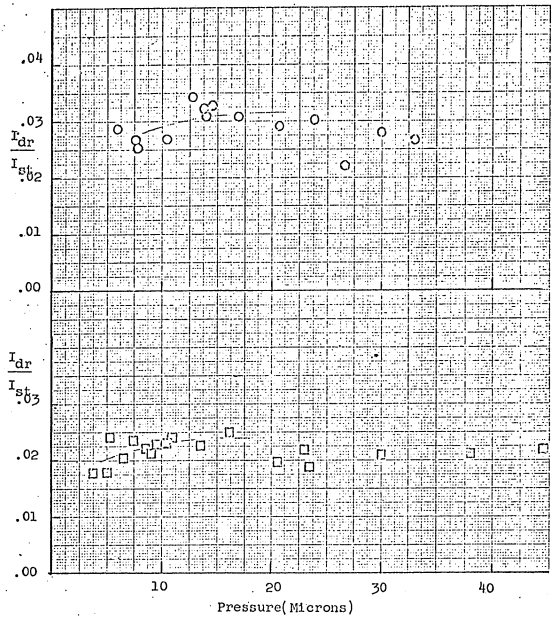

ICN-ICN Relative Intensity-Pressure

Observe $5,\frac{13}{2} - 6,\frac{15}{2}$

Pump o $3,\frac{11}{2} - 4,\frac{11}{2}$

□ $3,\frac{9}{2} - 4,\frac{11}{2}$

Figure 5

Reproduced with permission of the copyright owner. Further reproduction prohibited without permission.

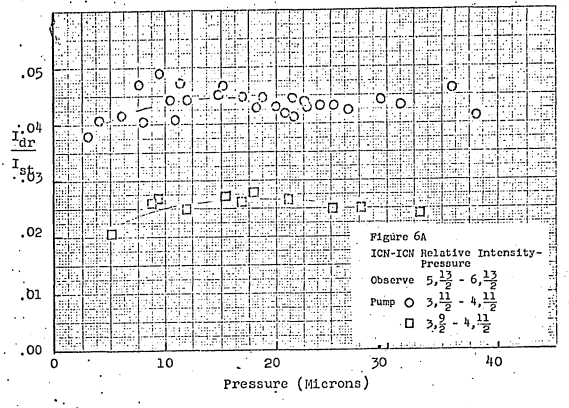

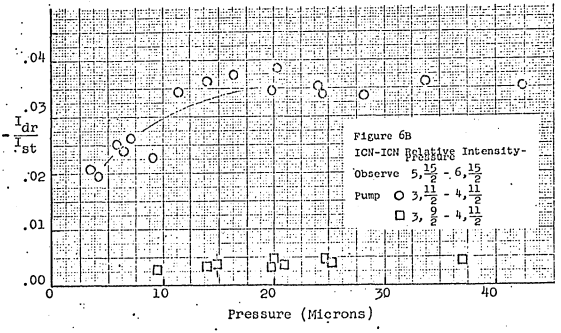

Reproduced with permission of the copyright owner. Further reproduction prohibited without permission.

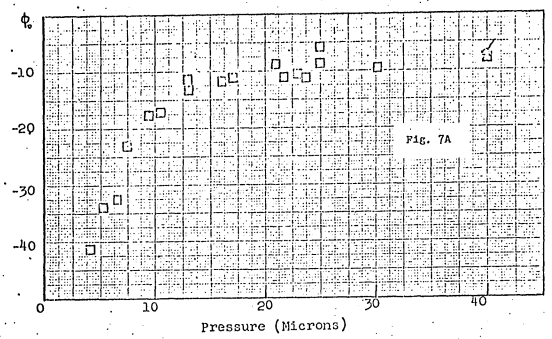

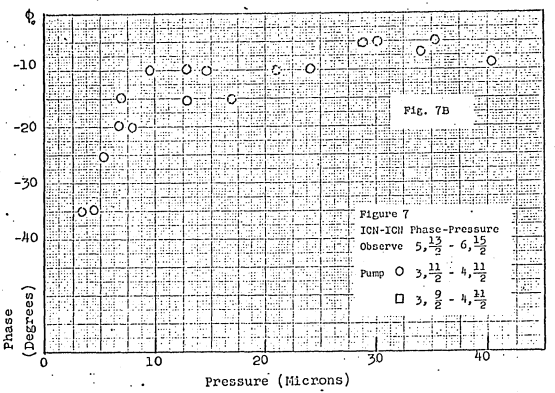

Reproduced with permission of the copyright owner. Further reproduction prohibited without permission.

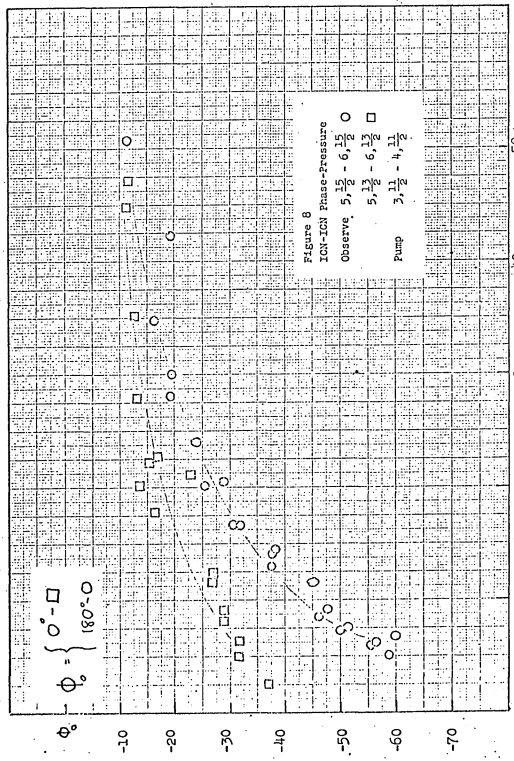

Reproduced with permission of the copyright owner. Further reproduction prohibited without permission.

HCN[12] where there is a definite decrease in double resonance signal intensity above 10 μ Hg. Though the radiation density in the guide is about the same for the two experiments, the pumping efficiency is much greater for ICN because the transition is strongly allowed while the HCN pump transition is only weakly allowed ℓ-doublet. More interesting, however, is that for one case (Fig. 6B) the relative intensity only reaches a maximum value at 12 - 15 μ Hg while for the other signal transitions reported, the maximum is reached below 10 μ Hg. This situation is reflected in the phase data as well where the phase of the signal at $|5, \frac{15}{2}> - |6, \frac{15}{2}>$ approaches a high pressure limit at higher pressures than the phase of the $|5, \frac{13}{2}> - |6, \frac{13}{2}>$ signal when the $|3, \frac{11}{2}> - |4, \frac{11}{2}>$ transition is pumped (Fig. 8).

E. Discussion

The first order perturbation theory evaluation of the cross sections for the ΔJ, ΔF collision-induced transition leads to the conclusion that the cross sections are closely related to the intensities of the corresponding spectral lines.[13] In first order theory, for ΔJ = +1 the ΔF = +1 transition is most favored, then the ΔF = 0 transition, with ΔF = -1 only very weakly allowed. In fact the probability of a collision-induced transition $J^iF^i \rightarrow J^fF^f$ is equal to the product of

---

12. R. G. Gordon, P. E. Larson, C. H. Thomas, and E. B. Wilson, J. Chem. Phys. 50, 1388 (1969).

13. See reference 1, Appendix I.

Reproduced with permission of the copyright owner. Further reproduction prohibited without permission.

the line strength of the spectral hyperfine component and a resonance function factor. Rabitz and Gordon[8] have presented calculations for the relative cross sections for the hyperfine components of $J = 3 \rightarrow 4$ of ICN. Comparison of their values with tabulated line strengths shows that for $\Delta J = +1$ collision-induced transitions, $\Delta F = -1$ and 0 transitions are more probable relative to $\Delta F = +1$ transitions than one would expect from the line strengths alone. With increasing J values, the $\Delta J = +1$, $\Delta F = +1$ transition is increasingly favored over the $\Delta F = 0, -1$ transitions. A second $\Delta J = +1$ collision would lead to a net $\Delta J = +2$, $\Delta F = +2$ population transfer with $\Delta J = +2$, $\Delta F = +1, 0, \ldots, -2$ being increasingly less likely.

The results obtained using the long copper cell show that many weak signals can be observed that can not be rationalized easily in terms of first order theory. The quantitative relative intensity and phase data presented are consistent with the dominant first order selection rules. The two signals for which the relative intensities were negative are the transitions for which the strongest connection would be $\Delta J = +2$, $\Delta F = +2$. The excess population of the $J = 4$ level would be transferred to the $J = 6$ level, and a decrease in absorption while the pump field is on would be expected. The pressure dependence of the relative intensity and phase shift confirm that multiple collision processes are important for that four-level system. Another feature of the relative intensity data is that for a given signal transition, pumping the $\frac{9}{2} - \frac{11}{2}$ level leads to smaller double resonances than pumping the $\frac{11}{2} - \frac{11}{2}$ transition. The reason for this is that the

Reproduced with permission of the copyright owner. Further reproduction prohibited without permission.

3, $\frac{9}{2}$ - 4, $\frac{11}{2}$ collision-induced transition is more favored than the $\frac{11}{2}$ - $\frac{11}{2}$ transition, and in this case the pumped levels can relax more efficiently as a two level system. However, whether all these experimental results are consistent with first order dipole selection rules can only be determined by fitting the data in terms of the linear kinetic theory rate constants, an analysis that is non-trivial and has not yet been performed.

Reproduced with permission of the copyright owner. Further reproduction prohibited without permission.

CHAPTER IV

ENERGY TRANSFER IN HCN-RARE GAS MIXTURES

I. Introduction

The first four-level microwave double resonance experiments demonstrated that collision-induced rotational energy transfer in dilute polar gases follows difinite "selection rules." In previous chapters further studies of rotational energy transfer processes in pure polar gases have been presented that show that the MMDR technique is sufficiently sensitive to study qualitatively the preferred "selection rules" in reasonably complex molecules. Perhaps the most powerful use of the double resonance techniques, however, is that it is possible to use the experimental results to determine a set of collisional rate constants. In order to determine rate constants one must, obviously, have a kinetic model that will relate the rate parameters to the experimental observables--the relative intensities and phases in the modulated double resonance experiments. Larson et al.[1] have shown that it is feasible to use a classical kinetic model to account for a set of four-level MMDR experiments in pure HCN.

In the pure polar gas, dipolar interactions dominate. If one studies a dipole-atom system, the nature of the dominant interactions is

---

1. R. G. Gordon, P. E. Larson, C. H. Thomas, and E. B. Wilson, J. Chem. Phys. 50, 1388 (1969).

Reproduced with permission of the copyright owner. Further reproduction prohibited without permission.

less well understood. Oka[2] has reported a number of experiments involving the NH_3-rare gas mixtures. He has studied a sufficient number of four-level systems to determine the nature of the selection rules. The complexity of his results suggests that it would be very informative to analyze an appropriate series of double resonance experiments quantitatively to determine a set of rate constants for energy transfer in a dipole-rare gas system.

The differential equations Eq.s (I-4, 6) and the result Eq. (I-21) of the linear kinetic theory outlined in Chapter I may be used to describe collision processes in gas mixtures. In this case $\underset{\sim}{n}(t)$ is the population vector for the polar molecule. The collisional rate matrix will be given as a sum of contributions:

$$\underset{\approx}{\Pi} = \underset{\approx}{\Pi}^{D-D} + \underset{\approx}{\Pi}^{D-FG} + \underset{\approx}{\Pi}^{D-wall}$$

where $\underset{\approx}{\Pi}^{D-D}$ represents the rate processes for dipole-dipole collisions, $\underset{\approx}{\Pi}^{D-FG}$ the rate processes for dipole-perturber collisions, and $\underset{\approx}{\Pi}^{D-wall}$ possible contributions due to collisions with the cell walls. In this model the total linewidths will be the sum of contributions from the different collisional processes (Eq. (I-2)), and the contribution of the pump field will be of the form Eq. (I-22a).

The work presented in this chapter involves new experimental studies on rotational energy transfer in pure HCN and in HCN-rare gas mixtures and their analyses by means of the linear rate theory presented

---

2. T. Oka, J. Chem. Phys. 49, 3135 (1968).

Reproduced with permission of the copyright owner. Further reproduction prohibited without permission.

in Chapter I. By way of introduction, the rotational energy levels of HCN are presented and there is a discussion about why HCN is a suitable system for study. Then, after a presentation of the experimental techniques, the experimental results are presented: double resonance experiments and collisional linewidth parameters.

The analysis of the results is presented in an iterative manner. First, using sensible HCN parameters we present a first set of rate constants for each of the rare gas partners. Then alternative sets of rates are presented for pure HCN and the mixtures. At that point we are trying to determine the likelihood that the parameters have physical as well as computational significance. A qualitative theoretical discussion is then presented to try to relate the rate constants to a potential function and to allow us to determine a favored set of rate constants. As will be seen, the analysis at that point suggests that a reasonable improvement in experimental accuracy would enable a more certain determination of rate constants. A last series of experiments is summarized which shows that important sources of uncertainty are probably very fundamental in nature--quantum coherence effects that have been neglected completely in the kinetic model. In conclusion, a brief summary is presented along with indications of sensible directions in which to proceed in the future.

II. Energy Levels in HCN: The Choice of the System

In the lowest vibrationally excited state of HCN, $v_2 = 1$, the interaction of the doubly degenerate bending modes with the rotational motion

Reproduced with permission of the copyright owner. Further reproduction prohibited without permission.

gives rise to a splitting of the ordinary linear molecule rigid rotor energy levels. This phenomenon, known as ℓ-type doubling, leads to the absorption in the microwave region for HCN. The transitions between the doublet components occur approximately at $224\ J(J+1)$ MHz. Part of the energy level diagram of the rotational spacings in the $v_2 = 1$ state is presented in Fig. 1.

The ℓ-doublet system has properties that make it well-suited for the double resonance studies. The system possesses the advantages of the energy level patterns of the linear molecule without the primary disadvantage of the linear molecule. The linear molecule has many fewer pathways by which a given saturated level can relax back to equilibrium than an asymmetric rotor has. Hence, the MMDR signals might be strong. However, for a true linear molecule the observed relative intensities tend to be weak because the effects of multiple collisions will counteract the single collision. If a single dipole-like collision induces a transition from $J + 1$ to $J + 2$, the second collision carries the molecule to $J + 3$. Experimentally one detects only $n_{J+3}(t) - n_{J+2}(t)$. Hence, there is expected to be some cancellation.

HCN in the $v_2 = 1$ state is a near-prolate rotor. The symmetric rotor wave functions in the Wang basis set are a good description of the wave functions. A given J level can be described[3] as

---

3. C. H. Townes and A. Schawlow, Microwave Spectroscopy, (McGraw-Hill, New York, 1955).

Reproduced with permission of the copyright owner. Further reproduction prohibited without permission.

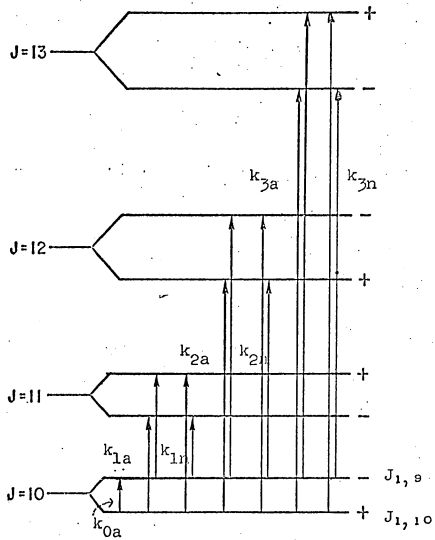

HCN ENERGY LEVELS

Figure 1

Reproduced with permission of the copyright owner. Further reproduction prohibited without permission.

Wang Functions

$$J_{upper} \qquad \frac{J_{K_{-1}K_{+1}}}{J_{1,J-1}} \sim \frac{1}{\sqrt{2}}[\,|J1M\rangle - |J-1M\rangle\,] \equiv |J1M-\rangle$$

$$J_{lower} \qquad J_{1,J} \sim \frac{1}{\sqrt{2}}[\,|J1M\rangle + |J-1M\rangle\,] \equiv |J1M+\rangle$$

where $J_{K_{-1}K_{+1}}$ is the usual asymmetric rotor nomenclature, K_{-1} being the near prolate rotor limiting quantum number, and K_{+1} the oblate rotor limiting quantum number. $|JKM\rangle$ indicates a symmetric rotor wave function with total angular momentum J, K the J projection on the body-fixed axis, and M the projection on the space-fixed axis.

If we assign a parity (+ or -) by whether the wave function is even or odd on rotation about the molecule c axis, one can show that for J even, the lower level is even while for odd J the upper level is even. These are the + and - notations of Fig. 1. For the near symmetric prolate rotor with an a-type dipole, there are dipole-allowed transitions for $\Delta J = 0$, $+ \leftrightarrow -$ and $\Delta J = \pm 1$, $+ \leftrightarrow -$. In the notation of Fig. 1, k_{0a} and k_{1a} are dipole-allowed transitions. For $\Delta J > 1$, the rate notation (k_{ja} or k_{jn}) is used to indicate whether a transition is allowed by a series of $\Delta J = +1$ dipole-allowed transitions (k_{ja} for $\Delta J = +1$ cascade transitions).

The $\Delta J = 0$ transitions occur in the microwave region while the $\Delta J = +1$ transitions occur in the far-infrared at a frequency of $\nu \cong 2 \cdot 44{,}000 \cdot (J + 1)$ MHz $\cong 2.9\,(J + 1)$ cm^{-1}. In the HCN system, as one pumps and detects $\Delta J = 0$ transitions, one has the situation where $\Delta J = +2$ collision-induced transitions do not directly affect

Reproduced with permission of the copyright owner. Further reproduction prohibited without permission.

$n_{upper} - n_{lower}$ of the $\Delta J = +1$ level.

The region most readily accessible experimentally is the ℓ-doublet system for moderately high J: J = 10-13. The appropriate dipole matrix elements are:

$$J+1 \leftarrow J \qquad |\mu_{ij}|^2 = \mu^2 \frac{(J+1)^2 - K^2}{(J+1)(2J+1)}$$

and HCN: K = 1 (2)

$$J \leftarrow J \qquad |\mu_{ij}|^2 = \mu^2 \frac{K^2}{J(J+1)}$$

We see that if we consider the collision process in terms of first order perturbation theory (Eq. II-3,5), and if the collisions follow dipole-like selection rules, then the $\Delta J = +1$ collision-induced transitions will dominate over $\Delta J = 0$ transitions for high J and low K values. In this case $\Delta J > 1$ signals should be observable. Furthermore, by working in the high J range, there should be reasonable simplifications that can be applied to the H matrix structure: the rate constants should be slowly varying functions of J--in fact perhaps almost J independent; the ΔJ rates should be almost the same for transfers from upper and lower levels.

The useful properties of HCN amount to the fact that the system is fortuitously simple. Insofar as those are desirable characteristics, one can not expect to study properties of inherently complex systems. As mentioned, Oka has done a great amount of work on rotational energy transfer in pure NH_3[4] and also for NH_3-foreign gas mixtures (O_2, H_2,

---

4. T. Oka, J. Chem. Phys. 48, 4919 (1968).

Reproduced with permission of the copyright owner. Further reproduction prohibited without permission.

He, Ar, Xe...).[2,5] NH_3 has inversion doubling analogous to the HCN ℓ-type doubling. One monitors and pumps $\Delta J = 0$ transitions. However, NH_3 is a symmetric top that has discrete JK levels, not simply the $|J,K=1>$ levels of HCN. In this more complex system one learns about K selection rules as well, but the analysis is also increasingly complex. As one finds ΔK collision-induced transitions, the minimal meaningful size of the Π matrix would be large indeed. Furthermore, for NH_3 there is less reason to assume k_{ij} to be J independent.

The factors discussed above that made HCN a sensible choice for the double resonance experiments in the pure polar gas also make it a suitable choice for polar molecule-atom experiments. The properties of the HCN energy levels themselves can not, however, guarantee that the results for HCN-rare gas experiments should be "interesting." As the previous work[1] found that the semiclassical rate model is applicable to HCN energy transfer experiments, it should also be applicable to the HCN-rare gas experiments.

III. Experimental

A. MMDR Experiments

1. The Spectrometer

The modulation spectrometer used is similar to the basic spectrometer described by Woods, Ronn, and

---

5. P. Daly and T. Oka, J. Chem. Phys. 53, 3272 (1970).

Reproduced with permission of the copyright owner. Further reproduction prohibited without permission.

Wilson[6] and also to Larson's[7] apparatus. A block diagram of the particular configuration used in this work is found in Fig. 2. To pump the J = 10 doublet at 24,660 MHz, an Oki 24V11 klystron with a rated output of about 1 watt was used. Frequency modulation of this klystron was achieved by introducing a square wave voltage to the klystron power supply reflector circuit. The source of the square wave was a 100 KHz Stark generator and a square wave of about 50 volts is sufficient to frequency modulate the klystron by about 25 MHz. Because the pump klystron is free running, it is necessary to adjust and readjust the applied square wave voltage to keep one of the pump frequencies on resonance as one performs a double resonance experiment. A 10 db coupler in the pump arm couples about 10% of the pump power to a mixer for frequency measurement. It was found useful to maintain the capability of frequency measurement while experimenting as one readjusts the applied square wave or switches from Stark to double resonance modulation. A band pass filter is used on the pump arm to cut out harmonics of the pump. This filter should also isolate the pump klystron from the higher frequency signal field. The EH tuner is used for impedance matching to obtain the maximum possible pump power through the cell.

The signal transitions for J = 11, 12, and 13 are at 29585.1,

---

6. R. C. Woods, A. M. Ronn, and E. B. Wilson, Rev. Sci. Inst. 37, 927 (1966).

7. P. E. Larson, Ph. D. Thesis, Harvard University, 1970.

Reproduced with permission of the copyright owner. Further reproduction prohibited without permission.

Reproduced with permission of the copyright owner. Further reproduction prohibited without permission.

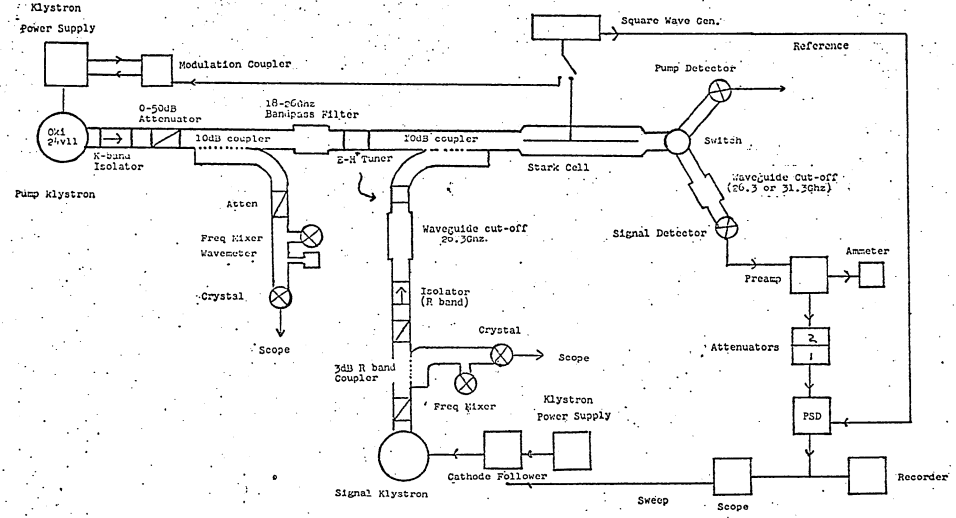

Figure 2. Block Diagram of MMDR Spectrometer

34953.5, and 40,766 MHz respectively. They were observed using EMI R9518, Oki 35V10, and Beam 40BTA tubes. Because not much signal power is needed, the efficiency with which the signal radiation is introduced into the sample cell is not particularly crucial. To measure the signal frequency and monitor the power output of the signal klystron, a 3 db R-band coupler splits the signal radiation into two fields of similar strength. The microwave attenuators are used to adjust the signal power level, and the isolator and waveguide cutoff filter are necessary to isolate the signal arm from the pump field. A 10 cm section of Q-band waveguide with a TE_{10} cutoff at 26,430 MHz should attenuate a field of frequency 24660 MHz by more than 100 db. The EH tuner on the signal arm can be adjusted to optimize power transfer from the signal arm into the cell. The R band radiation is fed into the cell via a 10 db K-band coupler. The impedance mismatch is horrendous, but at the particular frequencies of interest, sufficient power is introduced into the cell.

The signal klystron is frequency swept through an absorption line, and the radiation is detected by an appropriate silicon diode. The rectified signal is amplified by a tuned 100 KHz preamplifier, attenuated by a calibrated attenuator system, and amplified by a phase sensitive detector (Princeton Applied Research HR-8, to be called PSD). It is very useful to monitor the output of a pump crystal detector after the cell as one tries to optimize the experimental arrangement. In this manner one can adjust the pump reflector voltages and EH tuner to maximize the power passing through the cell while at the same time

Reproduced with permission of the copyright owner. Further reproduction prohibited without permission.

matching the power levels at the two pump frequencies. If this latter condition is not satisfied, the residual amplitude modulated signal tends to present spurious signals that can be comparable to or larger than the signal of interest.

Once the magnitude of the double resonance signal is known, it is possible to adjust the various circuit elements in such a manner that the magnitude of the spurious signals is reduced to such a level that the double resonance information can be collected to the desired level of accuracy. This preliminary work can be done before any sample is admitted to the system. Of course, it is less than candid to suggest that this trivial process is easy. It is not unusual to have to spend long hours trying to get the system working.

The double attenuator arrangement between the preamplifier and the PSD is necessary to maintain detection system linearity. In order to match the input impedance of the HR-8 to the preamp-attenuator load, a transformer was wound that was to match the balanced 100 Ω HR-8 input impedance to the unbalanced 250 Ω attenuator load. Subsequent linearity tests showed that it was still necessary to use a single gain level of the PSD and a single attenuator level of attenuator 1. Then one can vary attenuator 2 over a 40 db range and preserve system linearity to within 3%. Furthermore, with this arrangement the phase of a Stark signal as determined by the PSD was shown to be constant to within 1° over a 30 db range of signal attenuation. To measure the signals with greatest accuracy and consistency, it was necessary to use the recorder rather than the scope, especially after it was found that the vertical

Reproduced with permission of the copyright owner. Further reproduction prohibited without permission.

deflection amplifiers of the available oscilloscopes were sufficiently nonlinear to present problems. It should be emphasized that any measurements will be unreliable if made on a system for which systematic linearity checks have not been made. This is especially true for measurements where one is comparing signals varying over considerable magnitudes.

The cell used to contain the sample is a 10 foot X-band nickel Stark cell. It was used primarily because of its excellent leak-free nature. After evacuation the leak rate from the outside was generally less than 0.4 microns/hour. The cell leak rate was no larger than the residual outgassing through the manifold stopcocks. It was felt that this factor more than compensated for the fact that the pump power would be somewhat lower than could be optimally obtained from the Oki klystron. Since nickel has a greater specific resistivity than copper (6.8 vs 1.7 μΩ-cm), the cell attenuation will be greater by a factor of two.[8] Also, had one chosen to construct a K-band cell, one would obtain greater power densities because of the smaller cross-sectional area.

2. Procedure

Each HCN-rare gas mixture was prepared in the cell and vacuum line. First, an appropriate pressure of pure HCN (about 5 μ of Hg) was established in the system. To achieve this, the system was initially dosed

---

8. See reference 3, page 385.

Reproduced with permission of the copyright owner. Further reproduction prohibited without permission.

with about 60 μ of HCN and this pressure was slowly reduced to the desired pressure allowing the system to reequilibrate at intermediate pressure points. In this manner, one could establish an HCN pressure that would be constant to about 5% over a period of an hour. This rather elaborate procedure is necessary because HCN adsorbs strongly to the walls of the system, and one must be careful to reach a proper steady state near equilibrium. After the HCN has reached equilibrium at the desired initial pressure, small doses of the rare gas can be introduced to the vacuum line and cell. Because the 500 ml rare gas sample bulbs were at a pressure of several hundred mm Hg, an extra stopcock between the sample bulb and the manifold was necessary to allow the addition of small gas doses on the order of 30 to 40 μ each. The volume between the stopcocks was about $\frac{1}{2}$% of the 1.4 liter cell-manifold volume, and by adjusting the extra Teflon hi-vac stopcock, one could leak the desired small pressure from the smaller volume into the cell-manifold volume.

Measurements of a double resonance relative intensity and phase shift could be made as a function of total sample pressure up to 400 μ of Hg for helium, 250 μ Hg for argon, and 125 μ Hg for xenon. The maximum of the foreign gas pressure is determined by dielectric breakdown characteristics of the cell at the high Stark voltages necessary, but it also coincides with very small signal-to-noise ratio. Comparison data was collected for pure HCN over the range from 4 to 60 μ of Hg.

The pressure measurements were made with an MKS Baratron pressure meter Type 77 using the 77 H-1 sensing head. The instrument is a

Reproduced with permission of the copyright owner. Further reproduction prohibited without permission.

capacitance manometer that was calibrated at the factory before these experiments against an air-dead weight tester and was found to be linear to 0.1% across the entire 0-1 mm range. The day to day reproducibility is rated at better than 0.1 μ.

The HCN, from American Cyanamid, was provided by the Klemperer research group, and it was purified by freezing with liquid N_2 and pumping away remaining gases. The most likely remaining impurity was thought to be water, and as a check, the water absorption at 22232 MHz was monitored by Stark detection as HCN sample was introduced into the cell. Although there is a very weak signal always present, there was no increase in signal intensity as the sample was introduced. Helium of 99.99% purity was obtained from Med Tech Gases, Inc., and was used without further purification. Argon was obtained from Matheson and xenon from Linde. The purity of the latter two gases was checked by mass spectral analysis, and no impurities were detected within the limits of the spectrometer sensitivity.

The relative intensities and phases were measured in the following manner. With one of the pump frequencies within $\nu_o \pm 0.5$ MHz, there is an observable signal for most settings of the variable phase shifter of the HR-8. The reference phase is set to null the double resonance signal, and then by shifting the reference phase by 90° the double resonance signal is maximized. At that point the final adjustment of the pump frequency is made to further maximize the signal. In practice, recordings are made over several sweeps through the signal resonance as the pump is readjusted to be certain that the signal is maximized.

Reproduced with permission of the copyright owner. Further reproduction prohibited without permission.

Then a 90° shift of the reference phase allows a check that the HR-8 phase has been set correctly. On noting the null phase setting and the setting of the calibrated attenuator one has recorded the necessary information to use with the recorded signal traces. The double resonance modulation is then switched off and the Stark modulation is turned on. The PSD reference phase is readjusted to null the Stark signal and then after a quadrant shift of the reference phase, the signal is recorded. In general it is necessary to use a different setting of the calibrated attenuator to keep the double resonance and Stark signals of comparable size.

In Fig. 3A and 3B are presented traces of sample experimental results. The traces are to provide an indication of the signal to noise ratios. The most noticeable feature, however, is that there is no unique null of either a Stark or double resonance signal when one is 90° out of phase. Examination of nulls of the Stark signal in pure HCN shows that the difference in phase of "null a" to "null b" varies from less than a degree at 40 μ pressure to 4 degrees at 1 μ. For the double resonance signal in pure HCN the phase differences range from less than one degree at 40 μ to about 7° ± 2° at 4 μ for the $\Delta J = +1$ signal. For $\Delta J = +2$ signals the phases differ by only 2° ± 1° at 4μ and for the $\Delta J = +3$ signal it is 4° ± 4° at 5 μ. This phenomenon will be discussed in detail later. Nevertheless, the variations of apparent phase null over the range indicated have no detectable effect on the signal intensity when the phase shifter is quadrant-shifted for maximum signal size.

Reproduced with permission of the copyright owner. Further reproduction prohibited without permission.

Reproduced with permission of the copyright owner. Further reproduction prohibited without permission.

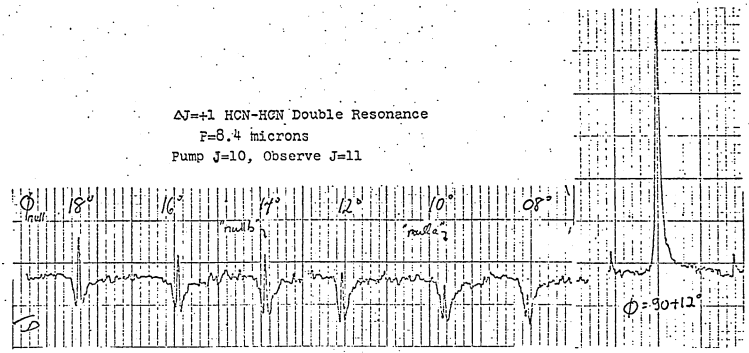

Figure 3A HCN-HCN Sample Traces

Reproduced with permission of the copyright owner. Further reproduction prohibited without permission.

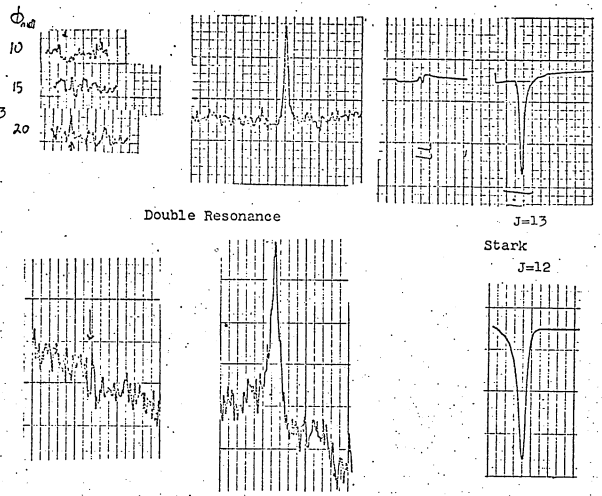

Figure 3B HCN-Foreign Gas Sample Traces

3. Results

a. Relative Intensities

The relative intensity is given by the ratio of the double resonance signal magnitude to the Stark signal magnitude times the ratio of the voltage attenuation factor. It has been found that within the accuracy of the work, the signal magnitudes are proportional to the peak heights. The experimental relative intensities are plotted against pressure in Fig. 4 for pure HCN and in Fig.s 5-7 for HCN and helium, argon, and xenon. In each figure we present the results for the different foreign gases for a given ΔJ signal.

For each data point the error bars indicate the uncertainty in that particular measurement. They are omitted where they would be similar in size to the data symbol. The uncertainty is generally determined by the baseline uncertainty due to the spurious residual double resonance signals. In pure HCN the scatter of $\Delta J = +1$ points above the 10 μ region reflects the fact that the pump klystron is not saturating the pump levels in this region, and it was not possible to reproduce the pump power level from day to day as the experiments were repeated. In the region above 20 μ, the Stark signals are not fully modulated, and corrections must be made for this fact. By 35 μ the Stark signal is about 10% smaller than it should be.

In the rare gas experiments, as the pressure of the foreign gas is increased, the signal heights decrease because of line broadening. Examination of the area of Stark signals showed that the total area

Reproduced with permission of the copyright owner. Further reproduction prohibited without permission.

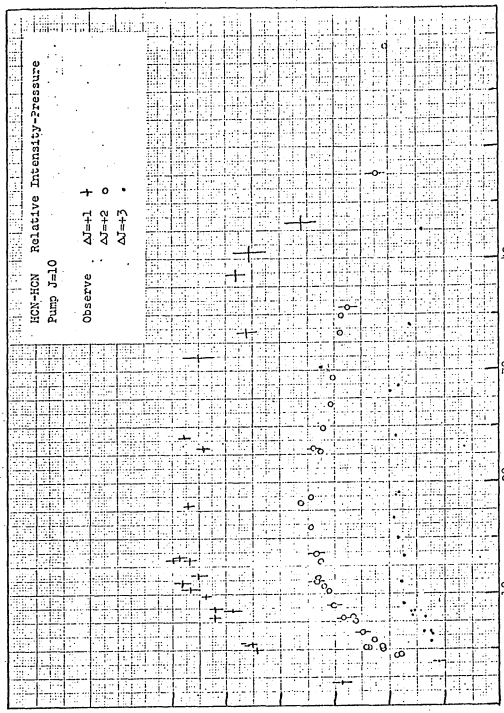

Figure 4

Reproduced with permission of the copyright owner. Further reproduction prohibited without permission.

Figure 5

Reproduced with permission of the copyright owner. Further reproduction prohibited without permission.

Reproduced with permission of the copyright owner. Further reproduction prohibited without permission.

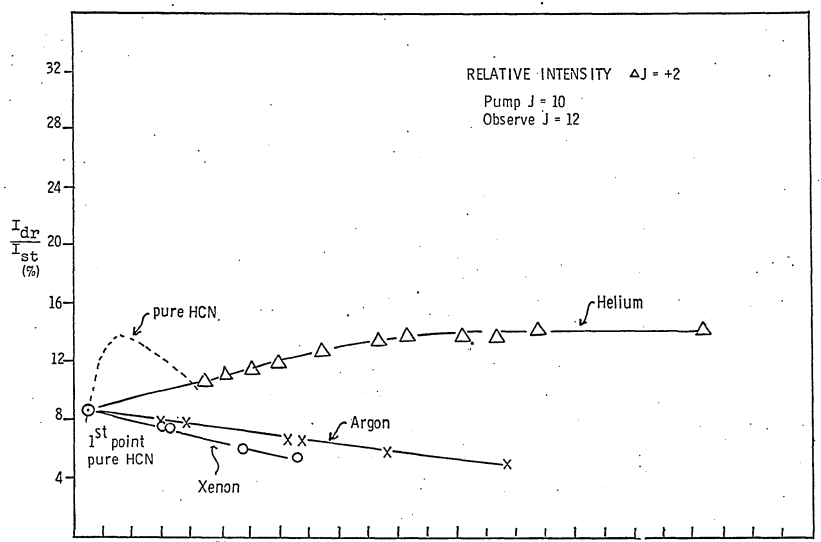

Figure 6

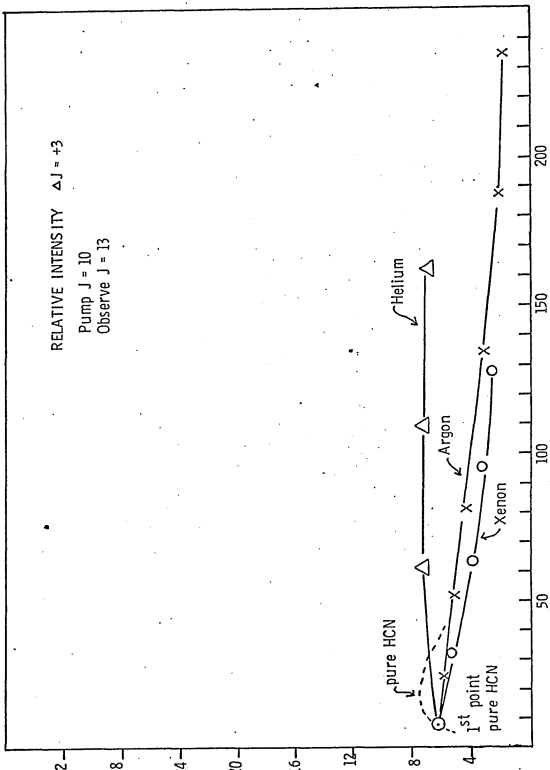

Figure 7

Reproduced with permission of the copyright owner. Further reproduction prohibited without permission.

remains constant to within several percent as the foreign gas pressure is increased. This demonstrates that HCN is not being forced off the cell walls by the foreign gases. For the higher pressures of xenon and argon, the uncertainties of the relative intensities are determined by the small signal to noise ratio of the double resonance signals.

Qualitative examination of the relative intensity data demonstrates that the results are "interesting." Helium behaves very differently than argon and xenon. In the former case we see an apparent preferential transfer to $\Delta J = +2$ and $\Delta J = +3$, while none to $\Delta J = +1$. These results imply that parity selection rules are followed. There is not equal population of upper and lower states. The $\Delta J = +1$ result might result from a large cross section, but no preferential population of the + or the - parity level. The high pressure plateau regions that are not observed in pure HCN reflect the fact that the linewidths for He broadening are less than 5% of the pure HCN parameter, and therefore, the pump transitions are saturated over greater pressure ranges. In the argon-xenon data we see that there is apparently no preferential transfer to either a + or - final parity state, but from a visual examination of the intensity data alone nothing can be said about the magnitudes of the ΔJ partial cross sections.

b. Phases

For a given gas and a given ΔJ double resonance experiment, the relative phase as a function of pressure was determined as described

Reproduced with permission of the copyright owner. Further reproduction prohibited without permission.

previously. The quantity of interest, however, is how the different phase curves for a given gas compare with each other. One must be able to measure absolute phases or to determine a suitable reference phase. There are two possible reference phases--the phase of the Stark signal or the phase associated with the applied pump modulation. The latter phase can be determined in principle by a simple procedure that has been used previously.[7] If a small portion of the modulated pump radiation is leaked to a detector crystal and the resultant rectified signal is fed into the preamp-amplifier system, there will be a large output signal associated with the residual amplitude modulation as the klystron oscillates alternately at one frequency and then the other. The reference phase shifter of the PSD can be adjusted to null this signal, and this provides a measure of the pump modulation phase itself. Once either this double resonance reference phase or the Stark reference phase is established, all double resonance phase shifts may be taken as the difference between the measured phase and the reference phase.

There are, however, logical objections to either reference in that both schemes omit part of the electronic circuitry that could be a source of phase variation in the double resonance experiment. The Stark phase completely omits the pump klystron and the circuitry by which the modulation is applied. Each time the pump klystron is readjusted, and certainly for each time the apparatus must be set up again, there could be different phase shifts. The phase detection of the pump power also has serious disadvantages. Which detector crystal should be used? The signal crystal, an R-band crystal, would be the most appropriate detector.

Reproduced with permission of the copyright owner. Further reproduction prohibited without permission.

It will rectify K-band radiation sufficiently well, but the isolating waveguide cutoff filter must be removed. The simplest detector to use is the K-band pump detector accessible in the general setup by the mechanical switch. If one uses this detector, one can not take into account properties of the R-band crystal and the signal radiation in general. That omission is undesirable as one wants to compare phases for different signal frequencies using different klystrons and different tuning characteristics of the R-band crystal detector. As will be seen later, a variable detector impedance and operating point do produce phase shifts.

An alternate approach is to assume that at the high pressure limit all phases should go to 0 or π as the linear model and our intuition insist. Examination of the phase data for pure HCN in the region of pressures greater than 25 μ is facilitated by considering the plot of phase as a function of $(\text{pressure})^{-1}$. A graphical analysis shows that the phase does vary linearly with 1/P in the high pressure region and that the slope of $\phi(1/P)$ for a given ΔJ experiment is well reproduced from experiment to experiment though the intercept is not. Least squares analysis of the data allowed the determination of slopes and intercepts. The intercepts could then be corrected to a standard intercept of π. With the data available, the intercepts determined by this procedure for $\Delta J = +2$ and $+3$ have uncertainties of $\pm 3\text{-}4°$, twice the value for the $\Delta J = +1$ uncertainty. Using this technique it is important that the crystal operating point remain constant only for a given experimental run.

Reproduced with permission of the copyright owner. Further reproduction prohibited without permission.

This last method was judged to be the most reliable method of comparing the phases from the different experiments. The uncertainty in a phase data point is then determined by the accuracy of the PSD phase shifter, the accuracy with which a null signal can be specified, and the accuracy of the calculated intercepts. These various sources of uncertainty are not independent. The apparent instrumental null of a pure HCN double resonance signal can usually be defined to within ± 1 or 2°. The uncertainty of this null is determined by signal to noise and the fact that as the pump frequency wanders, the null wiggles change magnitude. Of course, one must decide what lineshape is a null. Though "null a" of Fig. 3A is undoubtedly the correct effective null, for practical purposes at this point the difference between "a" and "b" may be considered a measure of phase uncertainties. The accuracy of the phase shifter of the PAR-HR-8 is conservatively rated ± 5% or 5°, whichever is smaller, but discussions with PAR representatives confirm that the phase shifts should be good to within 1° or 2°. For the experiments in pure HCN the high pressure phase data can be collected easily and therefore the intercept method is usable. Unfortunately, this is not true for the experiments with the foreign gases where the S/N ratio obtainable with the available technique is too small to determine high pressure phase to better than ± 5°.

In Fig.s 8-11 the phase information as a function of pressure is presented. The data for pure HCN in Fig. 8 represent phases corrected to the standard high pressure intercept. The uncertainties at lower pressures reflect the limiting accuracy of the phase due to the various

Reproduced with permission of the copyright owner. Further reproduction prohibited without permission.

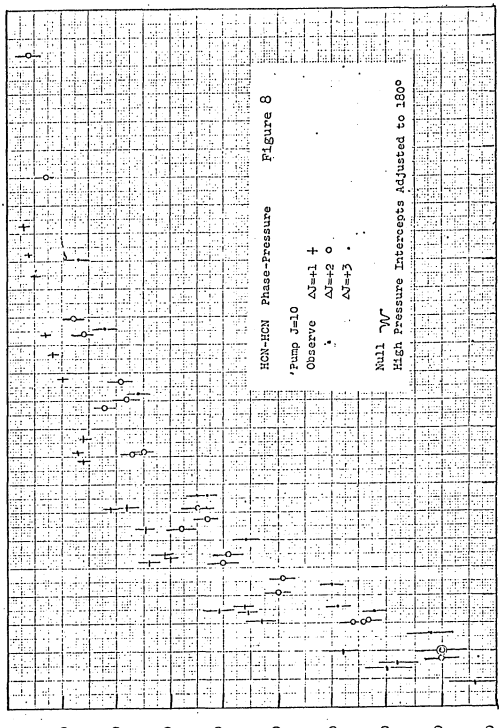

Reproduced with permission of the copyright owner. Further reproduction prohibited without permission.

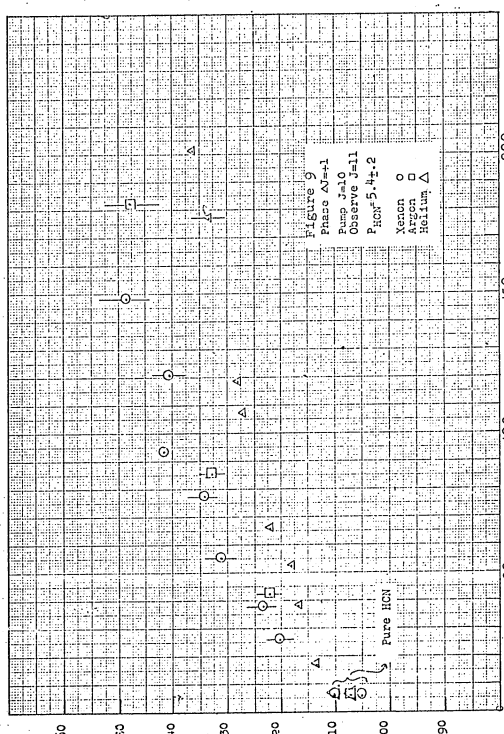

Reproduced with permission of the copyright owner. Further reproduction prohibited without permission.

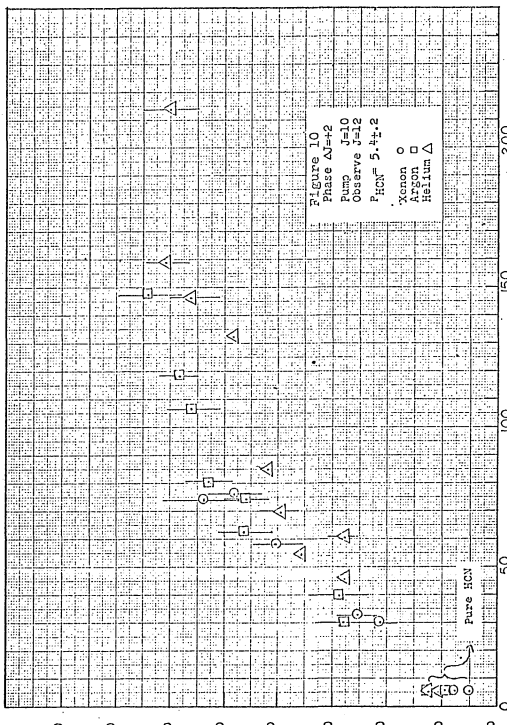

Reproduced with permission of the copyright owner. Further reproduction prohibited without permission.

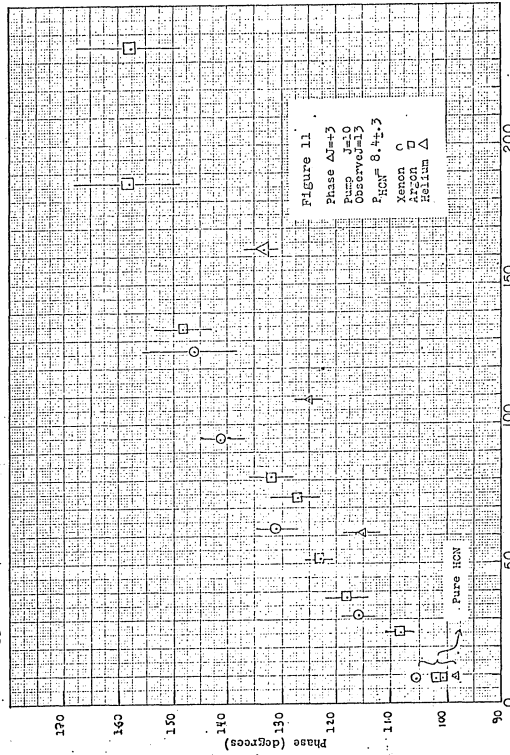

Reproduced with permission of the copyright owner. Further reproduction prohibited without permission.

sources of uncertainty. The data for the foreign gases has been corrected using the reference intercept from the pure HCN data taken at the same time. As with the relative intensities, the data is presented in a form that emphasizes the variation from gas to gas.

Examination of the phase data emphasizes several important features. For the different foreign gases the rates at which the phases approach their high pressure values correlates with the Lennard-Jones effective interaction diameter for the different atoms. All of these curves approach a high pressure value much more slowly than the HCN-HCN data. Furthermore, the HCN-argon and HCN-xenon data are essentially indistinguishable within the accuracy attainable. This feature was also found to be present for the relative intensity data, though there, because of the smaller experimental uncertainties, the results were clearly distinct.

In concluding this presentation of experimental results, it is important to note the relative uncertainties involved in the two different experimental quantities, the intensity and phase. For the relative intensity data each ΔJ curve is determined independently, and the numerical values are on the order of 0.1 ± 0.005. The percent error ranges from $\pm$ 1% to $\pm$ 5%. For the phase data the uncertainties are much greater. A single ΔJ phase curve varies at most 60° over the accessible pressure ranges, and there can be uncertainties up to $\pm 5^\circ$ for the phase determination at a single pressure. The uncertainties occur because of small S/N at high foreign gas pressure but are present at low HCN pressure because of the null wiggle. Unfortunately, one has to

Reproduced with permission of the copyright owner. Further reproduction prohibited without permission.

compare the phases of one ΔJ curve relative to the others, and as the uncertainties of a single curve propagate through the intercept reference technique, the errors are compounded. Hence, one arrives at the situation where for pure HCN at 5 μ pressure $\phi_{\Delta J=+1}(P) - \phi_{\Delta J=+2}(P) \approx 20°$, but the uncertainty will be on the order of ± 5°.

In this sense one sees that the relative intensity and phase information are nearly apples and pears. By scaling phases by 1/250, 1° = 0.004 and 180° = 0.7. The phase values are at least the same order of magnitude as the relative intensity numbers, but one must be very careful as one tries to use both phase and relative intensity data in a least squares procedure to determine rate constants.

B. Pressure Broadening Linewidth Parameter of the Microwave Absorptions

In order to use the linear rate theory, the diagonal elements Π_{ii} must be known. As we have discussed in Chapter I, in many circumstances the collisional linewidth parameters are a good measure of Π_{ii}. In that instance, the microwave linewidth will be given by

$$\Delta\nu_{JJ'} = \frac{1}{2}\left(\frac{1}{2\pi\tau_J} + \frac{1}{2\pi\tau_{J'}}\right) . \qquad (3)$$

For HCN J and J' are the doublet levels, and there is good reason to assume $\tau_J = \tau_{J'}$. Furthermore, in terms of Anderson's rotational linewidth theory we would expect the linewidths to be determined by ΔJ transitions where the intermolecular potential is of such a form that

$$\langle J K_{-1} K_1 M | V | J K_{-1} K_1 M' \rangle = 0 . \qquad (4)$$

In terms of the HCN energy levels this will hold for a first-order

Reproduced with permission of the copyright owner. Further reproduction prohibited without permission.

dipole-dipole interaction potential, the dominant interaction for pure HCN.

Examination of the literature[9] shows that pressure broadening of vibration-rotation lines in pure HCN has been studied many times. Interpretations of these results have generally concluded that the broadening of vibration-rotation transitions is determined by the collision-induced rotational transitions. The observed linewidth parameters all indicate a similar trend in the J dependence of the widths, but the reported values vary significantly in terms of absolute magnitude and the steepness of the J dependence. Results for three different IR vibration-rotation bands are listed in Table 1.

For HCN-rare gas mixtures, IR linewidth studies have been reported[10] for HCN-argon only. Because trial calculations with the linear kinetic model demonstrated that the computed double resonance results are reasonably sensitive to the J-dependent linewidths, it was decided to determine the values for at least some HCN-HCN and HCN-foreign gas collisional parameters.

---

9. For example:

9a M. T. Pigott and D. H. Rank, J. Chem. Phys. 26, 384 (1957).

9b L. Hochard-Demolliere, C. Alamichel, Ph. Arcas, J. Phys. (Paris) 28, 42 (1967).

9c G. Kortum and H. Verleger, Proc. Phys. Soc. 63, 462 (1949).

10. R. J. Thibault, A. G. Maki, E. K. Pyler, J. Opt. Soc. Am. 53, 1255 (1963).

Reproduced with permission of the copyright owner. Further reproduction prohibited without permission.

TABLE 1

HCN-HCN Linewidths (MHz/mm Hg)

halfwidth at halfheight

J	A This work	B Piggott and Rank[9a] (000) - (002)	C Arcas[9b] (000)-(001)	D Kortum[9c] (000)-(003)
3		27.0	42.0	
				46.0
6	31 ± 2	36.7	52.5	
7	34 ± 2	37.5	55.5	
8	(38 ± 3)	39.0	58.5	
9		38.2		50.0
10	(39 ± 4)	37.5	55.5	
				46.5
12		33.7	49.9	
				36.0
14		31.5	43.5	
15		28.7	42.0	

Reproduced with permission of the copyright owner. Further reproduction prohibited without permission.

The procedure used was to sweep through and record the zero field Stark absorption lineshape of a given J doublet for different pressures of pure HCN or for fixed HCN and different pressures of foreign gas. To achieve satisfactory resolution, it was necessary to use a phase-stabilized klystron. For the HCN signals, it was found that a sweep rate of 1 MHz/sec was adequate. From the recorded traces it was possible to measure the full width at half height.

For pure HCN, widths were determined over a pressure range from 8 to 40 μ of Hg. For the foreign gas mixtures in each case the initial pressure was about 8 μ of HCN and the foreign gas pressure was varied up to the pressure at which electric breakdown occurs in the presence of the high voltage Stark field. It was found that with the Stark modulation voltages that were accessible (up to 2000 V), the lines that were studied in the double resonance experiments ($J \geq 10$) were not fully modulated. For $J = 10$ the lineshape was visibly asymmetric, and even for $J = 8$ there was a problem. In these cases, an estimate was made of the center frequency, and using that, the halfwidth at half height could be determined. For comparison purposes, both the observed full width and estimated half width were also determined for certain lower J lines, and it was found that where the lines looked symmetrical, the values agreed. The observed widths were corrected for the effects of the 100 KHz modulation frequency.[11] From the observed linewidths as a

---

11. R. Karplus, Phys. Rev. 73, 1027 (1948).

Reproduced with permission of the copyright owner. Further reproduction prohibited without permission.

function of pressure, the linewidth parameters, $\Delta\nu_o$ in MHz/mm Hg, were determined by the method of least squares. In Table 1, Column A, are listed the linewidth parameters of pure HCN as determined by this procedure. In Table 2 are presented linewidth parameters determined for several J doublets for helium, argon, and xenon. Also included in Table 2 are the parameters reported for the argon broadening of the (000)-(001) HCN band. In both tables the large number of infrared J values are reported to emphasize the J dependence and also because they will be used in the Π matrix model. It is to be noted that the IR J values are averages of the P and Q branches, and the linewidth variation between any two adjacent J levels probably reflects experimental uncertainty. The uncertainties in the microwave linewidth parameters represent two standard deviations of the uncertainty in the slope as determined from the data. However, these slopes are sensitive to systematic errors as is evidenced by the difference between the asymmetric signal and the symmetrized signal of the J = 10 level.

Although it was not possible to measure the linewidths of the levels used in the double resonance experiments, the results are useful. On the basis of the HCN-HCN microwave linewidths, it appears that the infrared linewidths of Rank,[9a] Column B of Table 1, are the most reasonable values. The agreement between the microwave and IR linewidths for the HCN-argon parameters is perhaps better than one might expect, but it certainly is pleasing. The measured values of HCN-helium show that some careful consideration must be given before extrapolating to

Reproduced with permission of the copyright owner. Further reproduction prohibited without permission.

TABLE 2

HCN-Rare Gas Linewidths (MHz/mm Hg)

J	A HCN-He This work	B HCN-Ar This work	C HCN-Ar IR[a]	D HCN-Xe This work
4			2.6	
5			2.5	
6	1.45 ± .1	2.15 ± .1	2.3	2.2 ± .1
7	1.55 ± .1	2.1 ± .1	2.2	2.3 ± .2
8	(1.65 ± .2)		2.2	(2.15 ± .1)
10	(1.9 ± .25)		2.0	(2.45 ± .2)
11			1.9	
12			1.9	

a Thibault et al., J. Opt. Soc. Am. 53, 1255 (1963).

Reproduced with permission of the copyright owner. Further reproduction prohibited without permission.

the many other J values that are necessary in the quantitative analysis. Also, the linewidths in Table 2 support the comment made in the presentation of the phase results: the rate at which the double resonance phase signal increased with pressure towards a high pressure value increased from He to A to Xe. In the case of the rotational linewidths, we see that they also increase with increasing mass.

It is interesting to compare the interaction distances for microwave line broadening with the parameters from transport properties. Using Eq. (I-2) it is possible to convert the microwave linewidths to effactive cross sections, and using

$$\sigma = \pi b_{eff}^2 , \qquad (5)$$

one defines an effective interaction parameter, b_{eff}. In Table 2A are collected the cross sections and effective collision dimensions from the microwave broadening parameters and a cross section and diameter based on viscosity data for pure HCN. Also, using the Lennard-Jones parameters for the rare gas atoms and the additivity rule for mixtures, the Lennard-Jones parameters for the gas mixtures are estimated.

Examining the table shows that for pure HCN, the transport cross section is only 10% of the microwave cross section. However, the Lennard-Jones diameter for HCN-helium is a little bit larger than the microwave parameter, and for argon and xenon the Lennard-Jones parameters are a little smaller. The Lennard-Jones parameters have only a very qualitative meaning. The parameter for pure HCN is based on the assumption that the interaction potential is isotropic. In any event, the

Reproduced with permission of the copyright owner. Further reproduction prohibited without permission.

TABLE 2A

Cross Sections from Rotational Linewidths

and Transport Data

	HCN-HCN	HCN-He	HCN-Ar	HCN-Xe
Rotational Linewidths				
$\Delta\nu$ (MHz/mm)	40	1.6	2.1	2.2
σ (A^{o2})	1570	23.	67.	76.5
b*(A^{o})	22.	2.7	4.6	5.0
Transport Parameters				
d (A^{o})	5.7[a], 3.06[b]	2.85[b,c]	3.3[bc]	3.6[bc]

a A diameter from viscosity data from G. Bird, J. Chem. Phys. 38, 2678 (1963).

b Stockmayer potential parameter from J. O. Hirschfelder, C. Curtis, and R. B. Bird, Molecular Theory of Gases and Liquids (Wiley and Sons, New York, 1954).

c $d_{HCN-FG} = \frac{1}{2}(d_{HCN-HCN} + d_{HCN-FG})$

Reproduced with permission of the copyright owner. Further reproduction prohibited without permission.

difference between the pure HCN and the HCN mixtures indicates that collisions in the gas mixture must represent relatively short range interactions, and this must be taken into account as one analyzes the double resonance results.

IV. Analysis of Experimental Results

It is the purpose of this analysis to find sets of rate constants, $\underset{\sim}{\Pi}$ and $\underset{\sim}{d\Pi}$, that reproduce the experimental results for energy transfer in pure HCN and in HCN-rare gas mixtures when used in a program to calculate the relative intensities and phase shifts. First we obtain a set of rate constants that accounts for energy transfer experiments in pure HCN. Once these constants are known, it is possible to find a set of constants for the HCN-rare gas interaction. Having found a zeroth-order set of constants, we then present a rather technical discussion about attempts to improve the values for each set of constants. In particular, we discuss the problem of the uniqueness of the rate matrices that reproduce the experiments. Clearly, if there are more than one set of rate constants that are satisfactory, one can not say on the basis of the fitting procedure alone which set is more likely to be physically meaningful.

A. A First Set of Rate Constants

For a single type of collision interaction, a rate matrix of dimension N has at most N x N parameters necessary to specify the entire matrix. There are, however, a series of constraints and physically

Reproduced with permission of the copyright owner. Further reproduction prohibited without permission.

reasonable approximations that reduce the number of parameters to a small enough number such that the model parameters might have physical meaning. Where the diagonal elements can be determined by independent experiments (linewidths), and because the double resonance experiment involves perturbation about the equilibrium population values (detailed balancing), for a single matrix there will be at most $\frac{N(N-1)}{2}$ parameters. On the basis of experimental results even further reductions are possible.

In Table 3 are presented sets of kinetic parameters that give reasonable reproduction of the experimental data, and in Figures 12-14 can be found average experimental data points and curves computed from the rate constants. The curves are smooth lines drawn between calculated points. Calculations at 8 pressures from 2 μ to 40 μ of pure HCN or up to 250 μ of foreign gas are sufficient to define the curves quite well. A Fortran IV computer program developed previously[1] for pure HCN has been adapted for running on the IBM 360 and a similar program has been written to calculate relative intensities and phase shifts for the case of HCN-foreign gas mixtures. Modifications of these programs are also used in conjunction with a non-linear least squares program[12] from the IBM 7094 share library. The least squares program was used to vary the parameter systematically to find better fits to the data. Pertinent details about the programs are found in an Appendix.

---

12. D. W. Marquardt, Least Squares Estimation of Non-linear Parameters, IBM Share Library, SDA 3094-01.

Reproduced with permission of the copyright owner. Further reproduction prohibited without permission.

TABLE 3

First Rate Constants that Account for

Energy Transfer Experiments

	A	B	C
	$\Pi^{HCN-HCN} + \delta\Pi$	Π^{HCN-Ar}	Π^{HCN-He}
	HCN-HCN	HCN-Ar	HCN-He
k_{0a}	0	1	1
k_{1a}	1	0.026*	0.03*
k_{1n}	0.21	0	0
k_{2a}	0.167	0.17*	0.97*
k_{2n}	0	0	0
k_{3a}	0.136	0.03*	0.17*
k_{3n}	0	0	0
DPA	1		

* Parameters varied to reproduce relative intensity data points found in Fig.s 13 and 14.

Reproduced with permission of the copyright owner. Further reproduction prohibited without permission.

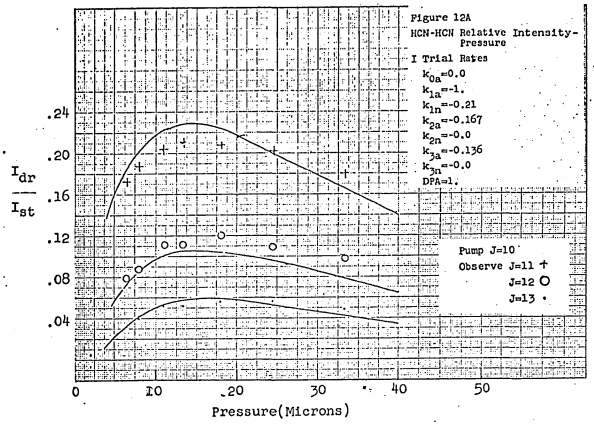

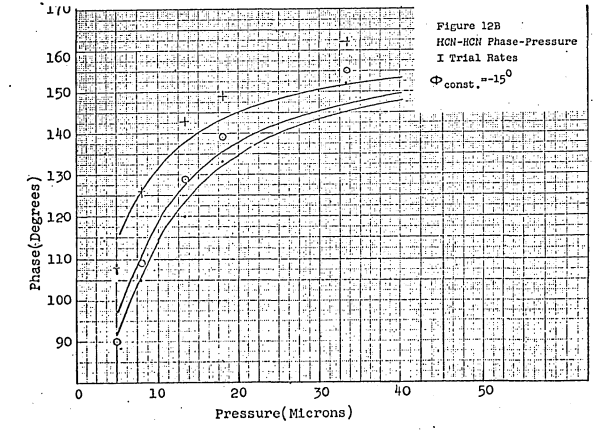

Reproduced with permission of the copyright owner. Further reproduction prohibited without permission.

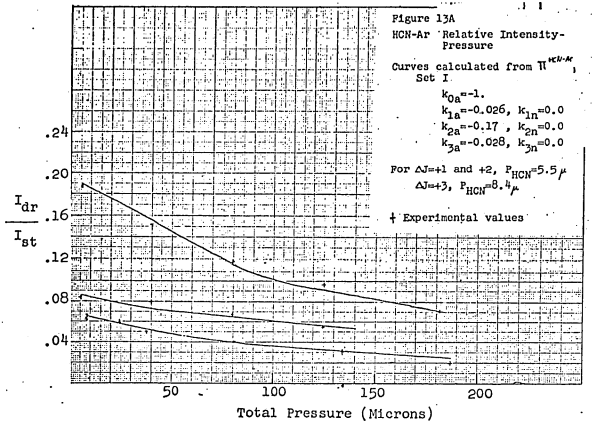

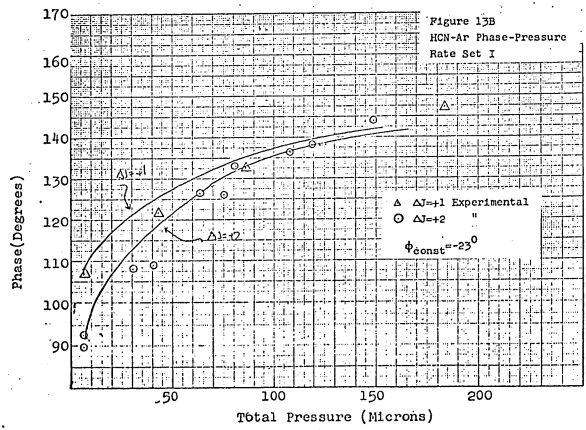

Reproduced with permission of the copyright owner. Further reproduction prohibited without permission.

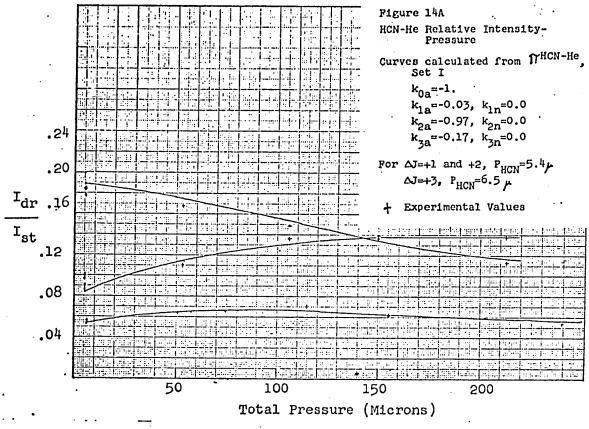

Figure 14A
HCN-He Relative Intensity-Pressure

Curves calculated from Γ^{HCN-He}, Set I

k_{0a}=-1.
k_{1a}=-0.03, k_{1n}=0.0
k_{2a}=-0.97, k_{2n}=0.0
k_{3a}=-0.17, k_{3n}=0.0

For ΔJ=+1 and +2, P_{HCN}=5.4μ
ΔJ=+3, P_{HCN}=6.5μ

+ Experimental Values

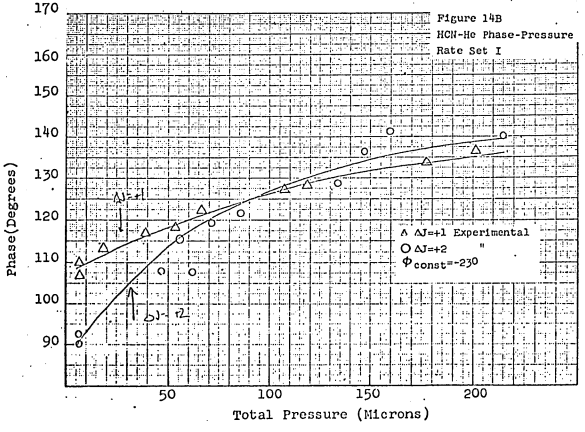

Figure 14B
HCN-He Phase-Pressure
Rate Set I

Reproduced with permission of the copyright owner. Further reproduction prohibited without permission.

1. HCN-HCN

To determine the rate constants for pure HCN, Larson, et al.[1] adopted several assumptions that dramatically simplify $\underset{\sim}{\Pi}^{HCN}$. A matrix of dimension 30 was used that was centered about the pump level J = 10. Because each J doublet must be included, the matrix was truncated to include from J = 3 to J = 17. Furthermore, they assumed that transitions of each type (k_{0a}, k_{1a}, k_{2a}, etc. of Fig. 1) make up the same fraction of the diagonal element for each state. It is certainly reasonable that the equilibrium rates should be the same for each level of a J doublet, and for pure HCN second order perturbation calculations by Rabitz[13] suggest that in the region studied by the experiments, the rate constants are slowly varying functions of J. This approximation of J independence must be very crude for the low J levels, and it necessitates that the final rates obtained will be at best an average over the region that provided the experimental data. With this assumption, however, it is necessary to specify the elements only for a single J level. There are then N - 1 parameters in the matrix. Because the experimental results showed that the dipolar interactions dominate and that the energy transfer signal decreases as ΔJ increases, it was assumed that Π_{ij} should have significant size only for small ΔJ. Energy transfer for polar gases will be dominated by collisions that change J only a small number of units: non-zero elements of $\underset{\sim}{\Pi}$ will be clustered

13. H. Rabitz and R. G. Gordon, J. Chem. Phys. 53, 1815 and 1831 (1970).

Reproduced with permission of the copyright owner. Further reproduction prohibited without permission.

in bands along the diagonal.

In this manner, the matrix $\underset{\sim}{\Pi}^{HCN}$ was reduced to five collisional parameters k_{0a}, k_{1a}, k_{1n}, k_{2a}, k_{3a}--only four of which are independent because of the constraint $\sum_i \Pi_{ij} = \Pi_{jj}$. Furthermore, the pump power was treated as a parameter by introducing in analogy to Eq. (I-22a)

$$\delta\Pi_{pq} = \frac{2\pi DPA}{\sqrt{0.01 + \Delta\nu^2 P^2}} \tag{6}$$

where DPA is a pump power parameter that is to be fit to the experimental results, and the 0.01 in the numerator is to include the other line broadening factors that enter at low pressure.

Lastly, a specific model of the wall collision was assumed:

$$\Pi_{ij}^{HCN\text{-}wall} = c\,(\delta_{ij} - n_i^{eq}) .$$

The model asserts that the collisions with the wall return the population to Boltzmann equilibrium, a view that is generally espoused in theories of gas collisions.[14] With this model

$$\frac{k_{\Delta J = +7}}{k_{\Delta J = +1}} \approx 0.47 ,$$

while the energy that must be converted to rotation from translation is 0.15 kT for J = 10 → 11, but 1.4 kT for J = 10 → 17. This classical kinetic theory model is based on a picture where a molecule spends time on the wall at each collision, and it is not obvious that wall inter-

---

14. For example, R. H. Fowler, Statistical Mechanics, (Cambridge University Press, London, 1929).

Reproduced with permission of the copyright owner. Further reproduction prohibited without permission.

actions affecting the rotational lifetimes must be that strong.

However, the effects of wall collisions on microwave broadening have been studied, and the rate of wall collisions, c, in an X-band cell is much smaller than the intermolecular collision rate over the pressures used in these experiments. Furthermore, in terms of experimental observables, the magnitude of c would be highly correlated with the effective pump power level.

Elementary gas kinetic theory shows that

$$n = \frac{1}{4} N \bar{v} A \tag{7}$$

where n is the number of molecules hitting a surface per time, N is the number density of the gas, $\bar{v}$ is an average velocity, and A is the surface area. If

$$\bar{v} = \sqrt{\frac{8kT}{\pi m}}$$

then $\Delta\nu_{wall} = \frac{1}{2\pi\tau} = \frac{1}{4\pi^{3/2}} \frac{A}{V} \left(\frac{2kT}{m}\right)^{1/2}$. On considering the geometry of two infinite parallel plates separated by a distance a, Danos and Geschwind[15] found

$$\Delta\nu_{wall} \approx \frac{0.1}{a} \left(\frac{2kT}{m}\right)^{1/2},$$

a value approximately twice that from the cruder theory, while Johnson and Strandberg[16] feel a frequency still four times greater would be appropriate. Using the Danos formula and noting that the appropriate

---

15. M. Danos and S. Geschwind, Phys. Rev. 91, 1159 (1953).

16. R. H. Johnson and M. W. P. Strandberg, Phys. Rev. 86, 811 (1952).

Reproduced with permission of the copyright owner. Further reproduction prohibited without permission.

dimension in a Stark cell is the septum to wall distance, one finds

$$\Delta\nu_{wall} \approx 0.0082 \text{ MHz} .$$

Even at 2 microns of pure HCN, the collisional linewidth is almost eight times this quantity. In Fig. 2 of Appendix II can be seen the effects of different wall collision rate constants. In the computation to follow, a value of $\Delta\nu_{wall} = 0.0093$ MHz is used.

For a starting point for our calculations it is reasonable to use the same assumptions to limit the number of the parameters but to use the new linewidths of Table 1 Column B. It was found that the rate constants listed in Table 3 Column A reproduce the energy transfer experiments in pure HCN reasonably well. These constants were selected because they reproduce the experimental relative intensity and phase data in the region 4-8 μ of Hg of HCN, the region that was used as the experimental starting point for the gas mixtures. In fact, as can be seen in Fig. 12 these constants do not reproduce the HCN data over all pressures within experimental uncertainty. In these curves the experimental points of Figures 4 and 8 have been reduced to a smaller number of averaged points. To the calculated phase values a single constant scaling parameter has been added, $\phi = -15°$. For the relative intensities, one notes that $\Delta J = +1$ is overemphasized while the $\Delta J = +2$ values are a little low. This discrepancy is necessary as one seeks to produce the proper lag between the $\Delta J = +1$ and $\Delta J = +2$ phase curves while using only five nonzero rates. On the phase curves it can be seen that the calculated values do not generate the apparent steepness of the change in phase with pressure. It should be remembered that the experimental

Reproduced with permission of the copyright owner. Further reproduction prohibited without permission.

curvature will be related to the null wiggles, and also that because the experimental curves are corrected to the high pressure intercept of 180°, there should be no additive phase factor. Hence, the additive factor that has been introduced is used to compensate for the insufficient curvature in the computed values.

2. Argon-Xenon

The experimental double resonance results for argon and xenon were very similar. There is reason to believe that the differences can be accounted for by the linewidth parameters alone and that the rate matrices for the two collision partners will be very similar. Since there are no available xenon infrared linewidth parameters for the many J states necessary, it was considered adequate to try to find rate matrices to account for the argon results only.

For argon, there is no apparent preferential population of final states for $\Delta J = +1$, $+2$, or $+3$. The simplest starting point for fitting is to assume that $\Delta J = 0$, k_{0a} transitions dominate, and then find those small non-zero values for k_{1a}, k_{2a}, and k_{3a} that adjust the calculated curves to the observed data. Using the HCN-argon linewidth parameters from Table 2 Column C as the estimate of the diagonal elements, Π_{ii}^{HCN-Ar}, and the HCN-HCN parameters of Table 3, one finds that the HCN-argon parameters of Table 3 provide a best fit in the least squares sense to relative intensity data points. The calculated curves and the experimental points are presented in Fig. 13. One can see that the relative intensities are fit as well for the argon contribution as for the

Reproduced with permission of the copyright owner. Further reproduction prohibited without permission.

initial pure HCN starting point. In this phase plot and in all others to follow for the gas mixtures, only $\Delta J = +1$ and $\Delta J = +2$ curves are presented. The experimental scatter is of the same magnitude for the $\Delta J = +3$ data. For the calculated phases an additive phase shift of -23° has been included that adjusts the calculated phases for pure HCN to the experimental values.

3. HCN-Helium

With helium as the perturber we had observed collision induced population transfer that followed definite parity rules and demonstrated particular J preference. In this instance it is even difficult to find linewidth parameters to estimate Π_{ii}^{HCN-He}. In order to make calculations one must estimate the J dependent linewidth parameters on the basis of the four microwave linewidth parameters. In Table 4 are listed three different sets of linewidth parameters that demonstrate slightly different J dependencies. For a first approximation the values in Column A are used for the diagonal elements of the rate matrix. The linewidths might be chosen by analogy to the CO-He parameters because CO and HCN have comparable masses and rotational constants (B_o(CO) = 57.9 GHz vs B_o(HCN) = 44.4 GHz). However, some authors report a slight decrease[17] of linewidth with J for the CO-He broadening while others[18] suggest a

---

17. D. Draegert and D. Williams, J. Opt. Soc. Am. 58, 1399 (1968).

18. D. H. Rank, D. Eastman, B. S. Rao, and T. H. Wiggins, J. Mol. Spect. 10, 34 (1963).

Reproduced with permission of the copyright owner. Further reproduction prohibited without permission.

TABLE 4

Some Possible J Variations for

HCN-He Linewidths
(MHz/mm-Hg)

J	A	B	C
3	1.75	1.2	1.55
4	1.60	1.3	
5	1.50	1.4	
6	1.45	1.45	
7	1.55	1.55	
8	1.65	1.65	
9		1.8	
10		1.9	
11		2.0	
12			
13			
14			
15			

Reproduced with permission of the copyright owner. Further reproduction prohibited without permission.

slight increase with J.

The basic structure for the foreign gas matrix was to assume k_{0a}, k_{2a}, and k_{3a} to be dominant and to allow for a small k_{1a} contribution. All other rates are set to zero. Since only relative rate constants are important, there are then three parameters to be adjusted. Once again, the parameters were adjusted to reproduce the relative intensities only. In Table 3 can be found the rate constants that generate the curves of Fig. 14. In this case we note that even the experimental phase points are reasonably well accounted for.

The foreign gas parameters presented reproduce the relative intensities as a function of pressure and, as we have seen, even the phases surprisingly well. In our fitting procedure one can determine residuals between calculated and observed data points, and from this one can determine parameter uncertainties. Before proceeding to that level, it is more important to make some evaluation of the basic model being used. Are there problems of multiple minima in a least squares fitting procedure?

B. Refinements of Results

In order to make some estimate of the physical significance of the derived rate constants, one has to consider other sets of parameters that might reproduce the results. To this point, the rate constants for the gas mixtures have been found from a consideration of relative intensities only. Do the phase curves contain new usable information? The work that follows is a rather technical discussion of various aspects

Reproduced with permission of the copyright owner. Further reproduction prohibited without permission.

of the model and the experimental data that lead to the conclusions:

(1) The uniqueness of the foreign gas rate constants can not be guaranteed. For both the argon and the helium cases we will find other relative rates that reproduce the relative intensity data. Various important sets of rate constants are presented in Table 5, and are discussed later.

(2) There is new information contained in the phase curves, but to be usable the accuracy of the curves would have to be accurate to within ±2°.

(3) There is strong evidence that difficulties in the determination of the phase data are partly caused by quantum mechanical phenomena that will not be accounted for by the semiclassical rate expressions.

1. HCN-HCN Parameters

As a starting point, it is interesting to note what the uncertainty of the calculated double resonance phenomena would be on the basis of approximations made in the calculations. In Fig. 1 of Appendix II are presented calculations that show how the relative intensities and phases vary with matrix size for an assumed set of rate constants and linewidths. A matrix of dimension 30 is in fact large enough such that no effects of the matrix truncation are found in the observed levels.

The errors introduced by assuming that $(\underset{\sim}{\Pi} + \underset{\sim}{\delta\Pi})$ is symmetrizable are less than experimental uncertainty even for relative intensities. $(\underset{\sim}{\Pi} + \underset{\sim}{\delta\Pi})$ can not be rigorously symmetrized. However, because the effect of pump perturbation is only a small change in the populations $(\underline{\delta n} \leq$

Reproduced with permission of the copyright owner. Further reproduction prohibited without permission.

TABLE 5

$\underset{\sim}{\Pi}^{HCN-FG}$

A. Rates for HCN-Argon

	I	II	III
k_{0a}	1.	1.	0.1
k_{1a}	0.026	0.57	0.9
k_{1n}	0	1.	1.
k_{2a}	0.17	1.9	0.35
k_{2n}	0	1.	0
k_{3a}	0.03	1.1	0.03
k_{3n}	0	1.0	0

B. Rate for HCN-Helium

	I	II	III
k_{0a}	1.	1.	0.24
k_{1a}	0.03	0.93	0.82
k_{1n}	0	0.9	1.0
k_{2a}	0.97	3.0	2.36
k_{2n}	0	0	0
k_{3a}	0.17	0.2	0.34
k_{3n}	0	0	0

Reproduced with permission of the copyright owner. Further reproduction prohibited without permission.

$\frac{h\nu}{2kT} < .01$), the matrix may be considered to be symmetrizable for the purposes of this work. Eq. (10) of Chapter I shows how $\underset{\sim}{\Pi}$ can be symmetrized, and if one applies a similar transformation to ($\underset{\sim}{\Pi} + \underset{\approx}{\delta\Pi}$) with the steady state populations of Eq. (I-11), the resultant matrix is nearly symmetric. Relative intensities and phases calculated by using either the top or bottom half of the resultant matrix differ by at most 1 part in 75 at 2 μ pressure and 1 part in 200 at 5 μ. An IBM System 360 Scientific Subroutine Package Program, ATE1G, was used that calculates eigenvalues for a general real matrix. It was found that the correct eigenvalues agree to 4 or 5 places with the approximate value. There are no complex eigenvalues for $\underset{\sim}{\Pi} + \underset{\approx}{\delta\Pi}$ for reasonable rates for pure HCN and for microwave powers up to 1000 times the power levels actually used.

In all the calculations, the equilibrium populations must be specified. For HCN in the $v_2 = 1$ state the rotational parameters must be estimated from various sources, and the rotational constant is known to only 1%. However, the uncertainties do not change the equilibrium populations by more than 2% in the levels of interest and hence have no effect on the calculations. For reference, in Table 1 of Appendix II can be found lists of the molecular parameters and the set of equilibrium populations found from the parameters.

If we are to decide whether or not the linewidths are proper estimates of the diagonal matrix elements, we must first know what variations in the calculations would be caused by the uncertainties in the experimental linewidths. In the gas mixtures, the magnitude of the

Reproduced with permission of the copyright owner. Further reproduction prohibited without permission.

mixture linewidth parameters relative to pure HCN parameters will clearly be important. Furthermore, for each set of linewidth parameters, the J dependence is important. These facts are demonstrated in Fig. 15 where we have calculations of the relative intensities and phases for pure HCN for two different sets of linewidth parameters, the values from columns B and C of Table 1. In particular, it is significant to note that the effects on the phases are dramatic. All curves go to a high pressure limit of 180° ± 1°, but the different parameters affect the steepness of the phase-pressure curves. In the low pressure region there is a shift of 10° between the curves while in the higher pressure region the shift is only 5°. Furthermore, one can see that there is also a small shift in spacing between the corresponding ΔJ curves. In the latter case the differences are not significant, only 2°. However, what is striking is that the $\Delta J = +2$ curve for one set of linewidths is superimposed on the $\Delta J = +1$ curve of the other set of linewidths.

Examination of the relative intensity curves suggests that the larger linewith parameters are behaving partly as higher effective pressures. The maximum value of the relative intensity is not changed much in magnitude, and its position is shifted to somewhat lower pressures.

2. Argon Analysis

Once we have a sense of the effects of the "constants" in the calculations, it is possible to consider alternate rate structures for the gas mixtures. Is it possible that the relative intensity data for the

Reproduced with permission of the copyright owner. Further reproduction prohibited without permission.

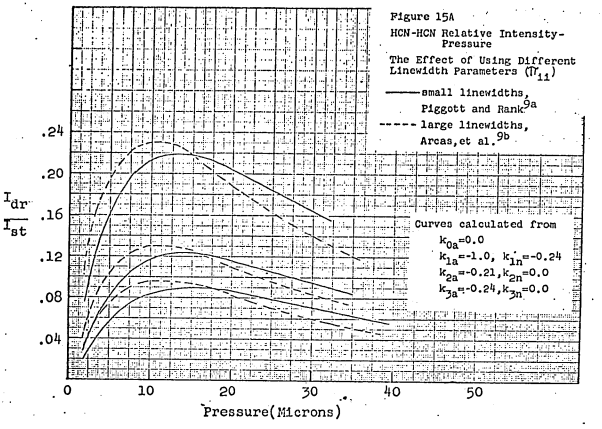

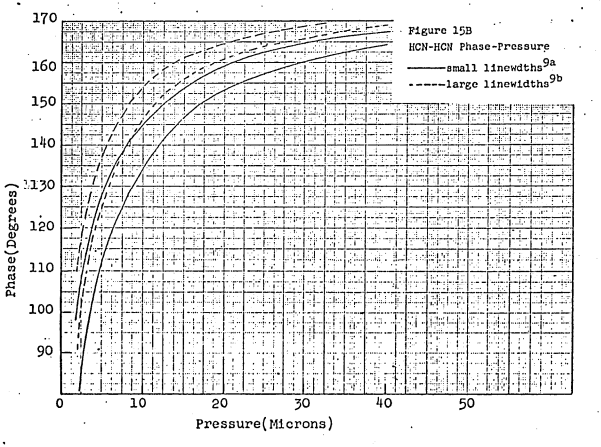

Reproduced with permission of the copyright owner. Further reproduction prohibited without permission.

argon-xenon experiments may be accounted for by sets of rates that do not possess parity preference, i.e. for $k_{ja} \approx k_{jn} > 0$? A dominant hard collision interaction that populates many levels with approximately equal probability, and, in particular, with no parity preference, would be one such set of rates. The hard collision rate proposed for the wall collisions suggests a possible structure for the rate matrix. However, as noted previously, that J distribution is probably much too broad. It is more sensible to assume that even a "hard" collision will only rarely cause a change in J for which the associated conversion between translational and rotational energy would be greater than kT. For HCN in the initial state J = 10, when $\Delta J = +5$, $\Delta E \approx kT_{room}$, but for $\Delta J = +8$, $\Delta E \approx 2.5\ kT_{room}$.

For a first trial, it was assumed that all constants up to $\Delta J = +4$ were equal--k_{0a}, ..., k_{4n}. Calculations were made comparing this assumption with the assumption that the linewidth was made up entirely of the "hard collision" model that distributes molecules according to equilibrium populations. It turns out that in terms of the double resonance observable, the results are identical, i.e. the relative intensities for the two calculations agree to within 0.003 and that the phases agree to within 1°. Then, starting with equal rates up to $\Delta J = +4$, the k_{1a}, k_{2a}, and k_{3a} parameters were adjusted to reproduce the relative intensities. A few adjustments were tried and with more time on the computer, a better fit can be obtained. What is important is that set II in Table 5 reasonably accounts for the relative intensity data as can be seen in Fig. 16-A-1.

Reproduced with permission of the copyright owner. Further reproduction prohibited without permission.

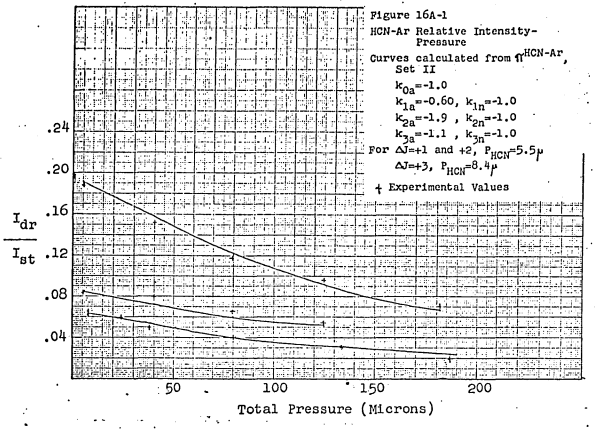

Figure 16A-1
HCN-Ar Relative Intensity-Pressure
Curves calculated from Π^{HCN-Ar}, Set II
k_{0a}=-1.0
k_{1a}=-0.60, k_{1n}=-1.0
k_{2a}=-1.9 , k_{2n}=-1.0
k_{3a}=-1.1 , k_{3n}=-1.0
For ΔJ=+1 and +2, P_{HCN}=5.5μ
ΔJ=+3, P_{HCN}=8.4μ
† Experimental Values

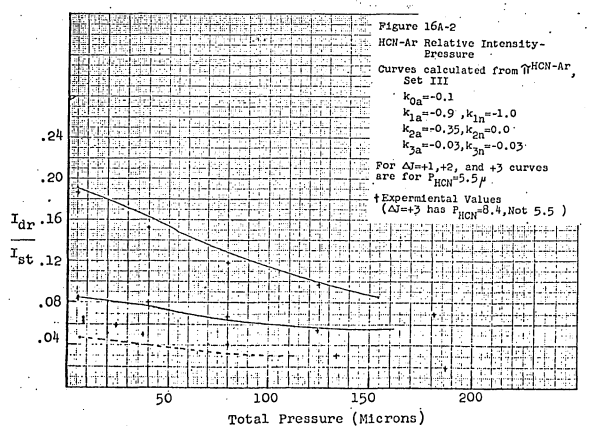

Figure 16A-2
HCN-Ar Relative Intensity-Pressure
Curves calculated from Π^{HCN-Ar}, Set III
k_{0a}=-0.1
k_{1a}=-0.9 , k_{1n}=-1.0
k_{2a}=-0.35, k_{2n}=0.0
k_{3a}=-0.03, k_{3n}=-0.03
For ΔJ=+1,+2, and +3 curves are for P_{HCN}=5.5μ
†Experimental Values (ΔJ=+3 has P_{HCN}=8.4, Not 5.5)

Reproduced with permission of the copyright owner. Further reproduction prohibited without permission.

In comparing the calculated and experimental phase curves (Fig. 16-B-1) for this second set of constants, we see that the rates do not reproduce the phases as well as the k_{0a} dominant mechanism (Fig. 13B). In comparing the calculated phase curves for this set with our initial set (see Fig. 16-B-2), we see that the predictions differ by as much as 8° in the $\Delta J = +2$ curves. In Case I where the $\Delta J = 0$, k_{0a}, rate dominates, the system approaches its high pressure limit more rapidly. This fact is emphasized in the steepness of the phase-pressure plots. Furthermore, the lag between the curves for the different ΔJ signals disappears at fairly low argon pressures. This too is an effect of a dominant k_{0a} relaxation mechanism.

A last set of rate constants to be considered is found in Table 5, Case III. In this instance it is noted that the $\Delta J = 0$ rate is considerably smaller than the other rates. The calculated relative intensities are presented in Fig. 16-A-2. As before the rates indicated are not refined. They can be refined to give a better fit of the relative intensity data. Calculations showed that these phases will differ by less than 2°-3° from Case II.

To summarize the various argon calculations, one can see that there is apparently information contained in the phase curves that will help distinguish various rate matrix structures. The rates at which the curves approach a high pressure limit appear to be most sensitive to the fraction that k_{0a} makes up of the diagonal element. Furthermore, the spacings between the curves are sensitive to the magnitudes of k_{ja} and k_{jn}, but these spacings are determined primarily by the starting points

Reproduced with permission of the copyright owner. Further reproduction prohibited without permission.

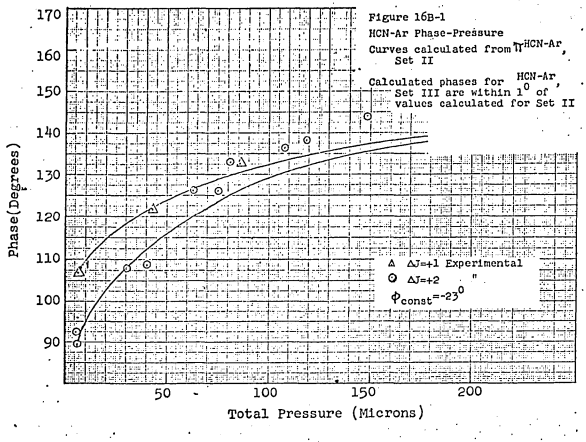

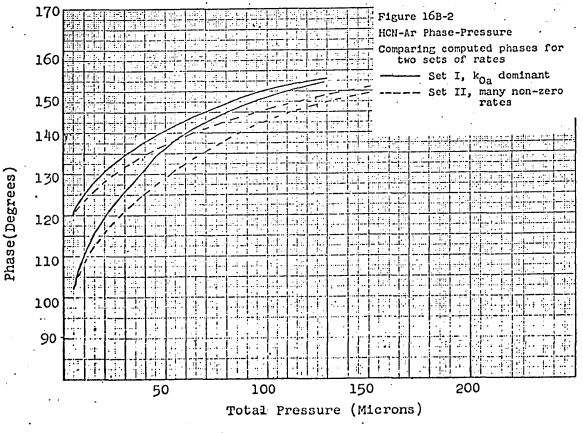

Reproduced with permission of the copyright owner. Further reproduction prohibited without permission.

in pure HCN. It appears that the three sets of rates account reasonably well for the relative intensities, but that on the basis of the phase data Set I would present a better fit.

3. Helium Analysis

The helium relative intensities showed collision induced transitions with definite J preferences and parity preferences. The different sets of helium rates listed in Table 5 point out the types of ambiguities present in the relative intensity data. As with the argon results, the $\Delta J = +1$ results can be attributed to either $k_{1a} \approx k_{1n} \approx 0$ or $k_{1a} \approx k_{1n} \neq 0$. The third set of rates emphasizes the possibility that k_{0a} is not really known relative to the other rates. In Fig. 17 are presented the relative intensities and phases calculated for these different sets of rate constants. As before, further improvement of the relative intensity fit for cases II and III is possible. The calculated phases for case II would lie between those calculated for I and III. These differences are on the same order of magnitude as the shifts in phases due to the HCN-He linewidth uncertainties as can be seen in Fig. 18. This is unfortunate since it makes it clear that even if the phases were known to ± 1 or 2°, our problem would not be solved. Because of these difficulties it is not possible to make a meaningful determination of a preferred set of rate constants on the basis of the fit of the calculated to the experimental phases.

At this point, it is worthwhile remembering why the phase information has not been used for fitting. In the argon experiments, the signal to noise ratio was sufficiently small that uncertainties of up to

Reproduced with permission of the copyright owner. Further reproduction prohibited without permission.

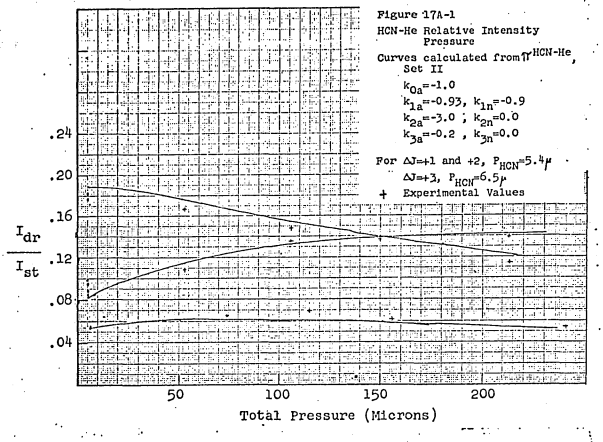

Figure 17A-1
HCN-He Relative Intensity Pressure
Curves calculated from γ^{HCN-He}, Set II
k_{0a}=-1.0
k_{1a}=-0.93, k_{1n}=-0.9
k_{2a}=-3.0 ; k_{2n}=0.0
k_{3a}=-0.2 , k_{3n}=0.0
For ΔJ=+1 and +2, P_{HCN}=5.4μ
ΔJ=+3, P_{HCN}=6.5μ
+ Experimental Values

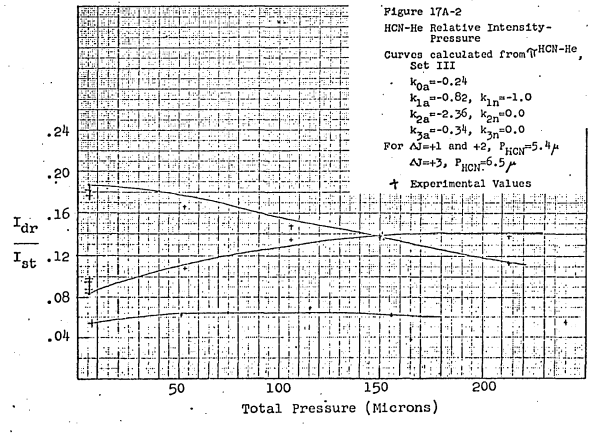

Figure 17A-2
HCN-He Relative Intensity-Pressure
Curves calculated from γ^{HCN-He}, Set III
k_{0a}=-0.24
k_{1a}=-0.82, k_{1n}=-1.0
k_{2a}=-2.36, k_{2n}=0.0
k_{3a}=-0.34, k_{3n}=0.0
For ΔJ=+1 and +2, P_{HCN}=5.4μ
ΔJ=+3, P_{HCN}=6.5μ
+ Experimental Values

Reproduced with permission of the copyright owner. Further reproduction prohibited without permission.

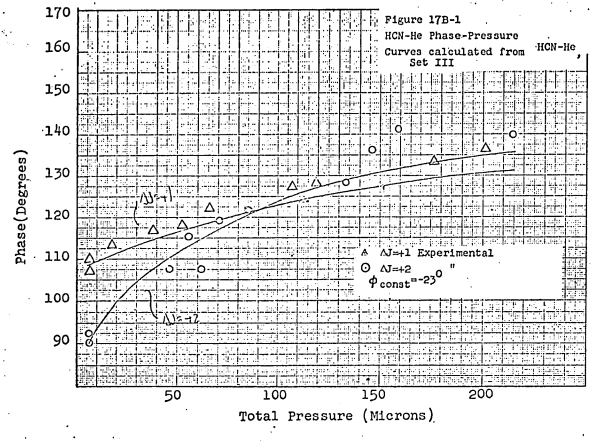

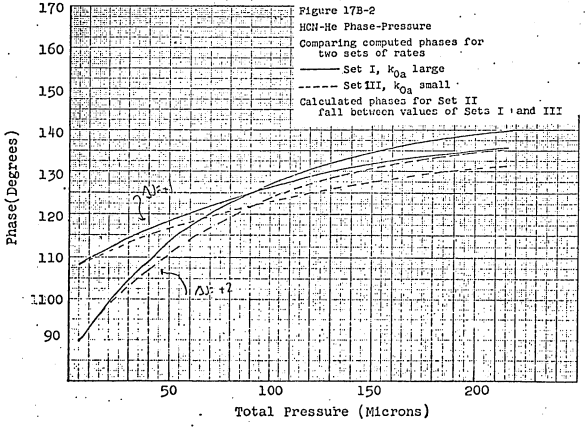

Reproduced with permission of the copyright owner. Further reproduction prohibited without permission.

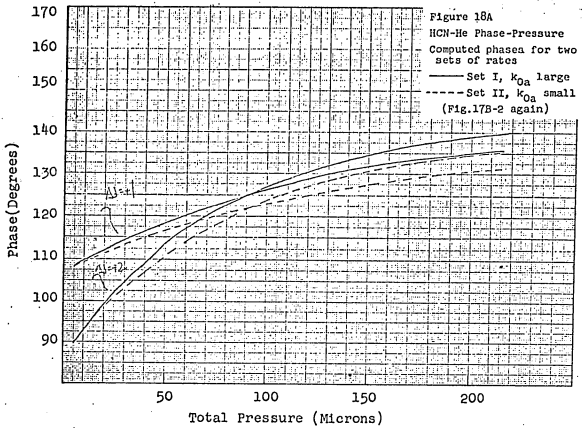

Figure 18A
HCN-He Phase-Pressure
Computed phases for two sets of rates
——— Set I, k_{0a} large
----- Set II, k_{0a} small
(Fig.17B-2 again)

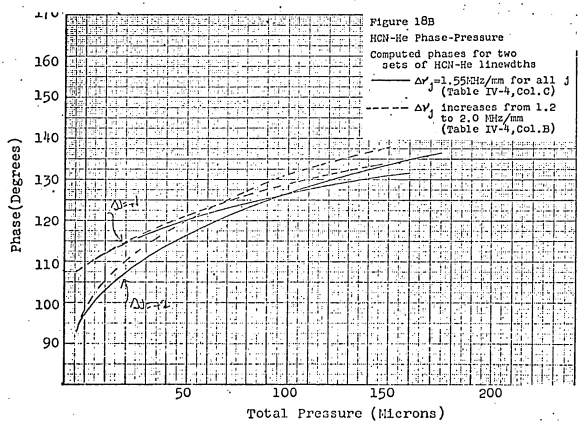

Figure 18B
HCN-He Phase-Pressure
Computed phases for two sets of HCN-He linewdths
——— $\Delta\nu_J$=1.55MHz/mm for all J (Table IV-4,Col.C)
----- $\Delta\nu_J$ increases from 1.2 to 2.0 MHz/mm (Table IV-4,Col.B)

Reproduced with permission of the copyright owner. Further reproduction prohibited without permission.

5° are present in any individual instrumental null. In the helium mixtures the apparent accuracy is somewhat better, but in both cases the data must be referenced to the HCN starting point. The phase curves will be useful only when the HCN phase curves can be well determined experimentally and theoretically.

4. Back to HCN

As noted previously, the rate matrix used for pure HCN in the gas mixture calculated was a compromise solution. It was based on a set of rates limited to $\Delta J \leq 3$ that gave a reasonable reproduction of both the relative intensity and phase data. Data has been presented for relative intensities and phases for $\Delta J = +1$, $+2$, and $+3$ double resonance experiments. Even if the experimental data were known very precisely, it would be difficult to systematically adjust the rate model to fit the results because the different ΔJ curves are not independent. k_{1a} transitions contribute to $\Delta J = +2$ signals. Hence, care is required in selecting data points for a least squares fitting procedure. In reality, the difficulties are compounded by the uncertainties in phase information. Whether the $\Delta J = +2$ phase curve lags behind the $\Delta J = +1$ curve by 13° or by 18°-22° at 5 microns of pressure is significant, but just at the borderline of the experimental uncertainties presented previously. It must be remembered, however, that we are considering variations of rate constants that are fairly small. The basic questions being asked are whether

$$\frac{k_{0a}}{k_{1a}} < 0.05 \qquad \text{or} \qquad \frac{k_{0a}}{k_{1a}} = 0.1 \text{ or } 0.2 \ .$$

Reproduced with permission of the copyright owner. Further reproduction prohibited without permission.

Also, one would like to know if

$$\frac{k_{1n}}{k_{1a}} = 0.1 \text{ or } 0.3$$

and if

$$\frac{k_{2a}}{k_{1a}} = 0.1 \text{ or } 0.3$$

and whether there is evidence for $k_{3a}/k_{1a} > .05$. For the polar molecules the k_{1a} transition is the dominant feature, but the purpose of the work is to determine how much more one can say than that.

To clarify these matters, more calculations will be presented to show the types of situations one is concerned with.

First, remark that the HCN curves have been calculated on the basis of 5 nonzero constants, k_{0a}, k_{1a}, k_{1n}, k_{2a}, and k_{3a} and a power parameter. In this instance, when one determines $k_{3a}/k_{1a} \approx 0.15$, the computed results will be sensitive to k_{3n} or k_{2n} parameters not considered previously. Even when k_{3n}/k_{1a} may be as little as 0.02, k_{3n}/k_{3a} will be considerably larger. In Fig. 19 curves are presented that point out this fact.

In Table 6 are presented a variety of sets of sets of rate constants and power parameters that reproduce the experimental data reasonably well. The first three sets are values that have been adjusted to fit the phase curves for a pressure of about 5 microns of Hg. Set IV is adjusted to reproduce relative intensity curves only. Set V is the set of constants derived previously[1] to account for energy transfer experiments in pure HCN. The calculated curves for the three new sets

Reproduced with permission of the copyright owner. Further reproduction prohibited without permission.

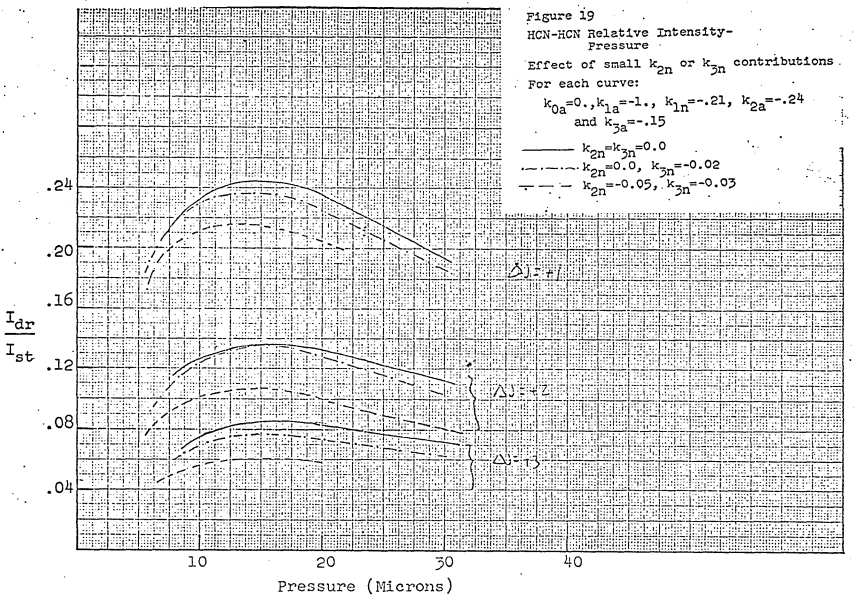

Reproduced with permission of the copyright owner. Further reproduction prohibited without permission.

TABLE 6

Alternate Sets of Rate Constants

for HCN-HCN Energy Transfer

	I (initial set)	II	III	IV	$V^{1,A}$
k_{0a}	0	0.16	0	0	0 (-.03,+.02)
k_{1a}	1.	1.	1.	1.	1.
k_{1n}	0.21	0.17	0.19	0.22	0.24 (0.21,0.26)
k_{2a}	0.167	0.26	0.18	0.32	0.21 (0.17,0.26)
k_{2n}	0	0	0	0	0
k_{3a}	0.136	0.13	0.04	0.11	0.24 (0.16,0.32)
k_{3n}	0	0	0	0	0
k_{4a}	0	0	0.24	0	0
DPA	1.	1.4	0.98	0.89	

A The quantities in parenthesis are the linearized 90% confidence limits estimated from the fit of the calculated to experimental values.

Reproduced with permission of the copyright owner. Further reproduction prohibited without permission.

are presented in Fig. 20.

At this point it is appropriate to compare this work with the previous work on pure HCN.[1] Comparison of the experimental data shows that there is agreement within experimental uncertainty between values for the $\Delta J = +1$ and $+2$ relative intensity data. The $\Delta J = +3$ relative intensity data of this work is new. There is disagreement between the phase information, and that reflects the uncertainty in comparing phase data for the different ΔJ experiments. The phase information presented in this work reflects a basic improvement in the experimental technique. More data has been collected; the $\Delta J = +3$ information is new; the method used to compare the phase data for the different ΔJ experiments is considered to be an improvement.

The analysis of the data in terms of the linear kinetic theory has been advanced. The values of the linewidth parameters have been shown to be important, and better values have been obtained. It has been found that it is not possible to determine a unique set of rate constants that satisfactorily accounts for all the data. The analysis confirms the dominance of the first order dipolar interaction: k_{1a} is dominant, k_{1n} and k_{2a} are about 20% of k_{1a}. It is shown that the highest J parameter fit (k_{3a} usually) does function as a pool for all other high J transitions. Also, the magnitude of k_{0a} must remain somewhat uncertain as long as the pump power in the cell is not known (compare case II with the others).

There is strong evidence that the phase data does contain new information when there is experimental data only for 3 ΔJ transitions.

Reproduced with permission of the copyright owner. Further reproduction prohibited without permission.

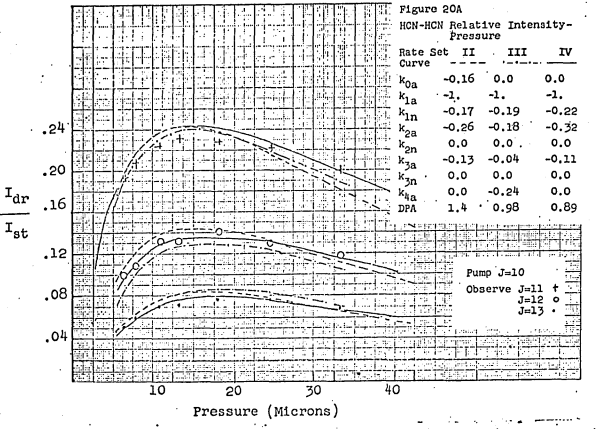

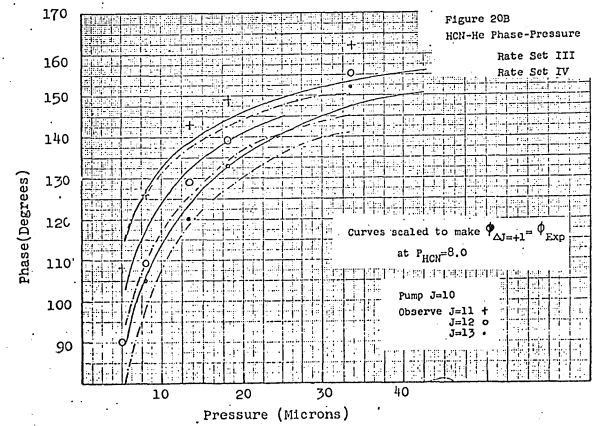

Reproduced with permission of the copyright owner. Further reproduction prohibited without permission.

Case IV fits the relative intensity data well, but the predicted spacing between the phase curves is less than experimental data warrants. The phase information used previously contains sufficient uncertainty that it does not contain new information. A test has been made where a least squares fit has been made of the relative intensity data alone, and it was found that the rates obtained are essentially the same as Case V.

In general, the new results emphasize that the linearized confidence limits[1] have little meaning. This is not because the problem is too non-linear: a test has been made of the estimated non-linear confidence limits,[12] and they are found to agree well with the linearized limits. Rather, the basic least squares problem is not well-defined. There is not a single unique minimum that can be found. It is very difficult to obtain the best mix of the different types of experimental data to obtain a meaningful fit.

An interesting fact is that for none of these constants is the steepness of the phase curves as great as the experimentally determined data. By introducing an arbitrary phase factor in comparing the calculated and observed phases one can compensate for this fact. However, the experimental curves have been corrected in such a manner that they all approach the high pressure limit of $\phi(\infty) = \pi$. Because the curvature of the HCN phase curves is not reproduced by the calculations, it is not wise to judge the goodness of the rare gas parameters by that criterion. Obviously, more attention must be paid to the experimental phases, but before doing that let us consider whether we can choose one

Reproduced with permission of the copyright owner. Further reproduction prohibited without permission.

set of parameters for each rare gas mixture that is to be preferred.

V. Discussion

We have indicated that it is possible to determine a set of rate constants for each foreign gas that accounts for the data, but it is not possible to claim that the set is unique. Having indicated other sets of constants, it is interesting to consider some general theoretical considerations to see whether there is an a priori reason for favoring one set over another. In considering the results for pure HCN, the dipole-dipole interaction is overwhelmingly predominant, even to the point where dipole-dipole potential must be considered to second order perturbation theory before considering other multipole interaction terms to first order.[13] In the HCN-rare gas interactions, there are, however, no clearly dominant interactions, and it is highly speculative to discuss the "likely" rate constants without very detailed calculations. However, reasons will be given that suggest that for HCN-He the set of rates presented as Case III, Table 5,

$$k_{0a} < k_{1a} \lesssim k_{1n} < k_{2a}$$

may be the most reasonable from a qualitative theoretical viewpoint.

Unfortunately, for the HCN-argon results, the various factors contributing to the magnitudes of the different rate constants are of an even more contrary nature, and it is even more difficult to state a preference between the rates. Though the atomic polarizability of argon is almost ten times that of helium, the fact that the average

Reproduced with permission of the copyright owner. Further reproduction prohibited without permission.

collision velocity is much smaller for the heavier atom makes $\Delta J > 1$ transitions relatively less likely. The kinematic factors lead one to favor (tentatively) the set of rates (Case III of Table 5) where

$$k_{0a} < k_{1n} \approx k_{1a}$$

and

$$k_3 < k_2 \lesssim k_1 .$$

A. Perturbation Theory Description of HCN-rare gas collisions

The theoretical formulation that is conceptually simple and has been applied with some success to microwave linewidth calculations is to use time-dependent perturbation theory along straight line trajectories to calculate collisional transition probabilities. In this manner the molecular rotations can be treated quantum mechanically. This approximate theory should be valid when the collision causes a small perturbation on the center of mass motion of the system, i.e. when $\Delta E/kT \ll 1$ and $\Delta J/L \ll 1$, where ΔE is the energy transferred from translation to rotation, ΔJ the angular momentum transferred from orbital to rotational motion, and L the orbital angular momentum. In Table 7 are presented values of $\Delta E/kT$ for $\Delta E = E(J_f = 10 + \Delta J) - E(J_i = 10)$ and values of μvb for the relevant collision couples. We see that even for the HCN-He collisions these conditions are reasonably well satisfied.

Obviously for purposes of a qualitative discussion it is possible only to consider first order perturbation theory in our search for dominant rates. In that case, $P_{i\to f}$, the probability that the collision induces a transition from $|i\rangle$ to $|f\rangle$, is

Reproduced with permission of the copyright owner. Further reproduction prohibited without permission.

TABLE 7

Some Numbers Relating to HCN Rotational Energy Transfer

A. $\frac{\Delta E}{kT}_{room} = \frac{E_{J\pm10+\Delta J} - E_{J-10}}{kT}$

ΔJ =	-7	+1	+3	+5	+7	+10
$\frac{\Delta E}{kT}$	-.6	+.14	+.5	+.9	1.4	2.2

B. $\frac{\Delta J}{L} = \frac{\Delta J}{\mu v b^*}$ where b^* = collision diameter from linewidths

μ = reduced mass of collision couple

v = average velocity of collision couple

	HCN-HCN	HCN-He	HCN-Ar	HCN-Xe
L($\hbar$)	~ 500	~ 20	~ 80	~ 100

Reproduced with permission of the copyright owner. Further reproduction prohibited without permission.

$$P_{i\to f} = \frac{1}{\hbar^2} \left|\langle f| \int_{-\infty}^{\infty} dt\, e^{iH_o t/\hbar}\, V(t)\, e^{-iH_o t/\hbar} |i\rangle\right|^2$$

where the time integral is actually the integral over the collision trajectory. For the rare gas collisions, states $|i\rangle$ and $|f\rangle$ refer to a single HCN molecule.

A collision coordinate system is defined in Fig. 21. We note that there are four coordinate systems: the instantaneous collision angle θ valid for a single $R(t)$; the space fixed collision axis system defined by the impact parameter b and the velocity v; the space fixed system that would be defined by the polarization of the microwave radiation; and the body fixed system associated with the HCN molecule. The potential is easily expressed in terms of $\theta(t)R(t)$ which must then be related to the collision axis system. Similarly the wave functions can be related in terms of the space fixed collision axis system. At some point in a calculation averages must be taken over all possible orientations of the collision axis system relative to the microwave system since all orientations of the collision plane are equally likely. For our purposes, however, we need only consider the problem in the collision axis system. The other necessary transformations require averaging over M, a fact that introduces some ambiguity in the relative probabilities but can only be handled by explicit calculations of all matrix elements.

What might be a reasonable potential? Buckingham[19] presents a

---

19. A. D. Buckingham, Adv. Chem. Phys. 12, 107 (1967).

Reproduced with permission of the copyright owner. Further reproduction prohibited without permission.

Figure 21

Reproduced with permission of the copyright owner. Further reproduction prohibited without permission.

general multipole expansion for the atom-linear molecule that is valid for non-overlapping charge distributions. Though the HCN wave functions are for a near prolate rotor, it should be quite sufficient to consider the linear molecule-atom interaction potential. The leading terms in the attractive branch of the potential then have the form

$$V = \frac{1}{[R(t)]^6}\left[A + \frac{B}{R} P_1(\cos\theta) + C\, P_2(\cos\theta) + \frac{D}{R}(\cos^3\theta) + \ldots\right] \quad (10)$$

where the P_j are the Legendre polynomials.

The B coefficient includes terms from the quadrupole-induced dipole interaction and dispersion contributions from anisotropic polarization effects (that the electrical charge center of the molecule does not coincide with the center of mass). The C coefficient includes contributions from dipole-induced dipole interactions and dispersion effects associated with the polarizability of the HCN molecule ($\alpha_\perp - \alpha_{||}$). The D coefficient includes dipole-quadrupole induction forces and further dispersion contributions from the polarizability tensor describing the molecular interaction with a field gradient.

At this time there is no good way of estimating the B or D coefficients for HCN. Furthermore, there is the repulsive branch of the potential that is also presumably anisotropic but is also a matter of speculation. It will certainly be important and perhaps dominant for HCN-He interactions. As one varies the collision partner, the changing parameters in the interaction are the rare gas polarizabilities and the collision kinematics, in particular the average velocity.

An example of the difficulties in estimating potential functions

Reproduced with permission of the copyright owner. Further reproduction prohibited without permission.

for use with perturbation theory can be seen from the HCl-rare gas rotational linewidth work. An estimate[20] has been made of attractive and repulsive branches for HCl-rare gas interactions in terms of P_1 and P_2. In that case the attractive P_1 term was based on the quadrupole-induced dipole interaction and reasonable rotational linewidths were obtained. For HCl-Ar such a P_1 term was felt to be the dominant line-broadening factor. Herman,[21] however, has found for HCl-Ar interactions that that P_1 contribution is only 1/7 of the magnitude of the coefficient one determines by taking into account the electrical-mass origin differences.

For rotational linewidths the general procedure is to use the perturbation theory expression to calculate a transition probability as long as the calculated $P_{i\to f}$ is less than 1. Then in the region of small b where the calculated probability exceeds unity, the theory is clearly invalid, and the value of $P_{i\to f}$ is set equal to one. It has been found, however, that the cutoff schemes are crucial, especially for molecule-atom interactions that are short range. In that case, over a small range of impact parameters $P_{i\to f}$ varies from less than 1 to greater than one, and in these situations the cross sections will be more sensitive to the cutoff procedures than the potential parameters. Furthermore, for these short range interactions where multi-term potential functions are considered to first order perturbation theory,

---

20. Krishnaji and S. L. Srivastava, J. Chem. Phys. 42, 1546 (1965).

21. R. M. Herman, J. Chem. Phys. 44, 1346 (1966).

Reproduced with permission of the copyright owner. Further reproduction prohibited without permission.

there is reason to suspect that higher order contribution from a dominant interaction may be too important to be neglected.

With all these caveats, let us examine the first order perturbation theory expression to see what it might suggest.

B. Parity Selection Rules

The parity selection rules can be determined from group theoretical considerations, but the particular ΔJ selection rules necessitate a more detailed consideration of the molecular wave functions and the interaction potential. The HCN wave functions have been introduced in terms of symmetric rotor functions, the interaction potential can be presented as linear combinations of spherical harmonics, and the selection rules can be derived from general considerations of properties of angular momenta. The necessary properties of tensor operators can be found in any of many books.[22]

The potential of Eq. 10 can be reexpressed in terms of spherical harmonics and, hence, rotation matrices, D^J_{KM}, in the collision axis coordinate system. The important result is that

$$P_1(\cos\theta) \propto \sum_{M=-1}^{1} f_M(t)\, D^1_{OM}(\hat{r}_{HCN}) ,$$

$$P_2(\cos\theta) \propto \sum_{M=-2}^{2} f'_M(t)\, D^2_{OM}(\hat{r}_{HCN}) ,$$

---

22. For example, D. M. Brink and G. R. Satchler, Angular Momentum (Clarendon Press, Oxford, 1968).

Reproduced with permission of the copyright owner. Further reproduction prohibited without permission.

$$\cos^3\theta \propto A\, Y^3_{00}(\theta,\ \phi=0) + B(Y^3_2 + Y^3_{-2}) ,$$

and, hence,
$$\cos^3\theta \propto \sum_{M=-3}^{3} f^{III}_M(t)\, D^3_{OM}(\hat{r}_{HCN}) .$$

The time dependence of the f functions reflects R(t) and $\psi(t)$ of Fig. 21, and $\hat{r}_{HCN}$ is the orientation of HCN in the collision axis system. The rotation matrices and, hence, spherical harmonics are related by a coordinate transformation only to matrices of the same order (a more general statement of the spherical harmonic addition theorem).

Alberts[23] has derived general selection rules for the Wang functions. They can be summarized:

	Non-Zero Elements	
	T even	T odd
$< J'lM';+\|D^T_{OM'}\|JlM;+ >$	(J' - J) even	(J' - J) odd
$< J'lM';+\|D^T_{OM'}\|JlM;- >$	(J' - J) odd	(J' - J) even

As we have noted |JlM;+ > is always the lower level of a doublet, but its parity is + for even J, - for odd J. Using the ± notation of Fig. 1 the parity rules for the transitions are

T even $\quad \begin{matrix} - \\ + \end{matrix} \leftrightarrow \begin{matrix} - \\ + \end{matrix}$,

T odd $\quad \begin{matrix} + \\ - \end{matrix} \leftrightarrow \begin{matrix} - \\ + \end{matrix}$.

Hence we note that only for T odd can there be $\Delta J = 0$, k_{Oa}, selection rules. For even T there can only be $\Delta M = 0$ transitions within a single

---

23. R. H. Alberts, Ph. D. Thesis, Harvard University, 1965.

Reproduced with permission of the copyright owner. Further reproduction prohibited without permission.

J level--a pure reorientation effect.

Furthermore, though the evaluation of the matrix elements is algebraically tedious, there are certain general rules:

(a) $|J' - J| \leq T$, the triangle rule, and

(b) $M + M' = M''$.

The parity and triangle rules lead to the conclusion that the $P_1(\cos\theta)$ interaction would lead to $\Delta J = 0, \pm 1$ transitions $\pm \leftrightarrow \mp$, the $P_2(\cos\theta)$ interaction $\Delta J = 0, \pm 1, \pm 2$, $\pm \leftrightarrow \pm$ transitions, and the $\cos^3\theta$ interaction to $\Delta J = 0, \pm 1, \pm 2, \pm 3$, $\pm \leftrightarrow \mp$ transitions. For our rate constants of Fig. 1 we can collect the possible first order contributions to the different rates:

Rates:	k_{0a}	k_{1a}	k_{1n}	k_{2a}	k_{2n}	k_{3a}	k_{3n}
Potential Terms:	$\cos\theta$	$\cos\theta$					
	$\cos^3\theta$	$\cos^3\theta$			$\cos^3\theta$	$\cos^3\theta$	
			P_2	P_2			

C. Relative Magnitudes of the Rate Constants

The relative magnitudes of these various rate constants depend on several factors:

(1) The molecular and atomic parameters (glopped in Eq. 10 as A, B, C, ...) $\equiv F_j$.

(2) The magnitude of the matrix elements after averaging over the various M components $\equiv C_j$.

(3) The integral over the collision path $\equiv R(x)$, where $x = \frac{\omega_{if} b}{v}$.

Reproduced with permission of the copyright owner. Further reproduction prohibited without permission.

In fact these terms do enter in a first order collision-induced transition probability as factors:

$$P_{i\to f} \propto \sum_j F_j{}^* C_j{}^* R_j(x)$$

where we sum over different interaction potential terms contributing to a given transition.

In Table 8 are presented values of x for the different transitions and in Table 9 are presented molecular parameters for HCN, the rare gas atoms, and some other molecules that might be informative. Birnbaum[24] presents the first order perturbation theory resonance functions $R_j(x)$ for different interactions. Each function is independent of particular molecular parameters. It is only a function of $x = \frac{\omega b}{v}$. The resonance functions R(x) vary from about 1 to 0 as a function of x. For the types of interactions we are considering, these first order resonance functions are all less than 0.2 for $x > 4$ and are monotonically decreasing for $x \geq 2$. From Table 8 we note that for HCN-He $x \approx 5$ for $\Delta J = +4$, but for argon or xenon $x \approx 5$ for $\Delta J = +1$. It is for this reason that the kinematic difference between collision partners may be the crucial factor.

Considering HCN-He, further analysis is possible in terms of the matrix elements. Where the resonance factor is near one for $\Delta J = +1$, the cos θ term would lead to $k_{0a} \approx 0.1\, k_{1a}$ as has been discussed previously in terms of dipole selection rules for HCN. Of course, it is wiser to say that because of the unfavorable matrix elements, even in

---

24. G. Birnbaum, Adv. Chem. Phys. 12, 487 (1967).

Reproduced with permission of the copyright owner. Further reproduction prohibited without permission.

TABLE 8

Values of $X = \frac{\omega_{if} b^*}{v}$ b^* dimension from linewidth

v average velocity of collision pair

ΔJ =	0	1	-1	+2	-2	+3	-3	+4	from $J=10_{1,10}$
HCN-									
He	.03	1.2	1.1	2.5	1.9	3.6		4.8	
Ar	.11	4.7	4.2	9.5	8.0	15.		20.	
Xe	.14	5.7	5.2	11.8	10.0	19.		24.	

Reproduced with permission of the copyright owner. Further reproduction prohibited without permission.

TABLE 9

Some Molecular and Atomic Parameters

	HCN	NH_3	N_2O	CO	HCl	He	Ar	Xe
μ, dipole (Debye)	3.	4.1	0.17	0.1	1.1			
α, polarizability (10^{25} cm^3)[a]	25.9	22.6	30.0	19.5	26.3	2.0	16.4	25.0
$\alpha_{\parallel} - \alpha_{\perp}$	20.0	2.0	27.9	9.75	7.4			

a Polarizability data from Hirschfeld, Curtis and Bird, Molecular Theory of Liquids and Gases, p. 95.

Reproduced with permission of the copyright owner. Further reproduction prohibited without permission.

the presence of the resonance function $R_J(x)$, $k_{0a} < k_{1a}$ is to be expected. Furthermore, without knowing the magnitude of the molecular parameters contributing to a $\cos^3\theta$, it is reasonable to expect that from it also $k_{0a} < k_{1a}$. In general

$$\langle i|\cos^3\theta|f\rangle = \sum_{l,j} \langle i|\cos\theta|l\rangle\langle l|\cos\theta|j\rangle\langle j|\cos\theta|f\rangle .$$

Hence, one can estimate the relative preferences of the allowed ΔJ transitions from the dipole selection rules and the estimate that

$$k_{if} \propto |\langle i|\cos^3\theta|f\rangle|^2 .$$

For this guestimate, if one assigns the $\Delta J = 0$ matrix element a weight of 0.1 relative to the $\Delta J = +1$ element ($|\mu_{10,10}|^2/|\mu_{10,11}|^2 \approx 1/50$), and if one counts the possible ways of making a particular ΔJ transition, one guesses an ordering for $\cos^3\theta$ rates

k_{0a}	0.4
k_{1a}	9.0
k_{2n}	0.1
k_3	1.0

As one subjectively takes into account the resonance functions, one suspects that if $\cos^3\theta$ is important, it still might manifest itself predominantly as a $\Delta J = +1$, +-transition.

Similar reasoning for the $P_2(\cos\theta)$ term leads to $k_{2a} > k_{1n}$, but also the feeling that the $\Delta J = 0$, ++transition could well be important.

Lastly, might something be said about the relative magnitude of the P_2 and P_1 coefficients? Not really--as noted from Table 9 the

Reproduced with permission of the copyright owner. Further reproduction prohibited without permission.

($\alpha_{\perp} - \alpha_{||}$) polarizability term that contributes to P_2 is larger for HCN than for CO, HCl, and NH_3. Furthermore, the larger dipole moment for HCN than CO or HCl also suggests that the P_2 term may well be dominant for HCN in the attractive branch of the potential. However, in light of the effective collision diameters, the repulsive branch of the potential must also be considered, and for this it is impossible to even make guestimates.

These rather general arguments suggest a preferred set of rate constants for HCN-He. The parameters of case III are consistent with an anisotropic potential containing P_1 and P_2 terms with P_2 dominating. There is evidence for possible $\cos^3\theta$ contributions. In fact, calculations show that the k_{3a} rate can not be replaced by k_{1a} rates as in HCN-HCN data. The other sets of constants are less likely. Case I would be likely only for the case where the resonance function was more important than it should be for HCN-He.

For the argon type results Case III is preferred because it allows for a P_2 dominant potential with the damping effect of the resonance functions. Case II where all rates are essentially equal is probably not realistic in light of the resonance functions, but the fact that rates of that type can be found to reproduce the data indicates that intermediate sets between Cases II and III can also be found. The data will be reproduced by rates for which the k_{0a} contribution is relatively small ($k_{0a}/\Sigma\, k_j$) and for which $k_{1n} > k_{1a}$, $k_{2a} > k_{2n}$. Furthermore, in light of the effects of the kinematics, there is reason to believe that $\Delta J = 0, \pm \leftrightarrow \pm$ ΔM relaxation mechanisms may be important. These would

Reproduced with permission of the copyright owner. Further reproduction prohibited without permission.

be allowed by a P_2 term, can not be observed by the experimental techniques used, and can not be fit by the model used.

VI. Further Experiments and Discussion About Phase Shifts

As we have seen, because of the limited number of J levels observed, the phase shifts contain new information in the double resonance experiments. Unfortunately, there have been difficulties in determining phase shifts with the same precision that the relative intensities have been determined. Where the phases have been determined most precisely, for pure HCN, it has not been possible to find rate constants that, while reproducing the relative intensities, also reproduce the phase shifts over the pressure range studied. Because of this fact it is interesting and important to consider the matter further.

First, let us consider the determination of the phase of the Stark signal. What might be the cause of the null wiggles that are found for both the double resonance and Stark signals? The most obvious explanation is that the apparent variation of phase across an absorption is an instrumental effect. If anywhere from the crystal detector through the PSD there is a shift of phase with signal amplitude, just such null wiggles might result. However, experiments have been performed that make such an interpretation unlikely:

(1) The phase null of a Stark signal changed less than 1° as the attenuation between the preamplifier and PSD was varied over 28 db.

(2) To test the crystal-preamp-PSD system a small quantity of

Reproduced with permission of the copyright owner. Further reproduction prohibited without permission.

100 KHz amplitude modulated microwave radiation was leaked to the detector and the incident power level was varied over 15 db. Over this range the phase null remained constant to within 1°.

(3) The fact that the magnitude of the phase variation appears to decrease with increasing gas pressure is not easily accountable in terms of an instrumental effect.

Examination of the J = 11 HCN signal led to the following conclusions:

(4) The center of the null wiggle ($\overset{\downarrow}{w}$) does in fact coincide with the zero field absorption frequency.

(5) There is a shift in the null of the Stark signal with pressure of the gas, as other variables (microwave power level, detector gain levels) are kept constant. Curves in Fig. 22 present the observed null phase as a function of pressure for different radiation power levels. The net result is that shifts of 4-5° are possible.

(6) It appears that the variation of phase with the microwave power level is primarily due to the varying impedance of the crystal detector as the crystal's dc operating point shifts with changing power levels.

a) By using a dc bias to maintain a constant dc operating current level while the microwave radiation was varied, it was seen that the variation of phase with power level was less than 1-2°.

b) A double attenuator experiment was performed where one could change the power reaching the crystal by attenuating the radiation alternately before and after the cell. In this case it was found that the phases agreed to within 1°, but there was still a pressure dependent phase shift of about 4° as sample pressure varied from 2 to 20 microns.

Reproduced with permission of the copyright owner. Further reproduction prohibited without permission.

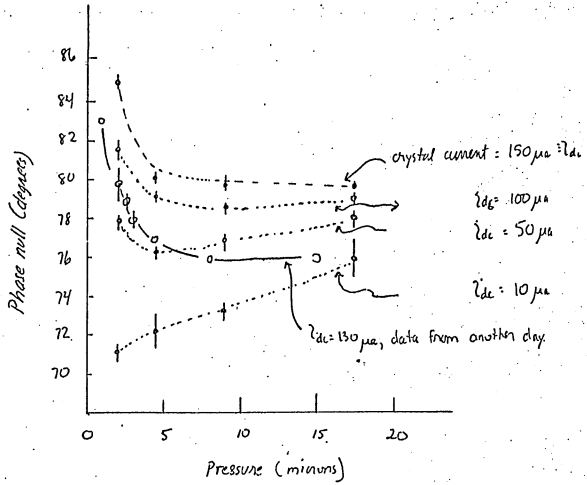

Null Phase of Stark Signal
as Function of Pressure

Figure 22

Reproduced with permission of the copyright owner. Further reproduction prohibited without permission.

These experiments suggest that the Stark absorption process is more complicated than the simple square wave absorption assumed in Chapter I. This fact has been confirmed by others. Howard Harrington[25] of Hewlett Packard has reported an experiment where the radiation frequency is fixed at the zero field absorption and the output of the crystal detector is monitored in the presence of Stark modulation of the molecular absorption. He looked at the J = 1 → 2 absorption of OCS at pressures from 0 to 20 μ of Hg and power levels from .6 μwatts to 6 mwatts. Instead of the expected square wave crystal output, a damped ringing waveform was observed (Fig. 23).

As an exercise, a crude Fourier analysis of the ringing square wave was performed. The waveform was assumed to be of the form

$$f(t) = \begin{cases} A + B\, e^{-\alpha t} \sin \omega_M t & 0 < t < T/2 \\ 0 & T/2 < t < T \end{cases}$$

where A would be the basic square wave magnitude, B the magnitude of the ringing effect, α a damping parameter, and ω_M the ringing frequency. Then, if one Fourier analyzes this wave form,

$$f(t) = \sum_1^\infty a_n \sin n\omega t + \sum_1^\infty b_n \cos n\omega t + b_0$$

where $\omega = 2\pi/T$, one finds that for n even only the damped sine wave contributes. For n even,

---

25. H. Harrington, Symposium on Molecular Structure and Spectroscopy, The Ohio State University, Columbus, Ohio, September, 1968 S4.

Reproduced with permission of the copyright owner. Further reproduction prohibited without permission.

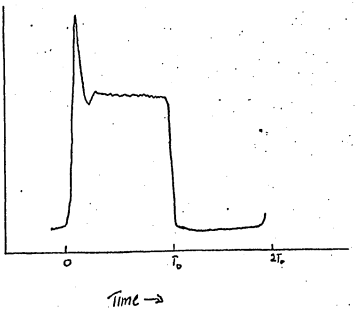

Output of Crystal Detector
(after Harrington[25])

Figure 23

Reproduced with permission of the copyright owner. Further reproduction prohibited without permission.

$$a_j = B\cdot(AS)_j$$

and

$$b_j = B\cdot(BS)_j,$$

while for n odd

$$a_j = \frac{2A}{j\pi} - B\cdot(AS)_j$$

and

$$b_j = -B\cdot(BS)_j.$$

where

$$(AS)_j = \{\frac{e}{T}^{-\alpha T/2}[\frac{(\omega_M - j\omega)\sin\frac{\omega_M T}{2} - \alpha\cos\frac{\omega_M T}{2}}{\alpha^2+(\omega_M - j\omega)^2} - \frac{(\omega_M + j\omega)\sin\frac{\omega_M T}{2} - \alpha\cos\frac{\omega_M T}{2}}{\alpha^2+(\omega_M + j\omega)^2}]$$

$$+ \frac{\alpha}{T}(\frac{1}{\alpha^2+(\omega_M - j\omega)^2} - \frac{1}{\alpha^2+(\omega_M + j\omega)^2})\}$$

$$(BS)_j = \{-\frac{e}{T}^{-\alpha T/2}[\frac{\alpha\sin\frac{\omega_M T}{2} + (\omega_M + j\omega)\cos\frac{\omega_M T}{2}}{\alpha^2+(\omega_M + j\omega)^2} + \frac{\alpha\sin\frac{\omega_M T}{2} + (\omega_M - j\omega)\cos\frac{\omega_M T}{2}}{\alpha^2+(\omega_M - j\omega)^2}]$$

$$+ \frac{1}{T}(\frac{(\omega_M + j\omega)}{\alpha^2+(\omega_M + j\omega)^2} + \frac{(\omega_M - j\omega)}{\alpha^2+(\omega_M - j\omega)^2})\}$$

A computer program has been written to evaluate these Fourier components, and in particular the possibility of phase shifts at the fundamental frequency has been examined. If one evaluates $\phi = \arctan b_1/a_1$ for different reasonable values of α, β, A, and B from Harrington's data, one finds ϕ changing by several degrees as the damping time changes from 2 to 4 microseconds if A/B = 1. Similarly shifts of 2° are

Reproduced with permission of the copyright owner. Further reproduction prohibited without permission.

possible as the period of ringing changes from 0.8 to 1.6 μs. However, B/A is a crucial parameter. As B → 0, clearly all shifts disappear.

This bootstrap approach to a waveform can and must be improved on. R. Karplus[11] has considered the absorption coefficient of a gas in the presence of square wave Stark modulation. Also many authors[26] have considered the saturation problem for two level systems. The authors generally focus on steady state results, which is unfortunate because what is of interest to us is the time dependent pulse phenomenon. However, certain persistent functional forms stand out. One feature is that there is a frequency-like term

$$\sqrt{(\omega - \omega_o)^2 + (\mu \cdot E/\hbar)^2 + 1/\tau^2} \equiv \sqrt{\gamma^2 + \frac{1}{\tau^2}}$$

where ω is the microwave field frequency, ω_o the molecular resonance, $\mu \cdot E/\hbar$ the power broadening parameter, and τ a lifetime parameter for relaxation to equilibrium. A preliminary examination[27] of these different theories suggests that the null wiggle phenomena of the Stark absorption is inherent in the modulation technique. The phase of the signal does change as one sweeps through an absorption because of

---

26. R. Karplus and J. Schwinger, Phys. Rev. 73, 1020 (1948), or A. Javan, Phys. Rev. 107, 1579 (1957).

27. This conclusion is based on discussions with Dr. H. Pickett and has been confirmed in a personal communication from Prof. R. Schwendeman of Michigan State who is continuing work on the phenomena originally reported by Harrington.[25]

Reproduced with permission of the copyright owner. Further reproduction prohibited without permission.

sin γt waveform terms. Furthermore, a pressure dependent phase shift would be expected, as well as a possible variation of phase with microwave power levels.

However, it is not really the place to go into these matters here. The preliminary experiments discussed here warrant further more careful examination. There is considerable information about molecular relaxation processes that can be found at the fundamental of the modulation frequency, but the theoretical treatments must be done carefully to unravel the effects of the modulation phenomena from the saturation relaxation processes.

This discussion started as an attempt to get a better understanding of the source of the difficulties in the double resonance phase. We must get back to that problem. As a concluding remark about the Stark phase it should be noted that it is not obvious that a theoretical treatment that fails to take into account specific collisional relaxation processes will be able to account for the Stark results for an arbitrary molecule.

Several experiments have been performed in an attempt to monitor the double resonance phase under various experimental conditions.

(1) As was mentioned previously, for the HCN double resonance signals where J = 10 was pumped and J = 11, 12, and 13 were observed, the null wiggle phenomenon was observed. In fact, the null wiggles are larger for the ΔJ = +1 signal than for the ΔJ = +2 signal or the ΔJ = +3 signal. Also, as can be seen in Fig. 3 the ΔJ = +1 null wiggles are a larger fraction of the signal size than the corresponding Stark null

Reproduced with permission of the copyright owner. Further reproduction prohibited without permission.

wiggles.

(2) a) For the $\Delta J = +1$ experiment at 5 microns pressure, the change in the null phase with pump power level was less than the experimental null uncertainty. Over a 15 db range, the phase changed less than 2°.

b) There is a definite change in null phase as the signal field power level is changed, but that change can be accounted for by the changing dc operating point of the crystal detector.

(3) The null phase of the double resonance signal does appear to shift slightly as the pump frequency is moved off resonance. Shifts of 3-4° were observed as the pump frequency was moved several MHz off resonance.

(4) The preceding result will have meaning only if the phase of the modulated pump radiation does not shift as the klystron power supply reflector voltages are changed. One of the reasons for not using the pump radiation as the time base (reference phase) was that when the power levels at the two frequencies of oscillation are nearly matched, there will be no well-defined phase. The square wave voltage applied to the reflector circuit is not by any means a perfect square wave. Under the best of circumstances, the rise time could be kept to less than 0.4 microseconds (100 KHz modulation means 5 μs per half cycle). Hence, the square wave spends almost 10% of its time getting turned on or off. This fact is compounded with the fact that a square wave modulated reflector voltage will not give rise to the same time dependence of both the frequency of oscillation and the amplitude of

Reproduced with permission of the copyright owner. Further reproduction prohibited without permission.

oscillation of the klystron. All these facts can be clearly observed by monitoring the output of a crystal that detects the frequency and amplitude modulated radiation. The output will look reasonably square. However, if it were truly square an absorption wavemeter tuned to one of the two frequencies would not have destroyed the shape, whereas in fact the waveform experimentally observed becomes distorted.

What can be said about these experiments? The null wiggles are probably interpretable in a manner analogous to the Stark wiggles. As the pump is turned on, there will certainly be damped oscillations within the pump levels. Furthermore, there will be molecules coming into the observed signal levels in a pulsed manner, and for these molecules the signal radiation field is suddenly turned on. It seems plausible that the absorption change due to the periodic modulation of populations that is detected by the double resonance techniques may have phase variations across a linewidth in a manner analogous to the Stark modulation effect. Since the molecules enter the $\Delta J = +1$ levels over a shorter time interval than the $\Delta J = +2$ or 3 levels, it might be expected that the effects would be more pronounced for the $\Delta J = +1$ signal.

The damped oscillations in the pumped levels are real population effects that cannot be included in the linear kinetic theory as presently formulated. We noted that even though the matrix $\underset{\sim}{\Pi} + \underset{\sim}{\delta\Pi}$ might in principle give rise to complex eigenvalues, it was found not to for reasonable rates for HCN energy transfer. In any event, oscillations of that type would not be adequate since a major approximation had been made when the steady state effect of the pump field was used as a trial

Reproduced with permission of the copyright owner. Further reproduction prohibited without permission.

form for $\underset{\sim}{\delta\Pi}$. If a time-dependent form for $\underset{\sim}{\delta\Pi}$ is necessary, everything becomes much more complicated. In practice population oscillations in the pump level can be built into the model mathematically without using a time-dependent $\underset{\sim}{\delta\Pi}$, but care will be necessary to construct a model in such a way as to preserve physical significance for the parameters.

The experiments and theory briefly touched upon in this section are very important in determining the sensible directions in which to proceed with double resonance and Stark studies of rotational relaxation processes. Clearly, if one wants to focus on that experimental region where steady state conditions do not hold at the end of a time cycle ($P \lesssim 6\text{-}7\ \mu$ for 100 KHz modulation), it is not surprising that the interpretation of the experimental results has to take into account these time dependent processes.

VII. Conclusions--Summary

It would be absolutely inappropriate to end on a pessimistic note. The experiments discussed in the previous section hint at the great quantity of information that can be contained in these microwave experiments. Insofar as there is much information, care will be needed to unravel the different contributing factors.

It may be useful to outline several details concerning the design of future experiments to study these processes.

In order to improve the phase measurements one must make certain that the time scale of the experiment is well defined. For the Stark

Reproduced with permission of the copyright owner. Further reproduction prohibited without permission.

experiments care must be taken to use the best square wave attainable. For the microwave double resonance experiments it is imperative that sharp square wave voltages be used to fm the klystron. It is probably desirable to use a low voltage waveform generator that is designed specifically for this purpose.

In general, phases should not be measured with a phase sensitive detector such as the HR-8. Commercial phase meters are obtainable that are much better suited for the purpose. Phase Meter Model 350 of Wiltron, Inc. of Palo Alto specifies an accuracy of $\pm 0.2^{\circ}$ for shifts up to 180° and it is suited for millivolt signals. A meter of this type will certainly be usable for Stark signals and probably be usable for double resonance signals.

There may be an advantage in using a broad-banded preamp rather than a tuned preamplifier. The resonant circuits of the tuned amplifier are potential sources of variable phases. One must perform phase experiments in such a manner that time variations are not confused with other possible causes of variations. It is dangerous to scan from high to low pressure monotonically since regular time variations might be mistaken for pressure effects. In any event, when one uses phase sensitive detection, little or no improvement in signal to noise is obtained by using a tuned preamp. Also, by utilizing suitable broadbanded preamplifiers the experimentalist will be able to do double resonance experiments at different modulation frequencies when the PSD or phase meter is of the variable frequency variety.

One interesting possibility in this vein is that it would be

Reproduced with permission of the copyright owner. Further reproduction prohibited without permission.

possible to detect double resonance signals at the harmonic of the pump frequency. This has been tested for the HCN $\Delta J = +1$ MMDR signal by pumping at 50 KHz and detecting at 100 KHz. The results are what one expects. There are essentially no horrendous baseline shifts since the modulation square wave contains essentially only even harmonics, but the signals are small. The observed relative intensity was only 4% of the Stark signal intensity while at the fundamental the relative intensity is 24%. Analysis of the linear rate model outlined in Chapter I leads to the conclusion that for the fundamental and even harmonics the complex relative intensity is proportional to $[\underset{\sim}{n}(0) + \underset{\sim}{n}(\pm t_o)]$ but for odd harmonics it is proportional to $[\underset{\sim}{n}(0) - \underset{\sim}{n}(\pm t_o)]$. Because such a detection procedure eliminates the spurious modulation signals, it is a technique that warrants further consideration.

In the technique of double resonance, the whole situation will be greatly simplified by the use of a frequency or phase-stabilized pump klystron. Though the existing phase stabilization apparatus in the lab is not suited for this purpose because of the Dymec response time, other frequency stabilizers with more suitable response times would be usable with a 100 KHz modulation frequency. If the pump were frequency stabilized, the signal to noise ratios of the double resonance signals can be easily improved by slower sweeps through the signal absorption.

For the double resonance experiments, the best method of comparing phase shifts for the different ΔJ experiments is to use the high pressure data to determine the limiting phase for high pressure. In fact it may be that the linear kinetic model may be used profitably in

Reproduced with permission of the copyright owner. Further reproduction prohibited without permission.

conjunction with accurate phase information from intermediate pressure regions.

It will be very interesting to continue work in the lower pressure regions where the effects of turning the fields on and off are important. For HCN the region of interest is pressures below 7 microns. As we have seen, a linear kinetic model has been unable to account for the full pressure dependent phase shift. Further careful experimental work on both the Stark and microwave phases will be necessary to trace out the nature of the different sources of phase shifts. One effect that must be included is the possibility that the signal radiation causes saturation effects in the low pressure region.

In conclusion let us remember that none of this invalidates the power of the double resonance technique for unraveling complicated relaxation processes. There is even more information obtainable than originally realized. The basic structure of the $\underline{\underline{\Pi}}$ matrices that have been presented are not in doubt. By focusing on the relative intensities at intermediate pressure regions and by using crude theoretical arguments about the angular dependence of the intermolecular potential, it has been possible to obtain preferred sets of specific rate constants for the HCN-rare gas collisions. The information about the dominant anisotropies of the HCN-He potential is indisputable, even if one does not know what the radial dependence is. Also, it is shown clearly that the major difference between HCN-He and HCN-Ar is the mean collision velocity and that this fact does cause significant differences in the predominant relaxation mechanisms.

Reproduced with permission of the copyright owner. Further reproduction prohibited without permission.

APPENDIX I

Rotational Transitions of Cis-Difluoroethylene

Molecular parameters and the calculated and observed rotational spectra for the ground and first vibrationally excited state of cis-difluoroethylene are listed. The programs used have been discussed in Chapter II. The observed frequencies have an estimated uncertainty of ±.1 MHz, and unless otherwise indicated they have not been reported previously.

Table I

Rotational Constants and Centrifugal Distortion Parameters[a]

	I	II	III
	Ground State	Ground State	v_5=1 State
A	21102.72	21103.41	21231.28
B	5930.09	5930.13	5929.44
C	4621.81	4622.26	4617.51
τ_{aaaa}	-.4331	-.4226	-.4359
τ_{bbbb}	-.0487	-.0469	-.0457
τ_{bbaa}	+.0976	+.1135	+.1086
τ_{baba}	-.0133	-.0166	-.0162
H_J	0	$-.161\times10^{-6}$	$-.222\times10^{-6}$
H_{JK}	0	$-.326\times10^{-5}$	$-.476\times10^{-5}$
H_{KJ}	0	$-.430\times10^{-5}$	$-.195\times10^{-5}$
H_K	0	$+.633\times10^{-5}$	$-.388\times10^{-5}$

a. The centrifugal distortion parameters are discussed in L. Pierce and N. Dicanni, J. Chem. Phys. 38, 730 (1963).

Reproduced with permission of the copyright owner. Further reproduction prohibited without permission.

Reproduced with permission of the copyright owner. Further reproduction prohibited without permission.

Table II. Rotational Transitions of Ground State Cis-Difluoroethylene

A. Spectrum Calculated from Parameters of Table I, Col.I

LEVELS	CALC	OBS	RIG. ROT.	P4	P6	2ND.	DEV	IN FIT
1(1, 1) - 2(2,-2)	25725.370	25725.580 *	25725.320	-0.084	0.000	0.134	0.210	
2(1, 2) - 2(2, 0)	27750.023	27750.080 **	27744.399	-1.443	0.000	-2.712	0.057	
2(0, 2) - 2(1, 2)	32478.156	32478.200 **	32486.575	-4.330	0.000	-6.089	0.044	
111(4,108) - 10(5, 5)	-24196.750	24196.800 **	-24177.411	-18.288	-0.000	-1.051	1.951	
23(7,17) - 22(8,14)	13174.581	13174.410 **	13611.014	-437.739	-0.000	-3.464	-0.171	
26(8,19) - 25(9,16)	14006.875	14006.070 **	14436.323	-425.374	-0.000	-4.174	-0.805	
28(10,19) - 27(11,16)	-30346.526	-30347.590	-29804.747	-537.917	-0.000	-4.762	-0.465	
26(10,16) - 27(11,17)	-30346.026	-30346.550	-29803.253	-538.000	-0.000	-4.747	-0.520	
25(9,17) - 24(10,14)	-31104.024	-31104.200	-30737.479	-362.694	-0.000	-3.851	-0.176	
25(9,16) - 24(10,15)	-31101.474	-31101.630	-30734.765	-362.856	-0.000	-3.847	-0.156	
25(12,14) - 26(13,13)	28158.073	28160.340	30352.946	-2193.873	-0.000	-4.034	1.767	
25(12,13) - 26(13,14)	28202.946	28202.340	30309.500	-2106.524	-0.000	-4.031	1.366	
23(10,14) - 22(11,11)	27116.111	27114.680	29467.821	-1347.009	-0.000	-4.431	-1.431	
23(10,13) - 22(11,12)	27139.466	27139.440	29494.349	-1349.987	-0.000	-4.425	-1.444	
2(1, 2) - 1(0, 1)	34965.683	34970.120 *	34969.357	-0.055	0.000	0.389	0.434	
2(1, 1) - 2(0, 2)	17870.062	17870.030 *	17870.427	0.039	0.000	-0.404	-0.039	
2(1, 2) - 3(0, 3)	20101.405	20101.490 *	20102.287	0.020	0.000	-0.859	0.040	
44(1,43) - 44(0,44)	23336.610	23338.470 *	23338.662	-0.000	0.000	-1.661	0.049	
4(0, 4) - 3(1, 3)	29159.863	29159.730 *	29160.464	-2.211	-0.000	-0.360	0.867	
6(2, 6) - 7(3, 5)	15852.666	15852.670 **	15820.406	-25.781	-0.000	-3.498	1.674	
23(7,16) - 22(8,15)	13438.437	13438.800 **	13925.343	-443.000	-0.000	-3.906	0.363	
24(7,18) - 23(8,15)	24637.225	24639.220 **	25069.919	-429.129	-0.000	-3.571	-0.405	
26(8,18) - 25(9,17)	14106.595	14105.260 **	14740.574	-631.064	-0.000	-4.274	-0.435	
22(6,15) - 21(9,12)	-31651.741	-31651.000	-31450.549	-229.109	-0.000	-4.047	0.767	
22(9,14) - 21(6,13)	-31654.756	-31654.100	-31452.243	-229.409	-0.000	-3.103	0.656	
26(11,16) - 25(12,13)	27686.643	27688.780	29430.418	-1736.464	-0.000	-4.311	-0.863	
26(11,15) - 25(12,14)	27697.561	27697.760	29440.119	-1737.881	-0.000	-4.297	-0.777	
1(1,-0) - 1(0, 1)	16481.103	16481.240 **	16481.282	-0.065	0.000	-0.113	0.069	
12(0, 3) - 12(1, 2)	17387.525	17388.220 **	17388.711	-0.904	-0.000	-0.279	0.444	
6(2, 5) - 5(3, 2)	-16965.729	-16964.720 **	-16965.409	-0.633	-0.000	0.313	1.009	
11(3, 8) - 10(4, 7)	14375.076	14327.270 **	14353.309	-63.976	-0.000	-4.975	2.184	
13(2,12) - 12(3, 9)	24585.615	24590.020 **	24662.867	14.186	-0.000	12.749	0.501	
12(3,11) - 12(4, 8)	24651.631	24652.270 **	24708.809	-58.627	-0.000	1.750	0.799	
16(2,15) - 15(3,12)	14261.044	14260.760 **	14100.371	135.242	-0.000	25.431	-0.394	
16(2,14) - 16(3,13)	-14015.766	-14015.710 **	-14409.615	355.259	-0.000	38.590	0.054	
25(5,21) - 24(10,15)	14752.767	14752.740 **	15624.769	-865.683	-0.000	-4.659	-1.367	
25(5,20) - 24(10,14)	14796.211	14796.060 **	15643.410	-868.656	-0.000	-4.502	-1.151	
28(12,17) - 27(13,14)	16618.631	16619.560 **	19555.764	-1931.337	-0.000	-4.295	0.929	
5(2, 3) - 4(3, 2)	-24691.608	-24692.600 **	-24693.621	1.932	-0.000	-1.001	1.008	
10(2, 9) - 9(3, 6)	15406.933	15407.830 **	15417.903	-15.255	-0.000	4.294	0.897	
12(3,10) - 11(4, 7)	15776.575	15780.330 **	15827.936	-48.474	-0.000	0.733	3.755	
28(12,16) - 27(13,15)	16621.186	16621.120 **	19597.155	-1931.673	-0.000	-5.296	0.934	

AV. DEV.= 0.651 RMS. DEV.= 0.880

* Frequencies reported in Reference 15 of Chapter II

** Frequencies reported in Reference 16 of Chapter II

Reproduced with permission of the copyright owner. Further reproduction prohibited without permission.

Table II. Rotational Transitions of Ground State Cis-Difluoroethylene
B. Spectrum Calculated from Parameters of Table I, Col.II

LEAST-SQUARES FIT OF OBSERVED TRANSITIONS

LEVELS	CALC	OBS	OBS.-CALC.	P4	P6	2ND	DEV	IN FIT
1(1, 1) - 0(0,-0)	25725.581	25725.580	25725.666	-0.076	-0.000	-0.008	-0.002	
1(1,-1) - 1(0, 1)	16481.169	16481.160	16481.196	-0.038	-0.000	0.007	0.004	
2(0, 2) - 2(1, 2)	17388.156	17388.200	17389.043	-0.899	-0.000	0.016	0.040	
5(1, 4) - 5(0, 5)	27756.057	27750.080	27751.684	-1.547	-0.002	0.162	-0.017	
5(0, 5) - 5(1, 5)	33476.232	33478.200	33482.183	-4.191	-0.004	0.245	-0.033	
6(2, 5) - 5(3, 2)	-16564.675	-16564.720	-16564.010	-0.643	-0.001	-0.021	-0.044	
11(3, 8) - 10(4, 7)	14327.262	14327.270	14390.939	-64.014	0.062	0.275	0.007	
11(4, 8) - 10(5, 5)	-24165.146	-24195.160	-24176.208	-19.005	0.006	0.040	-0.013	
12(2,12) - 12(3, 9)	24556.673	24550.020	24579.469	11.423	-0.210	-0.550	-0.053	
13(3,11) - 13(4, 8)	24652.242	24652.220	24913.545	-61.141	-0.019	-0.143	-0.022	
16(2,15) - 15(3,12)	14266.727	14260.760	14132.483	130.933	-0.925	-1.764	0.031	
15(2,14) - 15(3,13)	-14015.702	-14015.710	-14361.181	350.462	-2.452	-2.592	-0.009	
22(7,17) - 22(8,14)	13174.376	13174.410	13611.776	-439.473	1.482	0.595	0.031	
26(8,19) - 25(9,16)	14066.039	14066.070	14637.131	-634.855	2.774	0.668	0.031	
25(6,21) - 26(10,16)	14752.746	14752.740	15625.176	-878.834	4.809	1.586	-0.007	
25(5,20) - 26(10,15)	14765.160	14765.060	15664.244	-881.684	4.856	1.694	-0.040	
28(12,27) - 27(13,24)	16619.521	16619.540	18556.556	-1960.904	18.535	5.334	0.019	
28(10,19) - 27(11,16)	-30347.577	-30347.580	-29802.128	-549.387	2.934	1.004	-0.002	
28(11,18) - 27(12,15)	-30349.590	-30349.590	-29901.134	-569.464	2.935	1.004	0.000	
25(5,17) - 24(10,14)	-31104.200	-31104.200	-30735.514	-370.754	1.552	0.616	-0.099	
25(6,19) - 24(10,15)	-31101.537	-31101.630	-30732.805	-370.905	1.554	0.620	-0.093	
26(12,26) - 26(13,25)	28149.429	28149.340	30366.947	-2225.514	21.620	5.426	-0.089	
25(12,23) - 26(13,24)	28202.260	28202.360	30480.393	-2225.130	21.448	5.470	0.100	
32(10,24) - 32(11,21)	27114.715	27114.650	28468.452	-1366.202	9.431	3.035	-0.036	
33(10,23) - 32(11,22)	27138.567	27138.440	28494.886	-1368.962	9.460	3.154	-0.128	
2(1, 2) - 1(0, 1)	34570.128	34570.120	34970.175	-0.023	-0.000	-0.092	-0.009	
20(1, 1) - 20(0, 2)	17870.077	17870.030	17869.989	0.064	-0.000	0.024	-0.047	
3(1, 2) - 3(0, 3)	20101.444	20101.450	20101.320	0.071	-0.000	0.034	0.006	
4(1, 3) - 4(0, 4)	23336.666	23336.670	23336.886	-0.317	-0.001	0.069	0.003	
4(0, 4) - 3(1, 3)	29158.710	29158.730	29160.875	-2.186	-0.001	0.021	0.020	
5(2, 3) - 4(3, 2)	-24090.661	-24090.600	-24092.640	1.983	-0.002	0.048	0.001	
6(2, 6) - 7(3, 5)	15692.637	15692.670	15618.181	-25.769	0.011	0.215	0.033	
10(2, 9) - 9(3, 6)	15407.868	15407.830	15424.652	-16.554	-0.019	-0.271	0.021	
12(3,10) - 11(4, 7)	15780.266	15780.330	15830.680	-50.370	0.007	-0.061	0.034	
22(7,16) - 22(8,15)	13438.845	13438.800	13885.711	-449.200	1.580	0.755	-0.045	
24(7,18) - 23(8,15)	24437.268	24437.220	25470.369	-535.758	1.869	0.729	-0.011	
24(8,18) - 25(9,17)	14105.277	14105.260	14741.610	-460.300	2.846	1.121	-0.017	
28(12,26) - 27(13,25)	16621.122	16621.120	18558.443	-1961.220	18.544	5.356	-0.002	
22(6,16) - 21(9,12)	-31891.133	-31891.000	-31657.743	-234.447	0.734	0.372	0.133	
22(8,14) - 21(9,13)	-31884.113	-31884.100	-31650.449	-234.778	0.737	0.378	0.013	
26(11,26) - 25(12,23)	27688.892	27688.780	29431.102	-1751.306	14.537	4.476	-0.112	
26(11,25) - 25(12,24)	27697.354	27697.760	29440.861	-1762.630	14.571	4.553	0.405	

AV. DEV.= 0.046 RMS. DEV.= 0.080

Reproduced with permission of the copyright owner. Further reproduction prohibited without permission.

Table III. Rotational Transitions of v_5=1 Cis-Difluoroethylene Spectrum Calculated from Parameters of Table I, Col.III

LEAST-SQUARES FIT OF OBSERVED TRANSITIONS

LEVELS	CALC	OBS	RIG. ROT.	P4	P6	2ND	DEV	IN FIT
2(1, 1) - 2(0, 2)	18026.587	18026.540 *	18026.512	0.051	-0.000	0.024	-0.047	
3(1, 2) - 3(0, 3)	20243.545	20243.530 *	20243.438	0.054	-0.001	0.054	-0.015	
4(1, 3) - 4(0, 4)	23485.906	23485.960 *	23486.135	-0.326	-0.002	0.099	0.054	
1(1, 1) - 0(0,-0)	25848.692	25848.690 *	25848.782	-0.081	-0.000	-0.008	-0.002	
5(1, 4) - 5(0, 5)	27908.238	27908.280 *	27959.599	-1.520	-0.004	0.163	0.042	
4(0, 4) - 3(1, 3)	29020.766	29020.760 *	29022.861	-2.117	-0.001	0.023	-0.006	
2(1, 2) - 1(0, 1)	35083.732	35083.750 *	35083.791	-0.034	-0.000	-0.024	0.017	
25(9,16) - 24(10,15)	-33496.477	-33506.470	-33362.994	-335.766	1.446	0.617	0.007	
22(8,14) - 21(9,13)	-34210.667	-34210.700	-34001.241	-210.671	0.861	0.384	-0.033	
22(8,15) - 21(9,12)	-34217.474	-34217.490	-34008.304	-210.466	0.857	0.379	-0.016	
7(2, 5) - 7(1, 6)	36909.853	36909.900	36906.453	3.429	-0.038	0.011	0.046	
6(2, 4) - 6(1, 5)	40103.460	40103.400	40100.173	3.341	-0.024	-0.029	-0.061	
15(4,11) - 14(5,10)	25192.885	25193.010	25353.653	-161.605	0.350	0.487	0.125	
21(6,15) - 20(7,14)	23262.931	23262.860	23627.777	-366.790	1.175	0.770	-0.072	
24(7,18) - 23(8,15)	22859.463	22859.350	23363.350	-506.317	1.711	0.720	-0.114	
17(6,11) - 16(7,10)	-23952.432	-23952.440	-23845.563	-103.322	0.251	0.202	-0.008	
20(7,14) - 19(8,11)	-23459.960	-23459.930	-23278.936	-181.879	0.556	0.298	0.031	
20(7,13) - 19(8,12)	-23422.437	-23422.410	-23240.370	-182.919	0.569	0.313	-0.003	
23(8,15) - 22(9,14)	-22839.575	-22839.540	-22596.659	-294.568	1.196	0.495	0.036	
13(6, 8) - 14(5, 9)	-24440.596	-24440.530	-24390.375	-50.458	0.097	0.139	0.066	
13(6, 7) - 14(5,10)	-24693.656	-24693.610	-24645.826	-48.028	0.083	0.114	0.046	
12(5, 6) - 11(6, 7)	-24612.716	-24612.770	-24723.963	-18.887	0.031	0.102	-0.054	
12(4, 8) - 11(5, 7)	-13126.648	-13126.660	-13083.966	-42.890	0.060	0.148	-0.032	
13(3,11) - 12(4, 8)	23913.470	23913.450	23571.673	-57.986	-0.074	-0.143	-0.021	
12(3,10) - 11(4, 7)	14830.550	14830.600	14878.073	-47.491	-0.023	-0.060	0.100	
14(4,10) - 13(5, 9)	11716.652	11716.650	11828.159	-112.028	0.001	0.331	-0.012	
4(1, 4) - 3(2, 1)	-12848.878	-12848.930	-12846.915	0.124	-0.000	-0.087	-0.052	
25(9,17) - 24(10,14)	-33698.952	-33698.930	-33365.664	-335.624	1.663	0.613	0.022	
27(8,20) - 26(9,17)	23416.638	23416.710	24129.516	-717.260	3.177	1.203	0.072	
28(10,19) - 27(11,16)	-33236.052	-33208.080	-32711.744	-530.270	2.987	0.975	-0.028	
28(10,18) - 27(11,17)	-33207.168	-33207.140	-32710.793	-560.343	2.989	0.978	0.029	
23(8,16) - 22(9,13)	-22903.447	-22903.510	-22611.056	-293.982	1.147	0.484	-0.063	
38(12,27) - 38(13,25)	24814.948	24814.980	26886.771	-2097.545	19.789	5.934	0.032	
39(12,27) - 38(13,26)	24817.776	24817.730	26890.101	-2098.112	19.817	5.971	-0.046	
36(11,26) - 35(12,23)	24557.581	24557.540	26200.726	-1660.668	13.341	4.132	-0.041	
36(11,25) - 35(12,24)	24565.709	24565.760	26205.967	-1661.897	13.391	4.248	0.051	
33(10,24) - 32(11,21)	24240.630	24240.700	25517.856	-1283.718	8.685	2.864	0.070	
33(10,23) - 32(11,22)	24263.618	24263.570	25543.164	-1291.288	8.772	2.971	-0.049	
6(1, 5) - 5(2, 4)	28069.540	28069.400	28076.630	-10.230	-0.001	0.142	-0.140	
11(3, 8) - 10(4, 7)	13325.351	13325.350	13365.676	-40.684	0.073	0.285	-0.031	
12(2,11) - 11(3, 8)	22876.215	22876.230	22892.310	-5.291	-0.189	-0.615	0.015	
13(2,12) - 12(3, 9)	23936.812	23936.810	23926.621	11.404	-0.353	-0.859	-0.002	

AV. DEV.= 0.042 RMS. DEV.= 0.053

* Frequencies reported in Reference 15 of Chapter II

APPENDIX II

Programs and Computational Details for Chapter IV

A. Calculations for Pure HCN

1. Computer Program COLGVM

The Fortran IV computer program COLLI for the IBM 7094 has been listed and described in detail.[1] That program calculates relative intensities and phase shifts for double resonance experiments according to Eq. (I-21). As written, it is useful for pure HCN only. The program has been modified for use on the IBM 360-65 and is known as COLGVM. The main change is that different diagonalization subroutines are used that allow the calculations to be done with single precision arithmetic on the 360.

The input data is the same as for COLLI except:

Card	Input Data	Format
5	DPA, DPB, WCST1, WHC	5F15.8

WCST1 = wall constant

WHC = frequency (MHz/mm-Hg) of hard collisions between molecules. A hard collision is one that returns the populations to a Bolzman distribution. The same kinetic model is used as was used for the wall collisions:

---

1. Paul Larson, Ph. D. Thesis, Harvard University, Cambridge, Mass. 1969.

Reproduced with permission of the copyright owner. Further reproduction prohibited without permission.

$$\Pi_{ij} = WHC(\delta_{ij} - n_i^{eq}) \cdot P \cdot 2\Pi \qquad (1)$$

In Sections III and IV of COLGVM where $\underset{\sim}{\Pi}$ and $\underset{\sim}{\Pi} + \underset{\sim}{\delta\Pi}$ are diagonalized, an improved Givens procedure subroutine[2] is used that diagonalizes symmetric matrices. Several programming errors in COLLI have been corrected, and Section XVI of COLLI has been deleted.

It was found that a 30x30 rate matrix is large enough to allow the computed results to be independent of matrix size. There is no change in computed intensities and phases as the matrix is increased from dimension 28 to 30 by adding the J = 17 levels. A matrix of dimension 21 that includes J = 7 to J = 17 does have slightly larger relative intensities. A matrix including J = 7 to 14 produces phase shifts differing by 2-5° from the values computed for the ΔJ = +1, 2 and 3 experiments using the 30x30 matrix. In Fig. 1 are presented relative intensity curves for matrices encompassing J = 10-14, J = 7-14, and J = 3-17.

Several of the molecular parameters necessary to determine the HCN equilibrium populations have uncertainties that might affect the computed results. The energy levels for the lower level of the $v_2 = 1$ doublets are given by:

$$E_L = hB_v[J(J+1)-\ell^2] - hD_v[J(J+1)-\ell^2]^2 - \frac{a}{4}(v_2+1)J(J+1) \qquad (2)$$

where B_v = the rotational constant for the v vibrational state

D_v = a centrifugal distortion constant

---

2. This program was provided by Prof. Roy Gordon.

Reproduced with permission of the copyright owner. Further reproduction prohibited without permission.

Reproduced with permission of the copyright owner. Further reproduction prohibited without permission.

q = the ℓ-doubling parameter

ℓ = the units of angular momentum about the molecular axis (ℓ = 1 for this work).

The energies for the upper levels differ only by the sign of the ℓ-doubling contribution.

For HCN, $B(v_2=1)$ has been determined from infrared work,[3] D_v has been determined for the ground state,[4] and q has been determined by several authors.[5] Calculations have been made of the equilibrium populations determined by the different parameters, and it has been found that the effect on the calculated double resonance signals is less than 1 part in 100. In Table I are presented several sets of equilibrium populations and the molecular parameters on which they are based.

A third variable in the calculations is the wall constant parameter. In Fig. 2 are presented some calculated curves for a single set of collisional rates but different values for the rate of molecule-wall collisions. The wall constant has an observable effect. It is similar in nature for all observed transitions and is most important at lower pressures, unlike the pump power parameter.

2. Real Time Population Relaxation

---

3. I. R. Dagg and H. W. Thompson, Trans. Far. Soc. 52, 455 (1956).

4. C. A. Burrus and W. Gordy, Phys. Rev. 101, 599 (1956).

5. a. J. F. Westerkamp, Phys. Rev. 93, 716 (1954).

b. Miyahara et al., J. Phys. Soc. Jap. 11, 3352 (1956).

Reproduced with permission of the copyright owner. Further reproduction prohibited without permission.

TABLE 1

HCN Molecular Parameters and Equilibrium Populations

Microwave Parameters[4]

B_{000} = 44316.0 MHz and $D_{v=0}$ = 0.0904 MHz

Infrared Parameters[3]

B_{000} = 44346.9 MHz

B_{010} = 44451. MHz

ℓ-doubling parameter

$$q(J) = \begin{cases} 224.478 - 0.002667*J*(J+1) & \text{(Ref. 5b)} \\ 224.471 - 0.002614*J*(J+1) & \text{(Ref. 5a)} \end{cases}$$

Equilibrium Populations, J = 3 to J = 17

1. Populations used for calculations of Chapter IV, from (Ref. 1).

7.	6.99698412	8.50497246	8.49886632	9.68525589
9.67482734	10.51495302	10.49710605	10.98[illegible]0795	10.96693049
11.12184799	11.39312904	10.94460404	10.909289	10.50126803
10.45986903	9.84427965	9.79772604	9.02[illegible]7151	8.97954567
8.11446548	8.06160486	7.14991021	7.09619409	6.181[illegible]938
6.12893993	5.24819117	5.19708937	4.3765865	4.32875729

2. Populations using B_{010} = 44,451 MHz, D = 0.0904, q(J) from (Ref. 5b) and T = 300°K.

7.00000000	6.99698456	8.50353226	8.49742852	9.68159081
9.67116987	10.50837699	10.49254740	10.97902485	10.95693295
11.10822451	11.37956448	10.92739740	10.89217430	10.48082255
10.43955586	9.82118426	9.77481107	9.00501891	8.95480426
8.08848924	8.03590852	7.12362160	7.07043146	6.15662301
6.10393667	5.22417037	5.17355027	4.35464702	4.30722575

Reproduced with permission of the copyright owner. Further reproduction prohibited without permission.

Reproduced with permission of the copyright owner. Further reproduction prohibited without permission.

As mentioned in Chapters I and IV, $\underset{\approx}{\Pi} + \delta\underset{\approx}{\Pi}$ is not symmetrizable. Because of the nature of the energy level spacings, it can be treated as a symmetrizable matrix in terms of the calculated double resonance observables. The problem becomes more important if one is concerned with the populations themselves as a function of time. A program, RLGVD, has been written that calculates the populations as a function of time after the pump field is turned on or off. In the program analytic solutions to the equations

$$\frac{d\underset{\sim}{n}}{dt} = -\underset{\approx}{\Pi}\cdot\underset{\sim}{n} \qquad t > 0;\ \underset{\sim}{n}(0) = \underset{\sim}{n}^{ss} \tag{3}$$

$$\frac{d\underset{\sim}{n}}{dt} = -(\underset{\approx}{\Pi} + \delta\underset{\approx}{\Pi})\cdot\underset{\sim}{n} \qquad t > 0;\ \underset{\sim}{n}(0) = \underset{\sim}{n}^{eq} \tag{4}$$

are calculated for specified pressures and times. $\ln|n(t)-n^{eq}|$ and $|\ln n(t)-n^{ss}|$ are calculated for the appropriate times as well as $\frac{n(t)-n^{eq}}{n^{ss}-n^{eq}}$.

The data cards for RLGVD (Relax, Givens, Double Precision) are:

Card	Input Data	Format
1	title	10A8
2	N,NP,NT,IN	1615
3	K1,K2	1615
4	T(I), I = 1, NT	10F8.4
5	DPA,DPB,WCST	5F15.8

6-11 as in COLLI

Reproduced with permission of the copyright owner. Further reproduction prohibited without permission.

All variables have the same meaning as in COLLI except:

NT = number of times at which solutions are to be evaluated

T(I) = time (in microseconds)

Calculations have been made using HCN rate constants that account reasonably well for the HCN double resonance data. $\underset{\sim}{\Pi} + \underset{\sim}{\delta\Pi}$ has been considered to be symmetrizable, but in this case it is not a good assumption. In Table 2 we present a part of the population vector associated with the eigenvector of the zero eigenvalue of $(\underset{\sim}{\Pi} + \underset{\sim}{\delta\Pi})$ as calculated by the Givens subroutine from the upper and lower half of $\frac{1}{\sqrt{n_i^{ss}}} (\Pi + \delta\Pi)_{ij} \sqrt{n_j^{ss}}$. For reference we present the steady state and equilibrium populations. If one measures the error of a particular calculated population by $(n^{calc} - n^{ss})/(n^{eq} - n^{ss})$, examination of Table 2 shows that there are serious difficulties.

These calculations point out the fact that the double resonance intensities and phase shifts are not a terribly sensitive measure of the actual populations. Computationally, $(\underset{\sim}{\Pi} + \underset{\sim}{\delta\Pi})$ is diagonalized only in the low pressure region. Because $(\underset{\sim}{\Pi} + \underset{\sim}{\delta\Pi})^{-1}$ is calculated directly from $\underset{\sim}{\Pi}^{-1}$, no diagonalization is necessary where the system can be characterized by the steady state populations at the end of the pump half-cycle.

The solution to Eq. (4) has also been approximated by finding the eigenvalues and eigenvectors of a symmetrized matrix

$$S_{ij} = \frac{1}{2} (A_{ij} + A_{ji}) , \tag{5a}$$

where

$$A_{ij} = \frac{1}{\sqrt{n_i^{ss}}} (\Pi + \delta\Pi)_{ij} \sqrt{n_j^{ss}} \tag{5b}$$

The eigenvector of the zero eigenvalue of this symmetrized matrix does

Reproduced with permission of the copyright owner. Further reproduction prohibited without permission.

TABLE 2

Equilibrium and Steady State Populations, and Populations Calculated from Approximate Eigenvectors of $(\underset{\sim}{\Pi} + \delta\underset{\sim}{\Pi})$.

J		I[a] "n^{upper}"	II[b] n^{ss}	III[c] "n^{lower}"	IV n^{eq}
3_l		0.271559	0.271419	0.27128	0.271427
3_u		0.271487	0.271318		0.271310
10_l	} pumped levels	0.405650	0.406389	0.407130	0.407190
10_u		0.405647	0.406385	0.407125	0.405585
11_l	} $\Delta J = +1$	0.381475	0.381526	0.381518	0.381715
11_u		0.379804	0.380098	0.380393	0.379910
12_l		0.350094	0.350038	0.349980	0.350141
12_u		0.348180	0.348288	0.348395	0.348185

(a) Populations calculated from an eigenvector found for the symmetric matrix based on the upper half of A_{ij} of Eq. (5b).

(b) Populations calculated from $(\underline{\Pi} + \delta\underline{\Pi}) \cdot \underline{n}^{ss} = 0$.

(c) Populations calculated from the lower half of A_{ij} of Eq. (5b).

Reproduced with permission of the copyright owner. Further reproduction prohibited without permission.

generate the correct steady state populations. We present in Fig. 3 calculations of the populations as a function of time at 1μ and 8μ pressure for reasonable values of the kinetic parameters. The populations are presented as $\frac{n(t)-n^{eq}}{n^{ss}-n^{eq}}$ for convenience. Only the pumped levels are nearly equalized in the presence of the pump field.

For the half cycle with the pump on, an approximate solution has been constructed in such a manner that the system evolves to the correct steady state solution. However, in view of the material presented in Chapter IV concerning coherence effects, it does not seem worthwhile to consider in detail the approximate solution for that half cycle. An interesting feature about the other half cycle can be seen in Fig. 3. Since $\underset{\approx}{\Pi}$ can be symmetrized, these populations are calculated exactly in terms of the model, and we can see that the relaxation to equilibrium is governed by many relaxation times rather than a single time. When the pump field is turned off, the relaxation to equilibrium for the levels other than the pumped levels follows a complicated process. Because the collisional rate constant for the transitions between the pumped levels is very small, the perturbation is dissipated only by "flowing" through the other levels. At 1 μ pressure the populations of the adjacent levels actually become further removed from equilibrium for 10 μs. after the pump is turned off. At 8 μ of Hg this occurs for less than 1 μs.

The question of the meaning of the single microwave relaxation time associated with the collisional linewidth parameter certainly merits further consideration, and these calculations indicate one

Reproduced with permission of the copyright owner. Further reproduction prohibited without permission.

Reproduced with permission of the copyright owner. Further reproduction prohibited without permission.

Figure 3

$P_{HCN} = 1\mu$

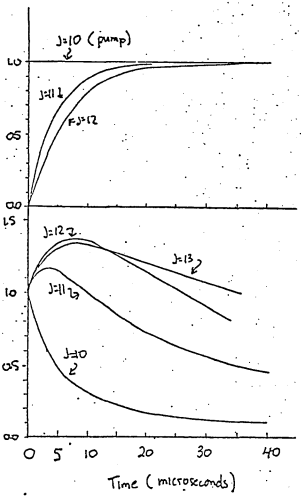

$P_{HCN} = 8\mu$

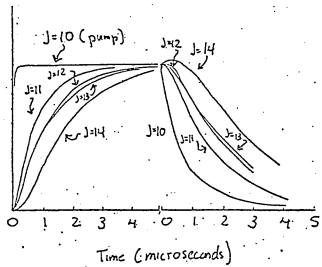

$$\left| \frac{\Delta n_J(t) - \Delta n_J^{eq}}{\Delta n_J^{ss} - \Delta n_J^{eq}} \right| \text{ vs. time}; \qquad \Delta n_J = n_{J,\text{lower}} - n_{J,\text{upper}}$$

direction that is being followed.

B. Calculations for HCN-Foreign Gas Experiments,

Computer Program COLFGGV

COLGVM has been modified to permit the calculation of the double resonance intensities and phases for HCN in the presence of a foreign gas. The program COLFGGV performs the calculations for a single pressure of HCN and many pressures of the foreign gas. There are two collision rate matrices that must be specified. The matrices are constructed for the specified pressures of HCN and the foreign gas and then combined into a final matrix

$$\underset{\sim}{\Pi}^{TOT} = \underset{\sim}{\Pi}^{HCN-HCN} + \underset{\sim}{\Pi}^{HCN-FG} .$$

This procedure must be followed because the two component matrices will not, in general, commute.

The input data are as follows (unless specified, parameters have the same meaning as in COLLI):

Card	Input Data	Format
1	Title	10A8
2	N,NP,NO,IN,NOPT	1615
3	K1,K2	1615
4	(MI(I), MF(I), I = 1,NO)	5F15.8
5	DPA,DPB,DPBF,WCST1,WHC,WHCFG	5F15.8
6	NE(I), I = 1,N	5F15.8
7	PHCN	F15.8

Reproduced with permission of the copyright owner. Further reproduction prohibited without permission.

8-11 as in COLLI		
12	JFGD	1615
13	PI2L(J), J = 1,2·JFGD	5F15.8
14	PI2U(J), J = 1,2·JFGD	5F15.8
15	N2FG(J), J = 1,N	16F5.1
16	P	F15.8

NOPT is an input variable. If NOPT = 0, specific rate constants for two columns of $\underset{\sim}{\Pi}^{HCN-FG}$ will be read in. If NOPT = 1, the only contribution to $\underset{\sim}{\Pi}^{HCN-FG}$ will be of the form

$$\Pi_{ij}^{HCN-FG} = WHCFG\cdot(\delta_{ij} - NE(I))\cdot P$$

and cards 12-15 must be omitted.

DPBF = the contribution to the pump power denominator from the foreign gas broadening. The pump power is given by

$$DP = DPA/(.01 + DPB*PHCN**2 + DPBFG*P**2)^{\frac{1}{2}}$$

where P is the pressure of the foreign gas and PHCN is the pressure of HCN (both pressures in mm-Hg).

WCST1 = wall constant.

WHC = frequency of "hard" HCN-HCN collisions.

WHCFG = frequency of hard HCN-foreign gas collisions. The rate matrix for the hard collisions is defined by Eq. (1).

PHCN = HCN pressure (mm-Hg).

2*JFGD = number of elements of PI2L(J) and PI2U(J) that are read in.

PI2L(J) = first column of the foreign gas rate matrix.

Reproduced with permission of the copyright owner. Further reproduction prohibited without permission.

PI2U(J) = second column of the matrix.

N2FG(J) = collision broadening parameters (halfwidth at half height in MHz/mm-Hg) for the foreign gas broadening.

P = foreign gas pressure (mm-Hg). Pressures must be listed on successive cards in ascending sequence.

There will be NP cards of type 16.

Reproduced with permission of the copyright owner. Further reproduction prohibited without permission.